



---

Publicly Accessible Penn Dissertations

---


1-1-2013

# Mechanical Development and Functional Mechanosensitivity During Early Cardiogenesis

Stephanie Feldman Majkut

*University of Pennsylvania*, [sfeldm@sas.upenn.edu](mailto:sfeldm@sas.upenn.edu)

Follow this and additional works at: <http://repository.upenn.edu/edissertations>

 Part of the [Biophysics Commons](#), and the [Developmental Biology Commons](#)

---

## Recommended Citation

Majkut, Stephanie Feldman, "Mechanical Development and Functional Mechanosensitivity During Early Cardiogenesis" (2013).  
*Publicly Accessible Penn Dissertations*. 895.

<http://repository.upenn.edu/edissertations/895>

This paper is posted at ScholarlyCommons. <http://repository.upenn.edu/edissertations/895>

For more information, please contact [libraryrepository@pobox.upenn.edu](mailto:libraryrepository@pobox.upenn.edu).

---

# Mechanical Development and Functional Mechanosensitivity During Early Cardiogenesis

## **Abstract**

This thesis addresses the questions of when and how mechanical stiffness arises during embryonic heart development and how mechanics affects early cardiomyocyte and myocardium contractile function and cytoskeletal organization. Previous studies addressing how mechanics influence the contractile and electrochemical capacity of mature cardiomyocytes on compliant substrates are reviewed in light of theory explaining how contractile striated fibers might optimally align on intermediate substrates. Embryonic heart and brain tissue stiffness through early development are measured by micropipette aspiration, and the earliest functional heart is found to be three-fold stiffer than early embryonic tissue while brain remains soft. Contraction strain in intact embryonic day 4 (E4) heart tubes shows an optimum relative to hearts with softened or stiffened extracellular matrices. Contraction wave velocity, however, goes linearly with softening or stiffening of tissue, consistent with a theory. Isolated E4 cardiomyocytes cultured on collagen-coated substrates of various stiffnesses show optimal contraction on substrates that match the stiffness of E4 tissue. Sarcomere organization shows optimal organization in intact tissue relative to soft and on intermediate substrates relative to soft or very stiff. The feedback between matrix stiffness and contractile capacity of cardiomyocytes in developing heart tissue is modeled and extended to include interactions with nuclear structural proteins, Lamins. A method for perturbing and imaging nuclear lamina in vivo is discussed and preliminary measurements indicate that the nucleus could act as a measure for intracellular stresses.

## **Degree Type**

Dissertation

## **Degree Name**

Doctor of Philosophy (PhD)

## **Graduate Group**

Physics & Astronomy

## **First Advisor**

Dennis E. Discher

## **Keywords**

cardiomyocyte, cytoskeletal organization, ECM, embryo, Lamin, mechanosensitivity

## **Subject Categories**

Biophysics | Developmental Biology

MECHANICAL DEVELOPMENT AND FUNCTIONAL MECHANOSENSITIVITY DURING EARLY  
CARDIOGENESIS

Stephanie Feldman Majkut

A DISSERTATION

in

Physics and Astronomy

Presented to the Faculties of the University of Pennsylvania

in

Partial Fulfillment of the Requirements for the

Degree of Doctor of Philosophy

2013

Supervisor of Dissertation

---

Dennis E. Discher, Ph.D., Professor of Chemical and Biomolecular Engineering

Graduate Group Chairperson

---

Randall Kamien, Ph.D., Professor of Physics and Astronomy

Dissertation Committee

Dr. Mark Goulian, Professor of Physics and Astronomy, Professor of Biology

Dr. Paul Janmey, Professor of Physiology and Adjunct Professor of Physics and Astronomy

Dr. Andrea Liu, Hepburn Professor of Physics, Dept. of Physics and Astronomy

Dr. Philip Nelson, Professor of Physics, Dept. of Physics and Astronomy

For my family

Especially for Mom and Yaya

## ACKNOWLEDGMENT

I would like to thank my advisor, Prof. Dennis Discher for his great support and guidance throughout my graduate study. I also greatly appreciate Dr. Christine Krieger for training in chick embryo dissections and manipulations in Chapter 3, Dr. Joe Swift for Mass Spectrometry analyses in Chapter 3, Prof. Andrea Liu and Prof. Timon Idema for their theoretical model and analysis in Chapter 3, as well as many informative discussions, and to Dave Dingal for the initial modeling work in Chapter 4.

## **ABSTRACT**

### MECHANICAL DEVELOPMENT AND FUNCTIONAL MECHANOSENSITIVITY DURING EARLY CARDIOGENESIS

Stephanie Majkut

Prof. Dennis E. Discher

This thesis addresses the questions of when and how mechanical stiffness arises during embryonic heart development and how mechanics affects early cardiomyocyte and myocardium contractile function and cytoskeletal organization. Previous studies addressing how mechanics influence the contractile and electrochemical capacity of mature cardiomyocytes on compliant substrates are reviewed in light of theory explaining how contractile striated fibers might optimally align on intermediate substrates. Embryonic heart and brain tissue stiffness through early development are measured by micropipette aspiration, and the earliest functional heart is found to be three-fold stiffer than early embryonic tissue while brain remains soft. Contraction strain in intact embryonic day 4 (E4) heart tubes shows an optimum relative to hearts with softened or stiffened extracellular matrices. Contraction wave velocity, however, goes linearly with softening or stiffening of tissue, consistent with a theory. Isolated E4 cardiomyocytes cultured on collagen-coated substrates of various stiffnesses show optimal contraction on substrates that match the stiffness of E4 tissue. Sarcomere organization shows optimal organization in intact tissue relative to soft and on intermediate substrates relative to soft or very stiff. The feedback between matrix stiffness and contractile capacity of cardiomyocytes in developing heart tissue is modeled and extended to include interactions with nuclear structural proteins, Lamins. A method for perturbing and imaging nuclear lamina in vivo is discussed and preliminary measurements indicate that the nucleus could act as a measure for intracellular stresses.

TABLE OF CONTENTS

<b>ACKNOWLEDGMENT .....</b>	<b>III</b>
<b>ABSTRACT.....</b>	<b>IV</b>
<b>LIST OF TABLES.....</b>	<b>VIII</b>
<b>LIST OF ILLUSTRATIONS.....</b>	<b>IX</b>
<b>PREFACE .....</b>	<b>X</b>
<b>CHAPTER 1 : CARDIOMYOCYTES FROM LATE EMBRYOS AND NEONATES DO OPTIMAL WORK AND STRIATE BEST ON SUBSTRATES WITH TISSUE-LEVEL ELASTICITY – METRICS AND MATHEMATICS .....</b>	<b>1</b>
<b>1-1: Introduction .....</b>	<b>1</b>
<b>1-2: Optimal Elasticity for Contraction and Calcium Excitation .....</b>	<b>1</b>
<b>1-3: Matrix Elasticity and Sarcomere Organization .....</b>	<b>6</b>
<b>1-4: Microenvironment of Early Cardiomyocytes .....</b>	<b>9</b>
<b>1-5: Conclusion .....</b>	<b>9</b>

<b>CHAPTER 2: HEART STIFFENING IN EARLY EMBRYOS PARALLELS MATRIX AND MYOSIN LEVELS TO OPTIMIZE BEATING.....</b>	<b>14</b>
2-1: Introduction.....	14
2-2: Results and Discussion .....	14
2-3: Experimental Procedures .....	21
2-4: Supplemental Analysis .....	33
<b>CHAPTER 3: ON THE INTERPLAY BETWEEN CARDIOMYOCYTES AND COLLAGEN-SECRETING CARDIAC FIBROBLASTS IN THE DEVELOPING HEART</b>	<b>60</b>
3-1: Introduction.....	60
3-2: Cardiac fibroblast and collagen content during development: .....	61
3-3: Systems biology in cardiac physiology and development .....	62
3-4: Model for Mechanical coupling between Collagen and Myosin production .....	64
3-5: From ECM to the nucleus .....	67
3-6: Lamins in development.....	67
3-7: Lamin A in cardiac development and disease.....	68
<b>CHAPTER 4: METHOD TO VISUALIZE AND STUDY EMBRYONIC CARDIOMYOCYTE NUCLEI AND LAMINS IN VITRO AND IN VIVO.....</b>	<b>77</b>



<b>4-1: Introduction .....</b>	<b>77</b>
<b>4-2: Methods .....</b>	<b>77</b>
<b>4-3: Results and Discussion .....</b>	<b>79</b>
<b>CHAPTER 5: CONCLUSIONS AND FUTURE DIRECTIONS.....</b>	<b>84</b>
<b>BIBLIOGRAPHY .....</b>	<b>87</b>

## LIST OF TABLES

Table 2-S1: Isolated cardiomyocytes plated on gels of various stiffnesses.	52
Table 3-1:Rate constants and coupling constants for Collagen-myosin coupled model	78
Table 3-2:Rate constants and coupling constants for Lamin-myosin coupled model	79

## List of Figures

Figure 1-1: Isolated cardiomyocytes plated on gels of various stiffnesses.....	11
Figure 1-2: Myofibril formation and registration modulation by substrate stiffness.....	13
Figure 2-1: <i>Mechanical development of heart and brain tissue parallels expression of abundant cell and matrix proteins.</i> .....	35
Figure 2-2: Effect of extracellular matrix softening and stiffening on heart tube beating.....	37
Figure 2-3: Isolated cardiomyocytes are sensitive to matrix stiffness, with striation dependent on actomyosin work. ....	39
Figure 2-4: Sarcomere breadth changes in softened heart and in isolated cardiomyocytes on compliant substrates. ....	41
Figure 3-1: Cardiomyocyte and Fibroblasts create a balance between contractile ability and ECM abundance during development.....	71
Figure 3-2: Model Collagen-I and Myosin mRNA and Protein expression during development ...	72
Figure 3-3: Lamin levels in heart and brain during development.....	73
Figure 3-4: Steady-state Lamin and Myosin levels given matrix elasticity .....	74
Figure 4-1: . Contractile beating of embryonic cardiomyocytes on elastic substrates.....	81
Figure 4-2: Sparse transfection of embryonic heart tubes for perturbation and imaging of nuclear Lamins.....	82
Figure 4-3: Nuclear deformation vs. cellular deformation. ....	83

## PREFACE

This thesis explores the influence of mechanics on the earliest functioning heart tissue from a soft matter physics perspective and introduces novel methods to study cardiomyocyte behavior in intact tissue. The following summarizes each chapter:

***Chapter 1: Cardiomyocytes from late embryos and neonates do optimal work and striate best on substrates with tissue-level elasticity: metrics and mathematics***

In this introductory chapter, we discuss recent studies on the mechanosensitive morphology and function of cardiomyocytes derived from embryos and neonates. For early cardiomyocytes cultured on substrates of various stiffnesses, contractile function as measured by force production, work output and calcium handling is optimized when the culture substrate stiffness mimics that of the tissue from which the cells were obtained. This optimal contractile function corresponds to changes in sarcomeric protein conformation and organization that promote contractile ability. In light of current models for myofibrillogenesis, a recent mathematical model of striation and alignment on elastic substrates helps to illuminate how substrate stiffness modulates early myofibril formation and organization. During embryonic heart formation and maturation, cardiac tissue mechanics change dynamically. Experiments and models highlighted here have important implications for understanding cardiomyocyte differentiation and function in development and perhaps in regeneration processes. This review was published in *Biomechanics and Modelling in Mechanobiology* last year.

***Chapter 2: Heart stiffening in early embryos parallels matrix and myosin levels to optimize beating.***

In development and differentiation, morphological changes often accompany mechanical changes [1], but it is unclear if or when cells in embryos sense tissue elasticity. The earliest embryo is uniformly pliable, and although adult tissues vary widely in mechanics from soft brain and stiff heart to rigid bone [2], cell sensitivity to elasticity is debated [3]. Here we focus on embryonic

heart and isolated cardiomyocytes, which both beat spontaneously, with added motivations from *regenerative medicine because rigid post-infarct regions limit pumping by the heart* [4]. Tissue elasticity,  $E_t$ , increases daily for heart to 1-2 kPa by embryonic day-4 (E4), and although this is ~10-fold softer than adult heart, the beating contractions of E4-cardiomyocytes prove optimal at  $\sim E_{t,E4}$  both *in vivo* and *in vitro*. Proteomics reveals daily increases in a small subset of proteins, namely collagen plus cardiac-specific excitation-contraction proteins. Softening of the heart's matrix with collagenase or stiffening it with enzymatic crosslinking suppresses beating strains in tens of minutes. Sparsely cultured E4-cardiomyocytes on collagen-coated gels likewise show maximal contraction on matrices with native E4 stiffness, highlighting *cell-intrinsic* mechanosensitivity. While an optimal elasticity for striation proves consistent with modeling of force-driven sarcomere registration, contraction wave-speed is linear in  $E_t$  as theorized for Excitation-Contraction Coupled to Matrix Elasticity. Mechanosensitive stem cell cardiogenesis helps generalize tissue results. This chapter concludes with a brief discussion of the interplay between cardiomyocytes and cardiac fibroblasts that secrete matrix and thus establish tissue stiffness.

### ***Chapter 3: Mathematical hypothesis on the interplay between Cardiomyocytes and Collagen-secreting Cardiac Fibroblasts in the developing heart***

As heart muscle stiffens due to deposition of collagenous extracellular matrix (ECM) by fibroblasts, cardiomyocytes must respond by increasing in contractile capacity through proliferation, growth and increased expression of sarcomeric proteins, which in turn influences fibroblast proliferation and ECM deposition. Ultimately this feedback between the ECM and contractile elements of the heart come to a stable balance. Here we review how fibroblast and collagen content evolves during heart development and suggest a model of how such a balance could be struck between myosin content and collagen content using the concept of tension stabilized biopolymers. We also discuss how this model could be extended to include interplay with nuclear mechanics and conclude with a model capturing results of past experiments on

mechanosensitive structural proteins in the nucleus, the lamins, that can also influence expression of contractility genes..

***Chapter 4: Method to visualize and study embryonic cardiomyocyte nuclei and Lamins in vitro and in vivo.***

This chapter outlines a method to visualize and perturb the lamina of individual nuclei within intact developing heart tissue and isolated cells on compliant substrates. Sparse Lamin-A transfection of E4 chick heart tubes was performed before isolating the cells on collagen-coated polyacrylamide substrates. We present and discuss preliminary data of nuclei strain relative to cell/matrix strain.

***Chapter 5: Conclusions and future directions.***

## **Chapter 1 : Cardiomyocytes from late embryos and neonates do optimal work and striate best on substrates with tissue-level elasticity – metrics and mathematics**

*Published: Majkut SF; Discher DE. (2012) Biomechanics and Modelling in Mechanobiology. 11(8), 1219-1225.*

### **1-1: Introduction**

The rhythmic beating of cultured cardiomyocytes, like the rhythmic beating of the heart, provides a clear and simple signature of the central function of these cells. Here we review recent single cell experiments and a mathematical model that have helped illuminate prominent effects of matrix elasticity on the function and structure of embryonic and neonatal cardiomyocytes. The elasticity of culture substrates has been shown by several groups to impact beating forces and beating velocities as well as the calcium dynamics of isolated heart cells. The effects extend, after many hours and thousands of beating cycles, to the expression and organization of the striated assembly of contractile proteins, even in dense co-cultures with cardiac fibroblasts. This protein assembly occurs dynamically over minutes, and a recent mathematical model for alignment of striations not only exhibits similar dynamics but also a dependence on matrix elasticity. The measurements and modeling have significant implications for understanding differentiation during early heart development and are particularly important to factor into the many efforts to generate mature cardiomyocytes from stem cells.

### **1-2: Optimal Elasticity for Contraction and Calcium Excitation**

Is the heart a pump or an excitatory tissue? It is both and more of course, but the fundamental function of the adult heart is to contract its internal volume in order to pump blood. Moreover, the only way that a solid-walled tissue such as the heart can contract in volume is if the wall of the

heart is elastically deformable. What has been less clear is whether the elasticity of the heart wall impacts the function of beating cardiomyocytes at the single cell level. The issue is both important and timely because there are many groups that aim to generate – from embryonic stem cells, induced pluripotent stem cells, and cardiac stem cells, among others [5, 6, 7] – cardiomyocytes that will repair adult hearts after a heart attack or other injury. Ultimately, heart is a muscle that does repetitive work on a load, and tissue elasticity  $E_{tissue}$  at the scale of a cell is a significant part of that load in contributing to remodeling at a basic molecular level.

Several recent studies have sought to physically quantify in culture the effects of matrix elasticity  $E_m$  on late embryonic and neonatal cardiomyocytes. Engler et al. (2008) [8] first made measurements of tissue elasticity  $E_m$  with Atomic Force Microscopy (AFM) of chick heart at embryonic days 4, 7, 10 (E4,7,10), and then isolated cardiomyocytes from E7 embryos and characterized the morphological and functional effects of substrate stiffness on cells. Collagen-I coated polyacrylamide gels provide a tunable matrix to which these embryonic cardiomyocytes attach firmly and beat spontaneously (**Fig. 1-1A**). Beating of cardiomyocytes, which, as in the human heart, occurs at approximately 1 Hz, applies periodic strains to the matrix that can be estimated from the displacement of beads embedded near the gel surface. The cells thus do an amount of work on the substrates that can be estimated by multiplying the square of the mean matrix strain under the cell,  $\epsilon_{out}$ , by matrix elasticity,  $E_m$ . The estimated strains were relatively constant up to about the mean elasticity for heart of ~10 kPa as measured by AFM, and then the strains decrease at higher  $E_m$ . The latter decrease reflects the fact that there must be some rigidity beyond which the cells simply cannot contract; it turns out that the limiting rigidity is close to the physiological tissue stiffness of ~10 kPa. Work done on the substrate goes as  $E_m \epsilon_{out}^2$  multiplied by a prefactor with units of volume that depends on the geometry of the system [9], and can thus be neglected. Engler et al. (2008) [8] estimate this work as  $\frac{1}{2} E_m \epsilon_{out}^2$ , which exhibits an optimum. Below about 10 kPa, the cells do little work on soft matrix (low  $E_m$ ), and above about 10 kPa, the cells cannot strain the stiff matrix (low  $\epsilon_{out}$ ). As pointed out, rigid matrix also arises in



scarring after a myocardial infarction in adults, which is well known to impede contractile function of the heart. Regardless, the optimal substrate stiffness aligns remarkably well with the micro-elasticity measurements for E7 myocardium.

Using a similar system of gel substrates, Jacot et al. (2008) [10] cultured neonatal rat ventricular myocytes (NRVM) and made careful measurements of both the rhythmic forces in beating as well as the much smaller 'resting' forces that are sustainably applied to a substrate due to a basal muscle tone in the cardiomyocytes (**Fig. 1-1B**). NRVM do not beat spontaneously and need to be electro-stimulated, whereas the embryonic cardiomyocytes studied by Engler et al. (2008) [8] beat spontaneously. Importantly, calcium spike dynamics measured by Jacot et al. (2008) [10] showed that 10 kPa matrix maximized both contractile force and the amplitude of calcium dynamics. Excitation-Contraction Coupling (ECC) is a classic phenomenon in muscle physiology [11], and these results are consistent with ECC, but highlight the key role of matrix elasticity as a load on cardiomyocytes. The results are clear for individual cells with no confounding impact of cell-to-cell electrical communication, which suggests that one needs to consider Excitation-Contraction-*Matrix* Coupling (ECMC) in order to understand heart development and pathophysiology.

Evidence in both studies above showed that the main protein motor in cardiomyocyte contraction, cardiac myosin, maintained a relatively constant level of expression. However, Jacot et al. (2008) used a pharmacological inhibitor of the nonmuscle myosin pathway, namely a drug that blocks Rho-associated kinases (ROCKs), and the results showed that this inhibitor suppresses the decrease in force exerted by NRVM on stiff gels (**Fig. 1-1B**). Such findings could lend insight into how and why the same drug protects against heart injury in animal models [12].

Co-cultures of NRVM and matrix-secreting fibroblasts derived from the same hearts were grown on PA gels for 5 days by Bhana et al. (2009) [13], who reported that – in their dense culture systems – cardiomyocyte function and cardiomyocyte numbers relative to fibroblasts appeared

optimal at substrate stiffness in the range of  $E_m = 22-50$  kPa (**Fig. 1-1D**). -The higher optimum in substrate stiffness is thought to match the mechanics of adult rat cardiac tissue, which the same group measured by a pipette aspiration method. It should be noted that cardiomyocytes beat synchronously when in direct contact with each other. Synchronously beating cardiomyocyte aggregates produce more force than individual cells [14], which may explain why these cells functioned so well on somewhat stiffer substrates than in the other studies and the neonatal tissue from which they were derived.

Bajaj et al (2010) [15] looked at similar dense co-cultures of E8 chick-derived cardiomyocytes and fibroblasts on PA gels of 1, 18, and 50 kPa and on tissue culture plates for 1-5 days. They found that the cells initially beat with frequencies modulated by substrate stiffness, with the fastest beating on the 18 kPa. However, after 5 days, as the cells proliferated and came into contact with each other, the beat frequencies became more uniform within each culture and across culture conditions, and the fastest beating occurred in the 50 kPa gel cultures. This is likely due to the cells in contact with each other beating in synchrony. Immunofluorescent imaging of focal adhesion (FA) formation and growth in the different culture conditions revealed increased FA area and number on stiff substrates over time and decreased FA area and number on the softest gels over time. Interestingly, this decrease in FA number and size corresponds to a less organized sarcomeric cytoskeleton on soft substrates relative to the well developed and aligned myofibrils observed on stiff substrates.

Using a very different type of substrate, Rodriguez et al. (2011) [16] cultured NRVM on fibronectin coated elastic micropilli arrays with effective shear moduli estimated to range from 3-20 kPa. The twitch force, work, and power generated by single cells once again increased with substrate stiffness (**Fig. 1-1C**). In addition, calcium activity increased in the NRVM on stiffer substrates. The authors also made direct comparisons of forces produced by neonatal myofibrils to adult myofibrils, showing that neonatal myofibrils generate only about one-third the power of adult

myofibrils. The results underscore the importance of developmental stage and age of the cells studied.

In addition to functional characterizations of the effects of substrate mechanics on force and work output of cardiomyocytes, several of the studies above also attempted to uncover some of the molecular changes that underlie measurable functional changes. Engler et al. (2008) [8] imaged alpha-actinin and noted that 1 day cultures on ~10 kPa matrix exhibited a maximum fraction of cells with sarcomeric striations. They also applied a novel method of labeling proteins within cells to expose differences in molecular structure or activity (Cysteine Shotgun Mass Spectrometry; [17]), and the analysis indeed identified substrate-stiffness dependent differences in myosin and other cytoskeletal proteins as well as one metabolic protein, the muscle-specific pyruvate kinase M1. The latter is intriguing because the studies of ROCK inhibition of the heart cited above also identified drug-dependent difference in several metabolic proteins [18]. On the other hand, such results are very sensible because differential force-generation by muscle places differential demands on metabolism. Moreover, in the drug studies of Jacot et al. (2008) [10], imaging of alpha-actinin in untreated cells revealed a tendency for reorganization of striated sarcomeres into stress fibers, whereas drug treatment blocked this reorganization. As mentioned above, Bajaj et al. (2010) [15] noted that disorganized and unaligned myofibrils in cardiomyocytes grown on soft substrates corresponds to decreased FA area and number relative to the those of cells grown on stiffer substrates, which had well aligned myofibrils. Rodriguez et al. (2011) [16] quantified the striations of cardiomyocytes on their microposts through measurements of sarcomere spacing and z-disk width. They reported that sarcomere spacing, a sign of myofibril maturity and an indicator of likely force output, fell within accepted values for mature myofibrils on all substrates, and increased with increasing stiffness. Z-disk breadth, which indicates increased coupling of sarcomeres within a myofibril, also increased with  $E$ . Increased sarcomere spacing is associated with increased force production because it allows for a greater number of cross-bridges to form during contraction. Increased z-disk breadth, in turn, maintains registry of

sarcomeres within a myofibril, minimizing myofibril buckling during contraction and maximizing contraction velocity.

### **1-3: Matrix Elasticity and Sarcomere Organization**

If organizational and structural changes in cytoskeletal structure underlie the functional, mechanical outputs of the cardiomyocytes, how might substrate mechanics modulate this organization? Cardiomyocytes sense and respond to intra- and extracellular mechanical stimuli through a variety of molecular mechanisms; integrins in costameres and focal adhesions transmit loads from the ECM to the cytoskeleton, cadherins connect myofibrils between cells at adherens junctions, and sarcomere-spanning proteins such as titin respond to intracellular stresses (reviewed in [19]). In considering what types of mechanisms may modulate myofibril organization as observed in the studies above, it is useful to consider how myofibrils form. Sanger et al. (2005) [20] proposed at least one pathway by which myofibrillogenesis occurs in striated muscle cells, and the process begins at the cell membrane, adjacent to matrix, with stress-fiber-like periodic premyofibrils. These progressively register with each other and mature into myofibrils through replacement of short filaments of nonmuscle myosin-IIB (NMMIIB) by long filaments of muscle myosin-II plus incorporation of other sarcomeric proteins (**Fig. 1-2A**). Premyofibril formation, registration, and maturation into mature myofibrils have been visualized in live spreading cardiomyocytes in culture (**Fig. 1-2B**), in precardiac explants, and also in whole embryonic hearts [21]. These studies were performed in a variety of vertebrate organisms; quail, chick, and zebrafish. However, this model is not universally accepted due to possible conflicting evidence from, for example, experiments in which NMMIIB knock-out mice still develop mature myofibrils. Sanger et al (2010) [21] argue that such evidence does not preclude their model because other NMMII isoforms might be upregulated or otherwise compensate for the loss of NMMIIB. Other mechanisms of myofibrillogenesis have been proposed, such as a self-templating model in which free actin and myosin filaments incorporate into preexisting myofibrils [22, 23, 20]. These different mechanisms may occur to different degrees in various circumstances and

different species, possibly explaining some of the observations contradicting the Sanger's premyofibril model. However, it does seem clear the premyofibril pathway to myofibrillogenesis is a prevalent if not a unique pathway.

Since premyofibrils form close to the surface of the cell, this first step of myofibril formation is a likely target of the substrate-stiffness modulation that leads to the variation in sarcomeric organization observed in the experiments above. Friedrich et al. (2011) [24] therefore proposed a general physical theory for how striated contractile fibers interactions with an elastic substrate could promote interfiber registry (**Fig. 1-2C**). They modeled the force transmitted by a fiber to the substrate as a periodic linear array of force dipoles, and the substrate as an elastic half space with a matrix elastic modulus,  $E_m$ , and a Poisson ratio,  $\nu$ . For two such fibers aligned parallel to each other, the elastic interaction energy between was derived as

$$W_{interaction} = \Phi\left(\frac{d}{a}, \nu\right) \frac{\rho_1^2}{aE_m} \cos\left(\frac{2\pi\Delta x}{a}\right) \quad (1-1)$$

Here,  $a$  is the sarcomeric periodicity of each fiber,  $d$  is the distance between the fibers, and  $\Delta x$  is the phase shift between the two fibers, (**Fig. 1-2C-i**).  $\Phi\left(\frac{d}{a}, \nu\right)$  describes the lateral propagation of the strain field produced by a single fiber. For simplicity, the dipole density was approximated as the first Fourier mode  $\rho(x) = \rho_0 + \rho_1 \cos\left(\frac{2\pi x}{a}\right)$ , so  $\rho_1$  is the amplitude of the dipole density. When  $\nu \approx \frac{1}{2}$ , as is the case for the polyacrylamide substrates of the experiments discussed previously and  $\frac{d}{a} > 0.247$ ,  $\Phi\left(\frac{d}{a}, \frac{1}{2}\right) < 0$ . This indicates that neighboring fibers should be inclined to come into registry such that  $\Delta x = 0$ .

The registration force on one fiber due to this elastic interaction with its neighbor is  $f_{reg} =$

$-\frac{\partial W_{interaction}}{\partial \Delta x}$ . Friedrich et al. (2011) [24] used this relation to model the overdamped sliding of fibers relative to each other, where the net force on the fibers is the sum of the interaction force

and a stochastic noise term. They further consider the experimental observations of substrate stiffness strengthening cell-substrate adhesions and active cell contractility. They model these

effects as  $\rho_1 = \frac{\rho_1^* E_m}{E_m + E_m^*}$ . This gives a maximal registration force that is a nonmonotonic function of  $E_m$

$$f_{reg} \sim -\frac{\rho_1^2}{E_m} \sim -\frac{E_m}{(E_m + E_m^*)^2} \quad (1-2)$$

and is modulated by an optimal  $E_m^*$ . Using this registration force, they simulated the sliding dynamics of an array of  $n = 10$  fibers over a range of  $E_m$ . To quantify the degree of interfiber registration, they defined the smectic order parameter for the resulting configurations

$$S = \sum_{i=1}^{n-1} \cos\left[\frac{2\pi}{a}(\Delta x_{i+1} - \Delta x_i)\right] / (n - 1) \quad (1-3)$$

The ensemble average of this order parameter,  $\langle S \rangle$ , as a function of matrix elasticity is plotted for various times in **Fig. 1-2C-iii**. The resulting curves are fit with the same functional form as the registration force **Eq. 1-2** and exhibit an optimum in matrix elasticity at  $\sim 10$  kPa. Therefore, elastic coupling between adjacent myofibrils can give rise to organizational trends much like those observed in the studies discussed above. Additionally, organizational dynamics predicted by this model occur on timescales of minutes to hours, which is thousands of cycles of rhythmic beating of cells.

A strong separation of time scales seems consistent with the slow re-organization of sarcomeres as a function of  $E_m$  as reported in the experimental studies above of Engler et al. (2008), Jacot et al. (2008), and Rodriguez et al. (2011). Thus, the clearest clock in the cell, its beating frequency, is not strictly coupled to formation or disruption of the central structure-function relationship in muscle, namely the contractile sarcomere. In materials science, processes such as work-hardening, which improves strength, and cyclic fatigue or failure, which compromise application, seem related to the force-dependent striation processes in muscle. The relation suggests the

importance of dislocations, defects, and cracks in heart development and disease, motivating further quantitative measures and mathematical models.

#### **1-4: Microenvironment of Early Cardiomyocytes**

It is important to note that in the developmental stages of the cardiomyocytes used in the studies above, the heart is a well-differentiated, 4-chambered organ with a substantial extracellular matrix. Although further growth and stiffening of cardiac tissue with development and aging occurs [13, 25], such mature tissue is already much stiffer at ~10 kPa than the earliest beating heart stages that have approximate elastic moduli of ~0.5-2 kPa [26, 27, 28]. Early embryonic cardiac tissue is very fragile, heterogeneous, and small. It is also only slightly stiffer than early embryonic tissue, which is typically measured to have  $E_{tissue}$  in the range of 0.1- 1 kPa [29, 27, 30]. Since the heart is the first functional organ to develop in the vertebrate embryo, initial myofibril formation, which shortly precedes the first heart beats, occurs much earlier in development than the stages from which the cells in studies cited here are derived. As a result, the impact of mechanical microenvironment on the earliest cardiomyocytes is less well less defined.

#### **1-5: Conclusion**

Given that cardiac mechanics develop progressively in an embryo, an important set of developmental questions emerges from the findings reviewed here that relatively well-developed cardiomyocytes “beat best” on matrices that mimic the mechanics of the original, mature tissues. A first key question is when do cardiomyocytes in the earliest embryo begin to respond to the micro-elasticity of the tissue? Do defects in striation emerge or are they avoided? Do such processes trigger new gene programs in development to promote (or undermine) robustness in structure-function? The experimental analyses and mathematical modeling summarized briefly here offer new tools to apply to such questions, and they are especially relevant to the current work with stem cells that may one day allow repair of adult heart tissue.

*Acknowledgements:* NIH T32, NIH R01, NIH P01, and NSF are all gratefully acknowledged.



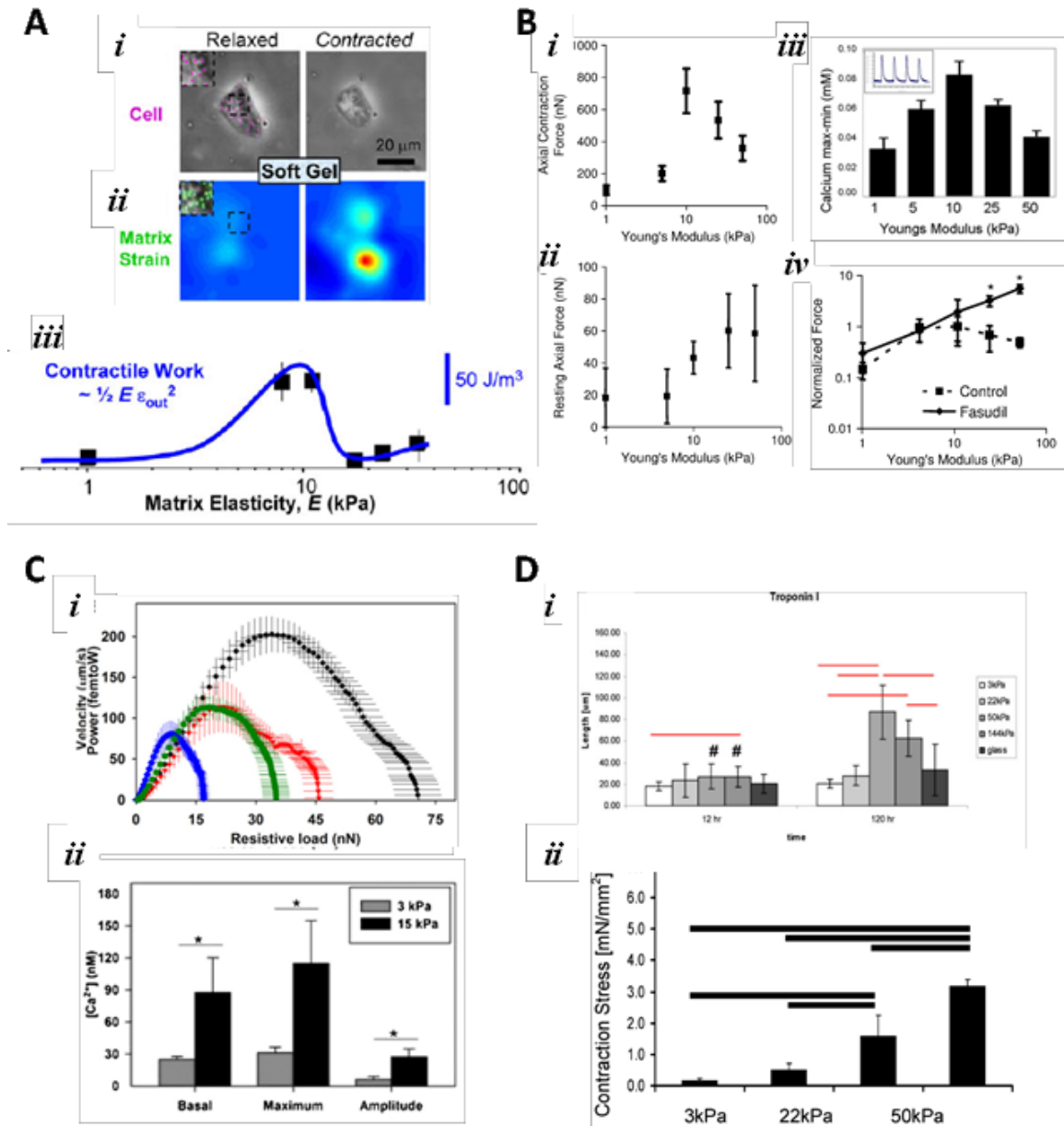


**Figure 1-1: Isolated cardiomyocytes plated on gels of various stiffnesses.** (A) Engler et al. (2008) [8] characterized the morphological and functional effects of substrate stiffness on embryonic cardiomyocytes isolated from E7 chick embryos cultured on collagen-I-coated Polyacrylamide (PA) gels. They found that the cells put out the most work on substrates of  $\sim 10$  kPa. This optimal substrate stiffness matches that of E7 myocardium as they measured by AFM. (B) Jacot et al. (2008) [10] cultured at neonatal rat ventricular myocytes (NRVM) on PA gels of 1 kPa, 10 kPa, and 50 kPa. They found that 10 kPa optimized NRVM function measured by contractile force generation and calcium activity. Furthermore, inhibition of ROCK and RhoA pathways eliminate the decreased force production of NRVM on stiff gels. (C) Rodriguez et al. (2011) [16] cultured NRVM on fibronectin-coated microposts with an narrow range of effective

moduli ranging from 3-20 kPa and found that twitch force, work, and power increased with substrate stiffness. In addition, calcium activity increased in NRVM on stiffer substrates. (D) Bhana et al. (2009) **[13]** co-cultured both NRVM and fibroblasts isolated from the same tissue on PA gels for 5 days, and monitored not just NRVM morphology and function, but the relative population changes of fibroblasts and cardiomyocytes. They found that cardiomyocyte function and population relative to fibroblasts were optimal at substrate stiffness of 22-50 kPa relative to soft (3 kPa) and stiff (144 kPa).

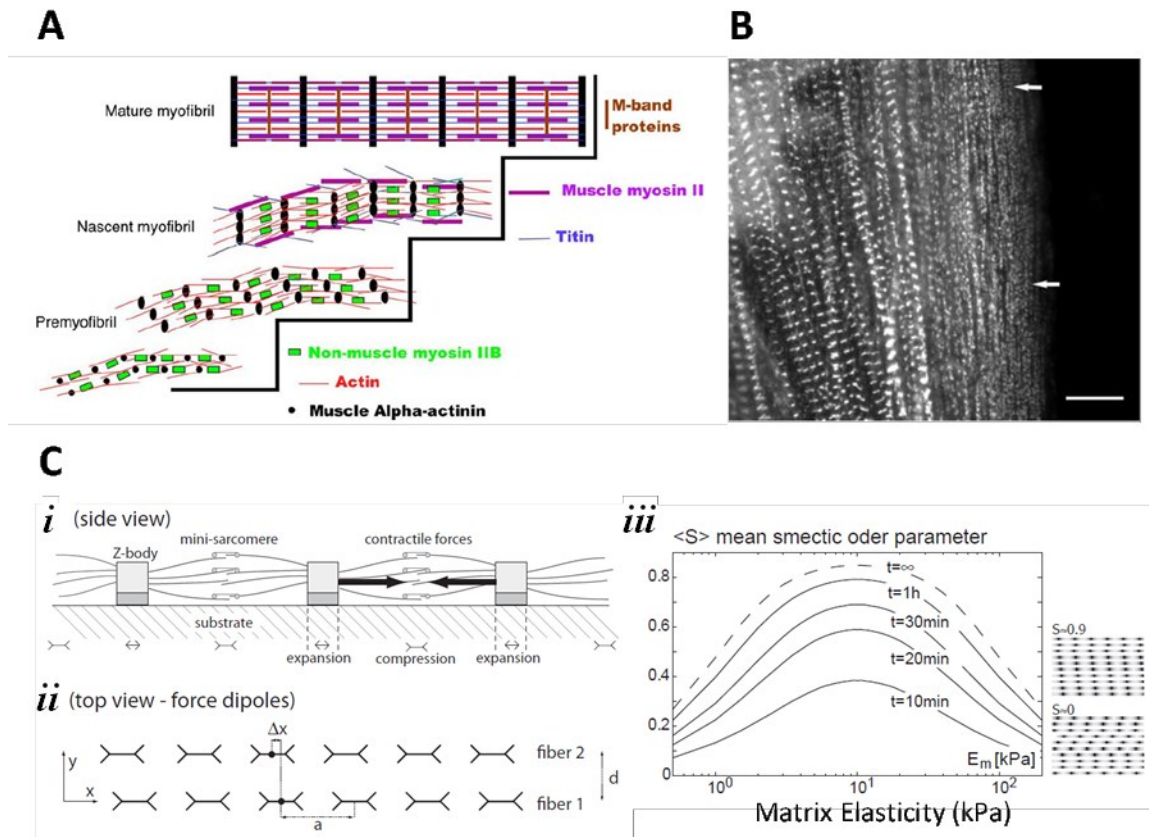


**Figure 1-2: Myofibril formation and registration modulation by substrate stiffness.** (A) Premyofibril model for myofibril formation (Sanger et al. 2005) [20]. Striated premyofibrils comprised of alpha-actinin-enriched z-bodies, short actin thin filaments and nonmuscle myosin IIB filaments mature into mature myofibrils by replacement of nonmuscle myosin IIB with muscle myosin II and incorporation of other sarcomeric proteins. (B) Premyofibril formation, registration, and maturation into mature myofibrils have been visualized in live spreading cardiomyocytes, as shown (Sanger et al. 2005) [20], in precardiac explants, and in whole embryonic hearts (Sanger et al. 2010) [21]. White arrows indicate premyofibrils deposited near the edge of the spreading cell. (C) Theoretical model proposed by Friedrich et al. (2011) [24] showing how aligned striated fibers on elastic substrates may come into registry in a substrate-stiffness dependent manner. (i) Striated fibers apply stresses at the cell-substrate interface that can be modeled as periodic line of force dipoles. (ii) Adjacent fibers interact through the laterally propagating strain fields they produce. (iii) These interactions lead fibers to come into registry with each other in a nonmonotonic substrate-elasticity-dependent way. The smectic order  $S$  of the resulting arrays of striations is a measure of the level of registration.

## **Chapter 2: Heart stiffening in early embryos parallels matrix and myosin levels to optimize beating**

*In Press: Majkut SF, Idema T, Swift J, Krieger C, Liu A, Discher DE. (2013) Current Biology.*

*Mass-Spec and analysis performed by Dr. Joseph Swift. Latrunculin recovery assay's performed by Dr. Christine Krieger. Modeling of contractile wave propagation and theory performed by Dr. Timon Idema with Prof. Dr. Andrea Liu.*

**2-1: Introduction** The heart is the first functional organ in vertebrate embryos, beating spontaneously as a tube by ~36 hr post fertilization (**Fig. 2-1A**). Subsequent stiffening has been described thusfar in terms of changes in cell volume, hyaluronic acid, and/or collagen-I [31] – but functional tests are lacking. Cardiomyocytes isolated from either late embryos [8, 32] or neonates [10, 16, 33] and cultured on substrates of varied stiffness suggest that gels which are stiffer than adult heart suppress contraction. Extremely soft substrates suppress sarcomere organization and limit contractile ability, with additional evidence of altered cytoskeletal conformation and assembly [8] in the absence of changes evident in other cells such as mechanosensitive degradation [34] or transcription [35]. Mature cells cultured on gels can thus exhibit an optimal stiffness for contraction, but the relevance to intact heart is unclear.

### **2-2: Results and Discussion**

***Heart stiffens with expression of Excitation/Contraction/Collagen proteins, while Brain remains soft***

Tissue aspiration into micropipettes (**Fig. 2-1B**) of diameter sufficient to probe dozens of cells [1] shows that heart at all stages behaves elastically (**Fig. 2-1C**) whereas midbrain tissue and

embryonic disk flow over minutes and fail to recover fully after release of the stress. The effective Young's modulus of each tissue,  $E_t$ , was calculated from the slope of aspiration pressure versus aspirated length (**Fig. 2-S1A**) [36], and for brain and embryonic disc, the (already large) aspirated length at 2 min was used. By E2, the presumptive ventricle is already 3-fold stiffer than undifferentiated embryonic disc and embryonic brain. The latter remains roughly constant through development at  $0.3 \pm 0.2$  kPa (**Fig. 2-1C**), consistent with adult brain [37]. Thus brain tissue is always soft whereas heart stiffens up to about 10-fold to reach neonate and adult heart stiffness by E14 [8]. Modest stiffness variations of  $\pm 20\%$  along the developing heart tube (**Fig. 2-S1B**) are also consistent with previous measurements [28].

Expression trends of at least some tissue proteins seemed likely to parallel the trends in tissue mechanics and to confer tissue stiffness. Quantitative mass spectrometry of extracts from embryonic discs, and E2-E4, and E10 heart and brain tissue identified over 200 diverse proteins (**Table S1**), of which fewer than 10% followed trends in expression similar to those of  $E_t$  (**Fig. 2-1D-G, 2-S1C-D**). Most trend-following proteins related closely to the excitation-contraction coupling system such as cardiac actomyosin contractile proteins, adhesion proteins, and the SERCA channel. Proteins that were notably not correlated with tissue stiffness included many nuclear proteins, intermediate filament proteins, and nonmuscle myosin. It should also be noted that this proteomic-focused analysis neglects other particularly important early embryonic heart tissue ECM components, such as Hyaluronic acid(HA). Changes in levels of HA, for instance could affect cell behavior, organization and development of these early cardiomyocytes outside of the mechanical changes of the surrounding tissue [38]. HA is also notably a prominent ECM component of adult brain. Of two ECM proteins detected, only collagen-I follows the  $E_t$  trends.

To begin to assess stiffness contributions of the actomyosin cytoskeleton or collagen, we inhibited myosin contractility with the myosin-II ATPase inhibitor blebbistatin or else disrupted the collagenous ECM with mild collagenase treatments, and then measured tissue stiffness. With

blebbistatin, heart tissue from E2 to E14 is softened by ~25% and brain tissue by ~50% (**Fig. 2-S1E**). In contrast, collagenase had no significant effect on brain tissue but considerably softened both early and late heart (**Fig. 2-S1F**) – without perturbing myosin-II levels (**Fig. 2-S1G**). The stiffness of brain tissue thus seems cellular in nature, whereas heart tissue mechanics have major extracellular matrix contributions at even the earliest functional beating stage.

***Optimal elasticity of embryonic heart: modest softening or stiffening impairs beating at E4***

Embryonic heart tubes beat spontaneously at ~1 Hz for up to 1-2 days after isolation, and we could easily measure local tissue strain heart tubes during beating by imaging GFP transfected cells as fiducial markers (**Fig. 2-2A**). This very visible activity is used to address the main question of our studies: whether cells in an intact living tissue are sensitive to microenvironment elasticity. Controlled dose-time treatments with collagenase provided a simple means of softening tissue matrix (in just 30 min), while enzymatic crosslinking of ECM with transglutaminase provided a method to stiffen tissue (**Fig. 2-S2A,B**). Enzyme permeated the tissue (**Fig. 2-S2C**), and for all but the most extreme softening treatment, embryonic heart behaved elastically in micropipette aspiration (**Fig. 2-S2B-inset**). By transfecting cells with a GFP membrane protein (SIRPA-GFP) we could also see that the contours of beating cells were unaffected by collagenase (**Fig. 2-2B, 2-S2D**), and so tissue softening is due primarily to cleavage of ECM rather than disruption of cell connections.

After the enzymatic treatments, hearts continue to beat rhythmically (**Movies 2-S1**), but the magnitude of local contraction (calculated from GFP expressing cells) was always affected. Each heart tube region was analyzed separately (**Fig. 2-S2E-I**), and normalization to pre-treatment measurements accounted for slight variations (~20%) in embryo age and/or lab temperature. Untreated tissue invariably showed the largest contraction, which was typically ~10% strain, while both softening and stiffening of the heart suppressed contractile strain (**Fig. 2-2C, 2-S2E**).

Stiffening of tissue should suppress strain since any muscle cell has a finite capacity to work against a very high load, but softening of the tissue matrix also decreased contractile strain. Consistent with these E4 results, softening of E6 hearts likewise impeded beating (**Fig. 2-2D**). A mathematical theory for striation [39] provided a basis for modeling contractile function (**Box 2-1**) and fits the experiments (**Fig. 2-2C**, dashed line). The optimal stiffness for heart contraction is thus the stiffness of native heart.

The speed of the contraction wave in each heart region increases monotonically with tissue stiffness, except for the most extreme rigidity (**Fig. 2-2E**). The linearity of wave speed can be predicted from a viscoelastic model of active media (**Box 2-2**). For the rigidified heart, beating was still evident, but the contraction wave did not propagate past the pacemaker region in the atrium (**Fig. 2-S2I**). Softening treatments also decreased the probability of contractions propagating out of the atrium.

#### ***E4 and stem cell derived cardiomyocytes are highly sensitive to matrix elasticity***

To assess whether variations in matrix elasticity affect E4-cardiomyocyte adhesion and beating, isolated cells and their properties were studied as sparse cultures on collagen-I coated polyacrylamide gels of varied stiffness (**Fig. 2-3A**). Most of the cultured cells beat at 0.5-1.5 Hz, similar to the heart, indicating high viability as well as sustained adhesion. Relaxed morphologies were measured after 24 hr in culture and showed that substrates stiffer than E4 heart tissue promote spreading and elongation (**Fig. 2-S3A**), as is common with other mesenchymal cell types (e.g. [35]). Cells on matrices of stiffness similar to that of the tissue of origin (~1-2 kPa) were relatively round and unspread compared to the maximum achievable elongation and spreading. Nonetheless, contractile deformation of an *E4 cardiomyocyte* and its local matrix *proves optimal at the matrix elasticity of native E4 tissue* (**Fig. 2-3B**). In vitro contractions were measured in terms of both 2D strains using cell edge displacements and changes in aspect ratio.

Cardiomyocytes derived from embryonic stem cells (ESC-CM), induced pluripotent stem cells (iPS-CM) or directly transdifferentiated cells hold great potential for regenerative therapies [40], and human ESC-CM and iPS-CM displace soft matrix more than stiffer matrix [41]. Here, ESC-CM on soft, intermediate and stiff substrates that match immature (1 kPa), mature (11 kPa), and diseased (34 kPa) myocardium express at day-4 in culture similar levels of sarcomeric proteins but myofibril organization is visibly optimal for intermediate stiffness and contracting edge-velocities decrease with substrate stiffness (**Fig. 2-S3B-E**). On soft substrates in day-6 cultures, myofibrils decrease and beating stops, while ESC-CM on the intermediate and stiff substrates bifurcated into either fast or slow contracting cell populations. Cardiogenesis is thus mechanosensitive to matrix.

#### ***Optimal striation depends on Myosin-II contractile activity***

Organization of the actomyosin cytoskeleton into sarcomeres and myofibrils within striated muscle cells is a well-established determinant of contractile activity [8, 10, 16], but in living zebrafish, fluorescence recovery after photobleaching shows striation proteins are mobile on timescales of 1-10 min [42]. Cardiomyocytes treated with the myosin-II ATPase inhibitor blebbistatin do not beat even though calcium transients are unaffected [43], and cells beat again within seconds after drug washout [44]. This is far quicker than contractility responses to heart matrix alterations in the 0.5-2 hr treatments here. To assess a role for myosin-II activity and contractile forces in striation as assumed in the modeling here [45] (**Box 2-1**), E7 cells with abundant striation were grown on gels optimal for striation [8], pulsed for 30 min with latrunculin to disassemble myofibrils, and then blebbistatin was added to half of the cultures (**Fig. 2-3C,D**). In the absence of blebbistatin, both premyofibrils and mature myofibrils recovered over a few hours from the induced disassembly, and most cells were filled with striations after 24 hr (**Fig. 2-**



**3D,E**), whereas sustained blebbistatin suppressed striation, consistent with striation requiring active myosin-II.

### ***Myofibril order depends on matrix elasticity in vivo and in vitro***

With E4 hearts, we sought to quantify any possible striation differences with and without matrix alterations. Sarcomeric  $\alpha$ -actinin-2 is a key crosslinker of 'z-discs' that is seen in mature myofibrils within embryos and also in shorter period premyofibrils using deconvolution microscopy [46]. In our confocal imaging, we measured sarcomere spacing lateral 'breadth' of z-discs along in-plane sarcomeres as a key metric of registry (**Fig. 2-4A**-inset). Whereas striation spacing peaked at 1.8  $\mu\text{m}$  and appeared unaffected by  $\sim 50\%$  softening of the E4 heart, the z-disc breadth was reduced relative to untreated control (**Fig. 2-4B**). This decreased registry of myofibrils shortly after softening of the matrix indicates a decreased coupling of sarcomeres and is consistent with the striation model [45], highlighting a molecular-scale mechanism for decreased contraction against decreased extracellular load.

Isolated cardiomyocytes beating on gels (**Fig. 2-4C**) show striation spacing of  $\sim 1 \mu\text{m}$  for premyofibrils, which conforms to expectations [42], and also the typical  $\sim 1.9 \mu\text{m}$  spacing of myofibrils (**Fig. 2-4D**) evident in intact heart. Striation spacing shows no variation with matrix, but the abundance of myofibrils relative to premyofibrils is maximized on matrices of elasticity 2-10 kPa (**Fig. 2-4E**). This is consistent with myofibril assembly from premyofibrils [42]. The z-disc breadth of myofibrils also exhibited a broad and significant ( $p < 0.05$ ) maximum (at  $\sim 2 \mu\text{m}$  breadth) within a similar range of matrix elasticities that promote myofibril formation (**Fig. 2-4F**). The premyofibrils exhibited a somewhat narrower ( $\sim 1.5 \mu\text{m}$ ) z-disc breadth that at least decreased on the stiffest substrates. Myofibril structural trends in response to substrate stiffness in culture are thus consistent with intact E4 heart and suggest a common mechanism of stiffness-dependent registration.

Z-disc breadth results for both mature myofibrils and premyofibrils (**Fig. 2-4F**) were also fit by the peaked function of Box 1 with respective  $E_m = 4.2 \pm 0.6$  and  $1.7 \pm 0.3$  kPa ( $n = 0.24 \pm 0.1$ ). Differences in  $E_m$  suggest myofibril organization favors a stiffer matrix or higher load. However, z-disc breadth also likely underestimates registration order within a cell, as it only includes immediately adjacent and perfectly registered striated fibers. Indeed, z-disc breadth trends for myofibrils and premyofibrils in isolated cells are broader than in simulation [45] but still consistent with trends for intact heart (**Fig. 2-4B,F**). What emerges systematically from fitting to Eq. 1 is that  $n$  increases with length scale: the smallest  $n$  is determined for z-disc breadth in culture and the largest  $n$  is found for strain in the intact heart. High cell density, 3D cell-matrix coupling, and cell-cell signaling in tissue (including calcium excitation waves) could all provide a basis for the enhanced sensitivity to matrix  $E$  of tissue.

Protein interactions that govern molecular mobility are force sensitive in living cardiomyocytes and vary with matrix elasticity [8]. An optimum stiffness for striation is thus understandable: while contractile activity 'massages' registration (**Fig. 2-3E, 2-4**) and these forces increase with matrix stiffness [1], high forces on stiff matrix tend to break bonds [8]. Myofibrils thereby mis-register if the load is either too low or high, which largely explains why *parallel and optimal* increases in actomyosin proteins and collagens (**Fig. 2-1**) must be coordinated in the tissue development program. Invading and proliferating fibroblasts make and remodel the matrix that stimulates cardiomyocyte proliferation [47] with increased expression of specialized contractile proteins ( $\alpha$ -actinin-2, cardiac myosin-II in **Fig. 2-1D,E**), and so it is sensible that this program requires matrix engagement by integrins [47] and extends to mechanosensitive, adhesion complex proteins such as talin [48] that also increase (**Fig. 2-1D**). Moreover, since collagen synthesis and organization by fibroblasts is regulated by strain (as reviewed in [49]), heart matrix is likely to be optimized by the optimal stiffness for cardiomyocyte striation and contraction (**Fig. 2-4**). The fact that the optimum shifts in development from 1-2 kPa at E4 and at E7 toward the stiffness of adult heart (eg. **Fig. 2-1C, 2-3E inset**) [8, 10, 16] is also consistent with initial observations that hearts which

were stiffened and stop beating are found to re-start their beating ten hours later. Lastly, Excitation–Contraction Coupling (ECC) in muscle physiology is well-established [11], but the broad effects of matrix stiffness on individual cells and structures even in sparse culture preclude the confounding impacts of cell-cell electrical communication and suggest that Excitation–Contraction–*Matrix* Coupling (ECMC) is required to truly understand muscle.

### **2-3: Experimental Procedures**

Heart isolation, enzyme treatments, micropipette analyses, tissue strain analyses, mass spectrometry proteomics, cell isolation, and the standard techniques are described in detail in the following subsections.

#### ***Tissue isolation***

White Leghorn chicken eggs (Charles River Laboratories) were incubated at 37°C, rotated once per day, until the desired developmental stage was reached. Embryos were extracted at room temperature by windowing eggs, removing extraembryonic membranes with forceps and cutting major blood vessels to the embryonic disc tissue to free the embryo. The embryo was placed in a dish containing PBS and quickly decapitated. For E2-E5 embryos, whole heart tubes were extracted by severing the conotruncus and sino venosus. For older embryos, whole hearts were extracted by severing the aortic and pulmonary vessels and the pericardium was sliced and teased away from the ventricle using extra-fine forceps. Brain tissue was collected from the presumptive midbrain. Embryonic discs were removed by windowing the egg, cutting out the embryo with the overlying vitelline membrane intact, lifting out the embryo adherent to the vitelline membrane and placing in a dish of PBS. Extraembryonic tissue was carefully cut away using dissection scissors and the finally embryo was teased away from the vitelline membrane using forceps. All tissues were incubated at 37°C in pre-warmed chick heart media (alpha-MEM supplemented with 10 % FBS and 1% penn-strep, Gibco, 12571-063) until ready for use.

### ***Mass-Spectrometry of tissues***

For proteomic studies, tissue of interest was washed three times by successive resuspension in ice-cold PBS and diced to sub-millimeter pieces. Proteins were solubilized by cellular disruption with a probe sonicator in ice-cold RIPA buffer with 0.1% protease inhibitor cocktail (approx. 5000 cells /  $\mu\text{L}$ ). NuPage LDS sample buffer (Invitrogen) with 1%  $\beta$ -mercaptoethanol was added to 1x concentration, followed by heating to 80°C for 10 min. Proteins were separated on SDS-PAGE gels (NuPAGE 4-12% Bis-Tris, Invitrogen), run at 100 V for 10 min followed by 25 min at 160 V. Sections of excised polyacrylamide gel (cut in two molecular weight ranges: 55-100 kDa and 100-300 kDa) were washed (50% 0.2 M ammonium bicarbonate (AB) solution, 50% acetonitrile, 30 min at 37 °C), dried by lyophilization, incubated with a reducing agent (20 mM tris(2-carboxyethyl)phosphine in 25 mM AB solution at pH 8.0, 15 min at 37°C) and alkylated (40 mM iodoacetamide in 25 mM AB solution at pH 8.0, 30 min at 37 °C). The gel sections were dried by lyophilization before in-gel trypsinization (20  $\mu\text{g}/\text{mL}$  sequencing grade modified trypsin in buffer as described in the manufacturer's protocol (Promega Corp. Madison, WI), 18 hr at 37°C with gentle shaking). Before analysis, peptide solutions were acidified by addition of 50% digest dilution buffer (60 mM AB solution with 3% methanoic acid).

Peptide separations (5  $\mu\text{L}$  injection volume) were performed on 15-cm PicoFrit column (75  $\mu\text{m}$  inner diameter, New Objective) packed with Magic 5  $\mu\text{m}$  C18 reversed-phase resin (Michrom Bioresources) using a nanoflow high-pressure liquid chromatography system (Eksigent Technologies), which was coupled online to a hybrid LTQ-Orbitrap XL mass spectrometer (Thermo Fisher Scientific) via a nanoelectrospray ion source. Chromatography was performed with Solvent A (Milli-Q water with 0.1% formic acid) and Solvent B (acetonitrile with 0.1% formic acid). Peptides were eluted at 200 nL/min for 3–28% B over 42 min, 28–50% B over 26 min, 50–80% B over 5 min, 80% B for 4.5 min before returning to 3% B over 0.5 min. To minimize sample carryover, a fast blank gradient was run between each sample. The LTQ-Orbitrap XL operated in the data-dependent mode to automatically switch between full scan MS ( $m/z = 350\text{-}2000$  in the

orbitrap analyzer with resolution of 60,000 at  $m/z$  400) and fragmentation of the six most intense ions by collision-induced dissociation in the ion trap mass analyzer.

Raw mass spectroscopy data was processed using Elucidator (version 3.3, Rosetta Biosoftware, Cambridge, MA). The software was set up to align peaks in data from samples derived from the same ranges of molecular weight. Peptide and protein annotations were made using SEQUEST (Thermo Fisher Scientific) with full tryptic digestion and up to 2 missed cleavage sites. Peptide masses were selected between 800 and 4500 amu with peptide mass tolerance of 1.1 amu and fragment ion mass tolerance of 1.0 amu. Peptides were searched against a database compiled from UniRef100 human (for proteomic studies, downloaded 05-Nov-2010) or UniRef100 gallus gallus (for matrix studies, downloaded 12-Jan-2011), plus contaminants and a reverse decoy database. Search results were selected with a deltaCn filter of 0.01 and mass error better than 20 ppm. Ion currents of oxidized peptides ( $\Delta = +15.995$  Da) were summed with their parent peptide; post-translational modifications of phosphorylation ( $\Delta = +79.966$  Da), acetylation ( $\Delta = +42.011$  Da) and methylation ( $\Delta = +14.016$  Da) were entered in the search. In matrix studies, we additionally looked for hydroxylation of proline, asparagine, aspartic acid, and lysine ( $\Delta = +15.995$  Da).

The two MW ranges of the proteomic dataset were analyzed separately. In the mid-MW range (55-100 kDa), the false-positive (FP) detection rate was estimated to be 11.4% (based on search hits of the decoy database) and only proteins with two-or-more peptides/protein were considered for further analysis (2015 peptides from 231 unique proteins). High-MW range (100-300 kDa): FP rate = 11.3%; subsequent analysis of 1223 peptides from 55 unique proteins. Label free relative peptide quantitation was performed with in-house software coded for Mathematica (Wolfram Research, Champaign, IL). Datasets were normalized against optimized housekeeping peptide sets that were found to be invariant between experimental conditions. A peptide-set optimization algorithm (PRF, [50]) was used to select peptides that show a similar 'fingerprint' behavior

between samples, and these peptides were used for the basis of quantification and normalization. We report only quantification of proteins with at least three PRF peptides/protein (total 178 proteins). Peptides from regions common to several proteins or isoforms were treated distinctly. Standard errors were calculated from at least 2 technical repetitions. As a further check of the peptide selection algorithm, ratio comparisons were made between all datasets and checked for consistency (for example, when considering data A, B and C, the ratio A:B should be consistent with A:C x C:B).

***Sample preparation, gel electrophoresis and immunoblotting.***

Frozen whole embryo (Hamburger-hamilton stage 5-8, n = 4) and tissue from E4, E6, and E14 chick heart (n = 4, 2, and 1, respectively) and brain (n = 3, 2, and 1, respectively) diced to approximately 10 mm<sup>3</sup>, was suspended in ice-cold 1x NuPAGE LDS buffer (Invitrogen; 1% protease inhibitor cocktail, 1%  $\beta$ -mercaptoethanol) and subjected to sonication on ice (3 x 15 x 1s pulses, intermediate power setting). Samples were then heated to 80 °C for 10 min and centrifuged at maximum speed for 10 min. SDS-PAGE gels were loaded with 5 – 15  $\mu$ L of lysate per lane (for LMNB1: NuPAGE 4-12% Bis-Tris, for MYH6: NuPAGE 3-8% Tris-Acetate; Invitrogen). Each sample was loaded in triplicate for averaging purposes. Additionally, sample concentrations were adjusted to match LMNB1 signal whilst avoiding overloading and smearing, diluting the lysates with additional 1x NuPAGE LDS buffer if necessary. Gel electrophoresis was run for 10 min at 100 V and 1 hr at 160 V. After blotting on a polyvinylidene fluoride membrane with an iBlot Gel Transfer Device (Invitrogen), the membrane was blocked with 5% bovine serum albumin in TTBS buffer (Tris-buffered saline, BioRad; with 0.1% Tween-20). Membranes were incubated with primary antibodies against LMNB1 (#332000, raised in mouse, Invitrogen; used at 1000-fold dilution) or MYH1/2/4/6 (sc-32732, raised in mouse, Santa Cruz; used at 1000-fold dilution) at 4 °C overnight. After washing, the membrane was incubated with 2000-fold diluted

anti-mouse HRP-conjugated IgG (GE Healthcare), at room temperature for 1 hour. The blot was developed with ChromoSensor (GenScript) for 3 min at room temperature. Blot images were obtained using a Hewlett-Packard Scanjet 4850. Densitometry was performed using ImageJ (version 1.45, National Institutes of Health). Immunoblots were performed in triplicate, and the mean MYH6 densitometry results normalized to LMNB1 values were reported  $\pm$  SEM.

### ***Micropipette aspiration of tissues***

Micropipettes were pulled from glass capillaries (World Precision Instruments, Sarasota, FL) with 1 mm inner diameters using a Flaming-Brown Micropipette Puller (Sutter Instrument, Novato, CA). Pulled tips were scored with the tapered base of another pulled pipette and broken to final inner diameters of 35-45  $\mu$ m. Pipettes were filled with PBS and attached to water-filled manometer-double reservoir set-up as described elsewhere [51]. Aspiration was performed at room temperature in PBS supplemented with 3% BSA, without  $\text{Ca}^{2+}$  to suppress beating. Before each experiment, we incubated the pipette tip in PBS/BSA solution for  $\geq 20$  min to prevent tissue sticking inside the pipette. During aspiration,  $\geq 3$  different pressures were applied from 0.5 – 1.4 kPa for neural tissue and 0.5-20 kPa for cardiac tissue. Aspiration experiments were imaged using a Nikon TE300 microscope with a 20x air objective and recorded using a Cascade Photometric CCD camera. The effective Young's modulus  $E_t$  of the local tissue was obtained from the linearity between the difference between the applied pressure inside the pipette relative to outside ( $\Delta P$ ) and strain  $L/R_p$ :  $\Delta P = \frac{2\pi}{3\Phi_o} E_t \frac{L}{R_p}$ , where  $L$  is the length of tissue aspirated measured from the mouth of the pipette,  $R_p$  is the pipette's inner radius, and  $\Phi_o$  is a shape factor  $\sim 2$  [36].

### ***Cell mechanosensitivity assay***

We isolated cells from heart tissue by dicing to sub-millimeter size and then digesting with Trypsin/EDTA (Gibco, 25200-072). To digest, we incubated tissue in approximately 1 mL Trypsin per E4 HT for 13 min rotating at 37°C, for 2 min upright to let large tissue pieces settle before carefully removing supernatant and replacing with an equal volume of fresh Trypsin, and finally shaking for 15 more min. We stop digestion by adding an equal volume of chick heart media. Cells were plated at concentrations of approximately  $2 \times 10^5$  cells/cm directly on collagen I coated PA gels of varying stiffness [8]. E7 cells were preplated for 2 hours on tissue culture plates to allow fibroblasts to adhere before removing medium with nonadherent cells and plating those cells on collagen I coated PA gels. Spontaneously beating cells were imaged using a Olympus I81 microscope with a 40x air objective configured for phase contrast after 24 hrs in culture, and recorded using a CCD camera at 23 frames/sec. Movies were analyzed using a custom Matlab program to segment cells and track cell area and aspect ratio using the Matlab regionprops function. Strain was calculated for 3 sets of 3 hand-selected seed edge points that were subsequently automatically tracked with a custom Matlab tracking program during beating. The 2D plane strain tensor was calculated for each set of 3 points, throughout and the maximal trace of the strain tensor during contraction was calculated as a measure of strain for a given beat. For each cell, at least 5-10 beats were analyzed. Results were pooled from 4 separate experiments of E4 cardiomyocytes beating on 0.3, 0.9, 2.5, 10, and 40 kPa gels (n = 15, 38, 32, 15, 8).

### ***Latrunculin Recovery Assay***

E7 cardiomyocytes were cultured on 11 kPa PA gels for 16 hrs. Cells were treated with 20  $\mu$ M lat-A. After 30 minutes, lat-A was removed. CMs were allowed to recover for 24 hours. In experimental samples (n = 32), 25  $\mu$ M blebbistatin was added to the media during the full



recovery time. In control samples (n = 9), CMs recovered in the presence of plain media. Premyofibril formation was measured by immunofluorescence of sarcomeric  $\alpha$ -actinin and non-muscle myosin IIb, where s- $\alpha$ -actinin spacing less than  $1.7 \pm 0.02 \mu\text{m}$  or the presence of NMMIIb within striated patterns indicated premyofibril areas.

### ***Whole heart tube transfection***

Lipofectamine/plasmid complexes were prepared as prescribed by the manufacturers (Lipofectamine 2000, Invitrogen). In particular, for each final 1 mL of transfection solution, 3-4 micrograms of plasmid (GFP or SIRPA-GFP [52]) and 10  $\mu\text{L}$  Lipofectamine were each diluted to total volumes of 50  $\mu\text{L}$  in Opti-MEM (Gibco, 31985-070) and stayed at room temperature for 5 min before combining both solutions to make the final transfection solution which again sat at room temperature for an additional 25 min. Heart tubes were preincubated in 0.9 mL pre-warmed chick heart media during lipofectamine/plasmid complex formation. The lipofectamine/plasmid complex was added to the heart tubes in heart media and left to incubate at  $37^\circ\text{C}$  5%  $\text{CO}_2$  for 8-12 hours. Transfection media was replaced with prewarmed chick heart media and the heart tubes continued incubating until use in stiffening or softening experiments and subsequent imaging.

### ***Tissue softening and stiffening treatments***

To soften collagenous ECM, tissue was incubated in solutions of Collagenase (Type XI, Sigma, C7657) in heart media at  $37^\circ\text{C}$  for the specified amounts of time, and rinsed 2x in heart media for 2 min each. Excised E4 HTs were incubated in 1.0 mg/ml, 0.3 mg/ml or 0.1 mg/ml Collagenase for 30 min. Excised E6 HTs were incubated in 0.3 mg/ml collagenase for the short periods (10-30 min) and long (50 min). To stiffen, E4 tissue was incubated in 20 mg/mL transglutaminase

(Sigma, T5398) in chick heart media for 1 hr or 2 hrs at 37°C (n = 3, 5, respectively, over 2 experiments). Micropipette aspiration was used to measure stiffness of E4 heart tissue before treatment and after 1 hour and 2 hours transglutaminase treatment (n = 2, 2, respectively) in coincidence with untreated controls (n = 1, 1)(**Fig. 1-S2A** ) Similarly, micropipette aspiration was used to measure softening of E4 HTs before and after 1.0, 0.3, and 0.1 mg/ml collagenase treatment(n = 2, 3, 2) (**Fig. 2-S2B**). For blebbistatin softening experiments, tissue was incubated in 20 µg/ml blebbistatin (EMD Millipore, 203390, stock solution 50 mg/ml in DMSO) in heart media for 30 min at 37 °C, and compared to a control of equal concentration of DMSO in heart media.

### ***Heart beat imaging and analysis***

GFP-transfected E4 chick hearts were imaged while beating by an Olympus I81, using 4x magnification, with phase-contrast and fluorescent illumination and movies were recorded using a CCD camera at rate of 23 and 17 fps, respectively. To calculate strain,  $\geq 2$  groups of 3 cells located within 20 microns of each other were hand chosen along the outer wall of anatomical region of interest (atrium, ventricle, or OFT) along the heart tube. The same procedure and Matlab program were used to track cells and calculate 2D strain as was used to calculate cell-edge strain for cells on gels. Unless HTs were not beating, strain was measured and averaged for at least 5 beats. The velocity of the contraction wave was calculated by dividing the distance along the heart tube between two groups of analyzed cell groups by the time difference their points of peak strains. To visualize cellular calcium, hearts were loaded with Fluo-4 AM (Fluo-4 AM F14217, Life Technologies) for 30 min at room temperature prior to imaging, following the manufacturer's protocol.

### ***Myofibril striation imaging and analysis***

To visualize myofibril structure and organization in intact heart tubes and isolated cardiomyocytes, samples were stained for sarcomeric  $\alpha$ -actinin-2, filamentous actin (TRITC-phalloidin, Life Technologies) and DNA (Hoechst 33342). Isolated cardiomyocytes and whole heart tubes were first incubated in relaxing buffer [53] for 5 min and 20 min, then fixed in 4% Formaldehyde for 5 min and 20 min, respectively. They were then rinsed three times in blocking buffer (3% BSA in PBS), then left in blocking buffer for 1 hr at room temperature. Samples were incubated in sarcomeric  $\alpha$ -actinin-2 primary antibody (1:500 in blocking buffer) overnight at 4°C rocking. They were again rinsed 3x in blocking buffer before incubating in secondary antibody (1:1000 in blocking buffer) with TRITC-phalloidin (1:2000). Finally, samples were incubated 10 min in Hoechst 33342 (1:1000) in blocking buffer and mounted with mounting medium. Cells on gels were mounted on coverslips and sealed with clear nail polish imaged by wide-field fluorescence imaging with a 60x oil-objective. All striated fibers were hand traced, and striation spacing was measured as the distance between peaks of the  $\alpha$ -actinin image by a peakfinder program in Matlab. Z-disc breadth was measured as the FWHM of the intensity profile perpendicular to the local myofibril direction, after subtracting the best fit linear trend line. Histograms of striation spacing for cells on gels fit to a bimodal:  $\text{count} = a \cdot \exp(-(s-\mu_p)^2/2\sigma_p^2) + b \cdot \exp(-(s-\mu_m)^2/2\sigma_m^2)$  where  $s$  is the striation spacing bin, and  $a$ ,  $b$ ,  $\mu_p$ ,  $\mu_m$ ,  $\sigma_p$ ,  $\sigma_m$  are best fit parameters. Relative premyofibril and myofibril fractions of  $a/(a+b)$  and  $b/(a+b) \pm$  least squares fit error are respectively in Fig. 2-4E, and premyofibril and myofibril spacing respectively are  $\mu_p \pm \sigma_p$  and  $\mu_m \pm \sigma_m$ , in Fig. 2-4D. To estimate the average z-disc breadth of premyofibrils vs. myofibrils, we took the striations with spacing  $\leq 1.3 \mu\text{m}$  to be premyofibrils and  $\geq 1.8 \mu\text{m}$  to be myofibrils and reported the mean  $\pm$  SEM z-disc breadth associated with each respective population. Whole untreated and treated HTs were imaged on a Zeiss LSM 710 confocal with a 40x air-objective, with z-plane spacing of  $0.48 \mu\text{m}$ . Striation in intact heart was analyzed using ImageJ. We converted the z-stack to a stack with z-plane spacing of  $1.96$  by grouped average

intensity z-projections of every 4 images. For a given z-plane, we selected 5 random in-plane, unbranched sections of myofibrils at least 20  $\mu\text{m}$  long using a random number generator to choose 5 random x-y coordinates from which we found the nearest candidate myofibrils. We used planes 6, 16, and 26  $\mu\text{m}$  into the ventricular tissue of untreated ( $n = 2$  HT,  $m = 479$  z-discs) and 0.3 mg/ml collagenase softened ( $n = 2$  HT,  $m = 479$  z-discs) E4 HT. Z-disc spacing and breadth were calculated as described for myofibrils in the cells on gels. The mean of all individual spacings and breadths  $\pm$  SEM were taken for each condition.

**Box 2-1. Friedrich-Safran Model of Matrix Elasticity optimized Registration Force: a Functional form**

Since striation is central to contractile function of any heart or skeletal muscle, a mathematical model of striation can help clarify striation mechanisms as well as processes dependent on striation, particularly the contractile strains measured here. Friedrich et al. (2011) account for matrix elasticity effects and force generation in calculating how striated contractile fibers in cells on elastic substrates interact with each other and come into maximal registry on substrates of intermediate stiffness [45]. The myosin-II based contractile force that drives myofibril registry in the Friedrich-Safran (FS) model follows a non-monotonic form  $f \sim E / (E_m + E)^2$  with a maximum at  $E = E_m$ . Striation organization dynamics in simulations were quantified in terms of a registration order parameter (i.e. ‘smectic’ order), and fit  $f^n$

$$\text{Striation} \sim [ E / (E_m + E)^2 ]^n \quad (2-1)$$

with  $n$  decreasing exponentially over time from  $n \approx 1$  to 0.6. Importantly, high  $n$  gives a sharper peak at half-max than low  $n$ . Moreover, because non-striated cardiomyocytes do not beat, striation is also key to rhythmic strains that we measured in tissue and isolated cells. Matrix strain in cultures of sparse cells indeed fit well to Eq.2-1 with an optimal elasticity  $E_m = 1.3 \pm 0.3$  kPa and  $n = 1$  (**Fig. 2-3B**). This result is particularly remarkable because  $f$  is relatively restrictive,

with only one fitting parameter. For the intact heart, Eq.2-1 also fits the measured strain with  $E_m = 1.6 \pm 0.2$  kPa but with  $n = 4 \pm 1$  (**Fig. 2-2C**). The higher exponent quantifies the much sharper peak for tissue, indicating a greater sensitivity to matrix elasticity in tissue compared to cells in sparse 2D cultures.

### ***Box 2-2. Mechanical Signaling Model for Contractile Waves***

Based only on Excitation-Contraction Coupling, the contractile wavefront speed should not depend on matrix elasticity. The excitable medium model here is linear in  $E$ : cells are coupled mechanically through extracellular matrix and cell contractions are triggered by mechanosensitive means, namely Excitation-Contraction-Matrix Coupling (see Supplement). The heart tube is considered per a two-fluid model [27] with isotropic linear elasticity (matrix plus cells) of elasticity  $E$  and Poisson ratio  $\nu$  as well as tissue viscosity  $\eta$ . Damping forces couple viscous and elastic components through a coupling constant  $\Gamma$ .

$$\begin{aligned} \Gamma(\partial_t u_i - v_i) &= \frac{E}{2(1+\nu)} \left( \partial_k \partial_k u_i + \frac{1}{1-2\nu} \partial_i \partial_k u_k \right) + \partial_j Q_{ij} \delta(\vec{x}) \Theta(t) \Theta(\Delta t - t) \\ \Gamma(\partial_t u_i - v_i) &= -\eta \partial_k \partial_k v_i + \partial_i p \\ 0 &= \partial_k v_k \end{aligned} \quad (2-2)$$

Here  $\delta(x)$  is the Dirac delta function,  $\Theta(t)$  the Heaviside step function, and  $\Delta t$  the duration of the contraction. The wavefront speed depends on two material parameters: an effective “diffusion constant”  $D = E / \Gamma$ , and a relaxation time  $\tau = 2 \eta (1+\nu) / E$ . A predicted threshold value of  $E_0 = 0.1 E_{\text{untreat}}$ , below which the system is too soft to support a contractile wavefront, is consistent with observations that – with softening treatments – the contraction wave failed to propagate sometimes into the ventricular region, which is softer than the atrium (**Fig 2-S1B**). The probability of propagating indeed decreased monotonically with softening (**Fig. 2-S2I**). Failure to propagate when  $E > E_0$  could be due to inhomogeneities in stiffness. Intriguingly, the stiffness of embryonic

heart when it first begins to beat at E2 is also roughly  $0.1E_{\text{adult}}$  (**Fig. 2-1C**), which is several-fold stiffer than the embryonic disc.

## 2-4: Supplemental Analysis

### ***Mechanical Signaling Model for Contractile Waves***

It is well recognized in biological contexts such as *Dictyostelium* [54] that chemical signaling can proceed via propagating wavefronts if a local increase in concentration of some chemical species can trigger further release of that species at that same location, thus amplifying the signal.

Analogously, we propose that *mechanical* signaling can proceed via the propagation of nonlinear contractile wavefronts through mechanically excitable heart tissue. When a cell contracts, it exerts a stress on the surrounding tissue. We approximate this stress as a dipole that conserves the volume of the contracting cell by expanding it perpendicular to the contraction. We denote the strength of the dipoles by  $Q$ . Note that tissue itself cannot sustain mechanical (sound) waves because they are damped out exponentially. However, a wave can be maintained if it is continually amplified. In our model, we assume that each cell contracts once the local stress exceeds a certain threshold value  $\alpha$ . This could occur, for example, if calcium release is triggered by stress [55, 56]. By contracting, a cell adds stress to the system, thus amplifying the signal. This mechanism can lead to a wavefront that moves at constant velocity down the heart tube.

More precisely, we treat the heart tube as a two-fluid model [57]. We model the tissue as having an elastic component (in matrix plus cells) that obeys isotropic linear elasticity and is characterized by the Young's modulus  $E$  and Poisson ratio  $\nu$ . The tissue also has a viscous component that obeys the Stokes equation, is characterized by a viscosity  $\eta$  and is incompressible. Damping forces couple the viscous and elastic components of the material through a coupling constant  $\Gamma$ .

$$\begin{aligned}\Gamma(\partial_i u_i - v_i) &= \frac{E}{2(1+\nu)} \left( \partial_k \partial_k u_i + \frac{1}{1-2\nu} \partial_i \partial_k u_k \right) + \partial_j Q_{ij} \delta(\vec{x}) \Theta(t) \Theta(\Delta t - t) \\ \Gamma(\partial_i u_i - v_i) &= -\eta \partial_k \partial_k v_i + \partial_i p \\ 0 &= \partial_k v_k\end{aligned}\tag{2-2}$$

Here  $\delta(x)$  is the Dirac delta function,  $\Theta(t)$  the Heaviside step function, and  $\Delta t$  the duration of the contraction. The wavefront speed depends on two material parameters: an effective “diffusion constant”  $D = E / \Gamma$ , and a relaxation time  $\tau = \eta / \mu = 2 \eta (1+\nu) / E$ , where  $\mu$  is the material’s shear modulus. Additionally, the speed depends on two dimensionless parameters: the Poisson ratio  $\nu$  and the rescaled threshold  $\underline{\alpha} = a^3 \alpha / Q$ , where  $a$  is the spacing between the cells. By purely dimensional considerations, there are two ways to construct a quantity with the dimensions of a speed:  $D/a$  and  $a/\tau$ . Because both scale linearly with  $E$ , we can immediately conclude that the wavefront speed  $v$  should scale with  $E$  as well. We have confirmed this by solving the model numerically. A full dimensional analysis shows that  $v \sim E a^{1-2n} \Gamma^{-n} \eta^{-(1-n)}$ , where  $n$  is a number between 0 and 1 that depends on the dimensionless parameters  $\nu$  and  $\underline{\alpha}$ . For fixed Poisson ratio  $\nu = 0.4$ , which is reasonable for soft tissues [8], we found numerically that  $n$  depends strongly on the dimensionless threshold stress  $\underline{\alpha}$ , increasing from 0.2 for  $\underline{\alpha} = 0.5$  to 0.4 for  $\underline{\alpha} = 0.75$ . At sufficiently high values of  $\underline{\alpha}$ , or equivalently, sufficiently low values of  $E$ , the tissue becomes too soft to trigger cells to contract; below that threshold (which we denote by  $E_0$ ) the wavefront can fail to propagate ( $v=0$ ).

Pipette aspiration measurements show the ventricle has an effective viscosity  $\eta \approx 25 \text{ Pa}\cdot\text{s}$ , and since this changes by only 20% for the stiffened and softened tissues, we treat it as constant. The coupling constant  $\Gamma$  is estimated by assuming the largest contribution arises from the relative motion of the cytoskeleton with respect to the cytoplasm. Therefore  $\Gamma \sim \eta/x^2$ , where  $x$  is the displacement during contraction, which we take to be  $5 \mu\text{m}$ , or half the radius of the cell, so that  $\Gamma \sim 1 \text{ Pa}\cdot\text{s} / (\mu\text{m})^2$ . We find  $\underline{\alpha}$  by fitting the numerical results to the slope of the  $(E, v)$  data for the ventricle, which is  $13 \text{ mm}/(\text{kPa}\cdot\text{s})$ , and the one-parameter fit yields  $\underline{\alpha} \approx 0.5$ . The threshold for initiating contractions is thus about half the force per unit volume exerted by the cells themselves while contracting.



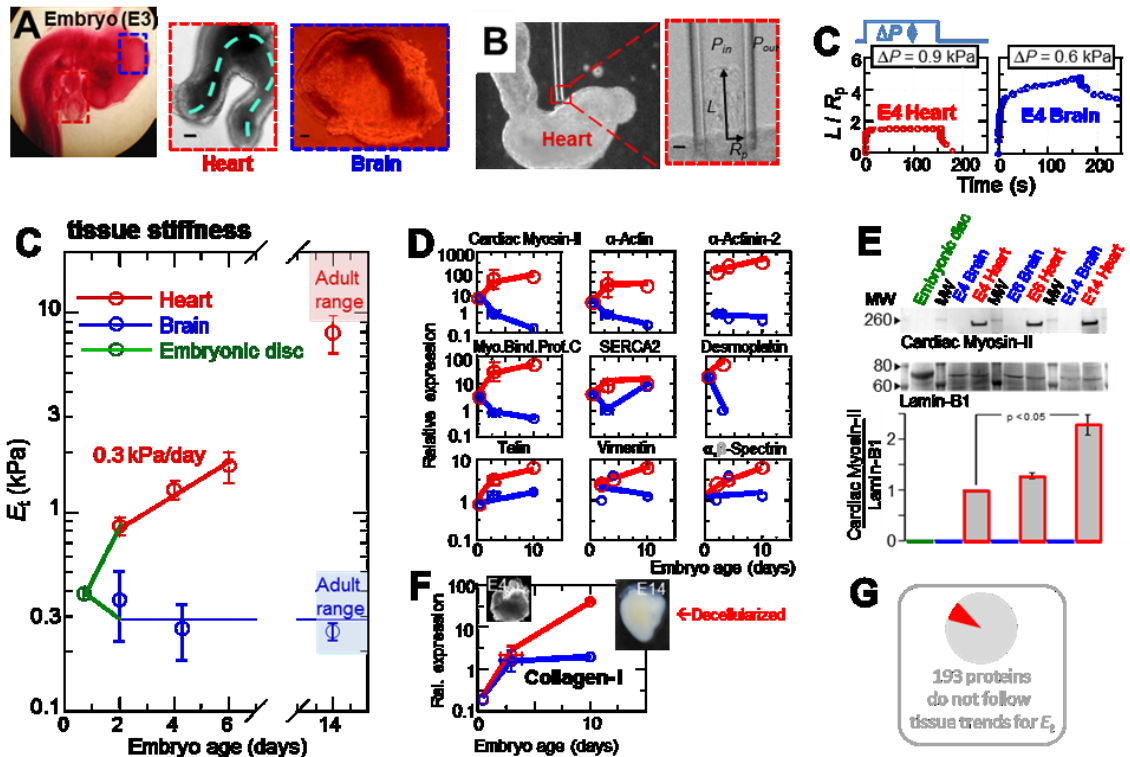


**Figure 2-1: Mechanical development of heart and brain tissue parallels expression of abundant cell and matrix proteins.** (A) E3 chick embryo with heart tube (red line) and midbrain (blue line) outlined *in situ* and after isolation. The heart continues to beat *ex vivo*, with contraction and flow propagating along the dashed turquoise line. Scale bars represent 100  $\mu\text{m}$ . (B) Micropipette aspiration of the inner curvature of an E3 heart tube, with close-up of aspirated tissue in phase contrast image. Scale bar represents 10  $\mu\text{m}$ . (C) Representative aspiration/relaxation curves for E4 heart and brain demonstrate the elastic and viscoelastic behavior of the tissues, respectively, as discussed in the text.  $L$ ,  $R_p$  and  $\Delta P = P_{in} - P_{out}$  are illustrated in (B). (D)  $E_t$  for heart and brain tissue throughout embryonic development, starting with day-1 embryonic disc ( $n = 2$  embryos), then E2, E4, E6, and E14 heart and brain ( $n \geq 3$  measurements each), respectively. By the time beating starts, the heart tube is already 3-fold stiffer than early embryonic tissue and then stiffens at a rate of  $\sim 0.3$  kPa/day (solid red line). Due to the thick epicardium of E6 hearts and older relative to the inner diameter of our micropipettes, measurements likely underestimate stiffness of the myocardium at those stages due to significant contribution of epicardium. Brain tissue does not stiffen during development and remains viscoelastic with a mean  $E_t = 0.3$  kPa. (E) Quantitative mass spectrometry (MS) of cellular proteins extracted from intact embryonic disc (Hamburger-Hamilton stage 3-4), E2, E3, E4, and E10 heart and brain tissue reveals a small set of detected proteins with expression patterns similar to heart or brain mechanics: namely, a general increase in heart and relatively little to no increase in brain. Expression is relative to average in brain E2-E3 ( $n \geq 3$  MS measurements). (F) Immunoblot confirms that MS measurements of Cardiac Myosin-II expression increase in heart during development. Samples represent pooled tissue from 3-4 embryos at each reported stage and were normalized to Lamin B1 ( $n \geq 3$ ). (G) MS indicates that collagen-I expression increases during heart development, but not greatly during brain development. Inset images: 1% SDS-decellularized E4 and E14 hearts. The insoluble matrices retain the shape of the embryonic hearts, but while E14 matrix (80% of MS ion current is collagen-1) appears solid,

the E4 matrix appears more reticulated and porous, consistent with having less mass. **(G)** Of the 209 proteins identified by Mass-Spec (**Table S1**), only 17 had expression levels across tissues and development that paralleled mechanics. Error bars in all figures represent SEM.

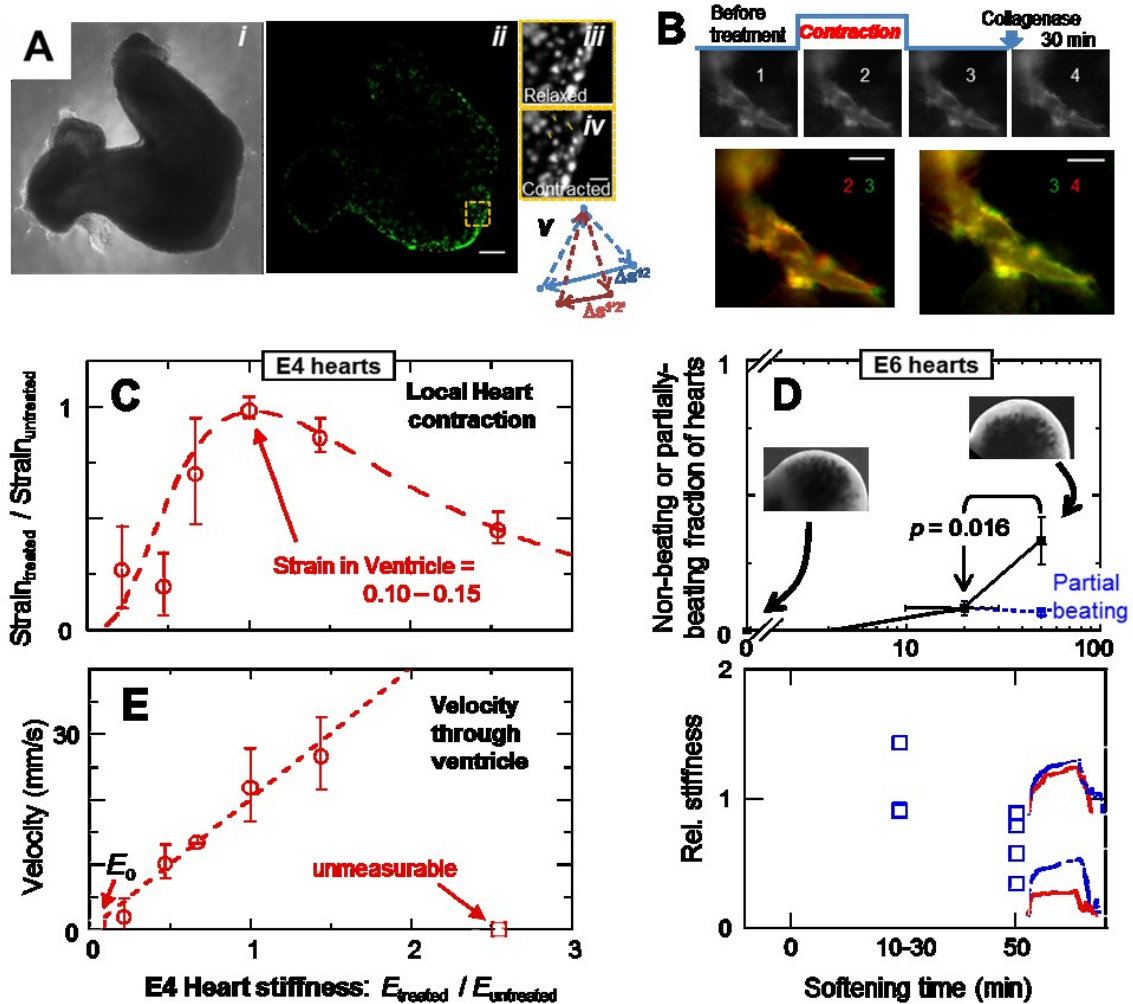


**Figure 2-2: Effect of extracellular matrix softening and stiffening on heart tube beating** (A) Extracted E4 heart viewed with phase contrast (i) and fluorescent imaging (ii) following sparse transfection with GFP. Scale bar = 100  $\mu\text{m}$ . Three GFP-expressing cells used to calculate strain during beating are tracked from their relaxed (iii) to contracted (iv, scale bar = 20  $\mu\text{m}$ ) positions. Strain is schematized in (v) and described in [58]. (B) SIRPA-GFP-expressing cell in transfected E4 heart tissue before and after softening. Overlays of SIRPA-GFP expressing cells over time help visualize any cell conformational changes during contraction and softening treatments. Overlay of the same cell pre-treatment while relaxed (green) and contracted (red) (bottom-left) shows less overlap (yellow) than the relaxed cell before and after softening of the tissue. This suggests that cells maintain morphology and adhesions during softening treatment. (C) Tissue strain during beating of GFP-transfected softened and stiffened E4 HT normalized to that of untreated and the resulting relative strain averaged for atria, ventricles, and outflow tract. Softened and stiffened tissues suppress contractions. Typical peak strains throughout the untreated heart tube were  $10 \pm 4\%$ . The dashed curve is a fit to Eq. 1 with  $n = 4 \pm 1$  and  $E_m = 1.6 \pm 0.2$  kPa. (D) E6 hearts treated with collagenase stop beating or beat partially with greater frequency over time of treatment. Beating is significantly hindered after 50 min softening treatment, relative to untreated or briefly (10-30 min) treated hearts. E6 hearts show clear

softening by 50 min softening treatment, unlike briefly treated hearts, which correlates with decrease in beating function. Insets are representative aspiration-relaxation curves for mildly and significantly softened hearts given the same 50 min softening treatment, in which red represents the untreated tissue and blue represents the treated tissue. (E) Velocity of the contraction wave through the ventricle vs normalized  $E_t$ . Wave-speeds in untreated ventricle, atria, and outflow tract of  $22 \pm 4$  mm/s,  $4 \pm 2$  mm/s and  $2.8 \pm 0.7$  mm/s, respectively, are consistent with past work [59]. For the most extreme stiffening treatment, contraction does not propagate past the presumptive pacemaker. The velocity in the ventricle increases linearly with tissue stiffness, consistent with theory. The dashed line is the theoretical prediction with a single adjustable parameter, namely the ratio of the stress threshold to the magnitude of the force dipole corresponding to a contracting cell.  $E_o$  indicates the theoretically predicted stiffness below which a contraction wave should not propagate. Error bars for all figures represent SEM ( $n \geq 3$  hearts).

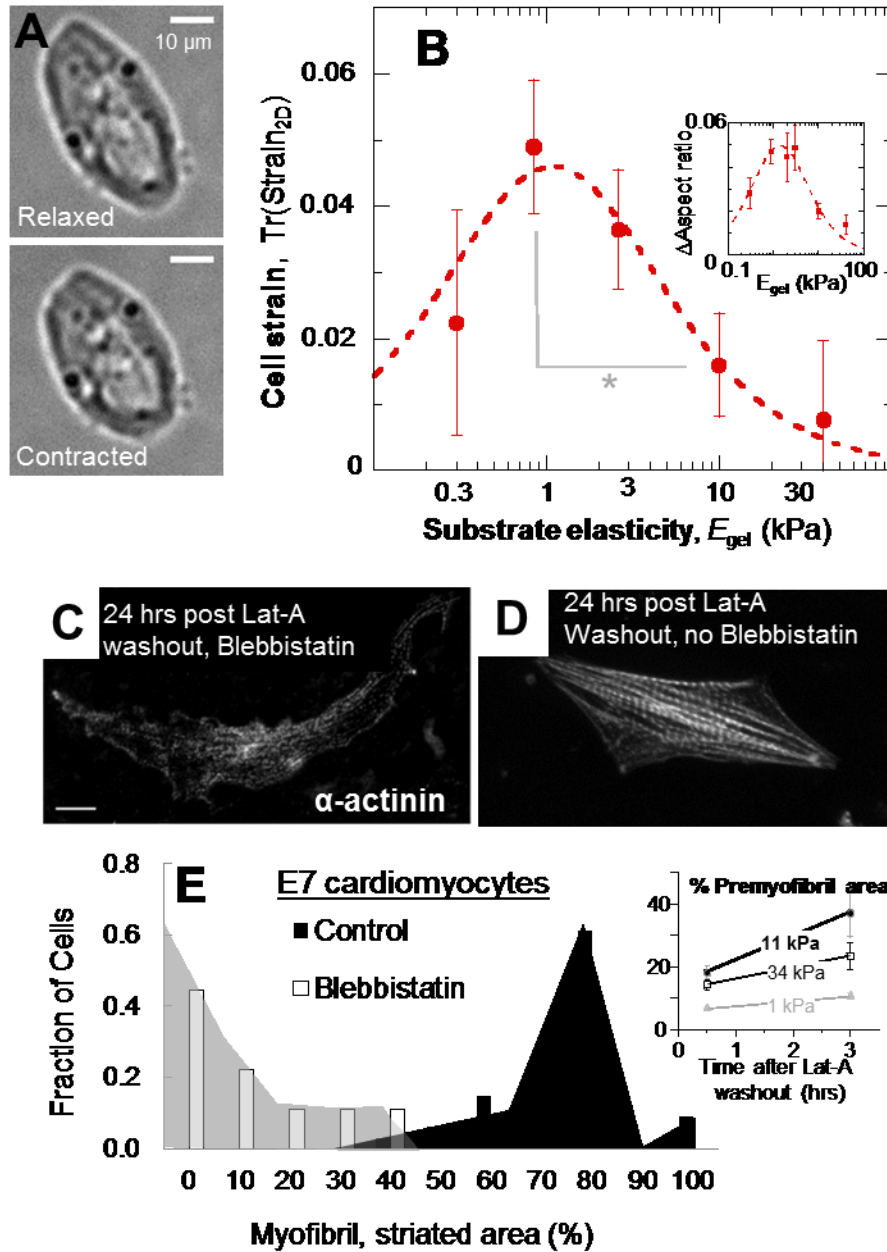


**Figure 2-3: Isolated cardiomyocytes are sensitive to matrix stiffness, with striation dependent on actomyosin work.** (A) Cardiomyocytes were imaged beating in culture after 18-24 hr in culture. Morphologies in the relaxed and contractile states and contractile strains were measured for beating cells. (B) Edge-strain of cardiomyocytes cultured on PA gels of various stiffnesses, measured as the trace of the 2D strain-matrix of cell edge points during beating, as described in methods. In beating, cell and matrix strain is strongly modulated by substrate elasticity with an optimal  $E_{gel}$  similar to that of E4 heart and much lower than that measured for more mature cells ([8, 10]). Softer and stiffer substrates impede beating of cultured cells. The Lorentzian fit gives  $E_m = 1.3 \pm 0.3$  kPa, consistent with the tissue elasticity of E4 hearts ( $E_t = 1.3$

$\pm 0.4$  kPa in Fig. 2-1). (C-D) Representative image of E7 cardiomyocytes recovering from latrunculin-A (Lat-A) treatment in the presence (C) or absence (D) of blebbistatin, which does not affect cell viability [35]. (E) Myofibril assembly was measured as the percentage of cell area covered by mature myofibrils (sarcomere spacing  $> 1.5 \mu\text{m}$ ). Inhibition of beating and actomyosin contractility by blebbistatin reduces the amount of new myofibrils formed following Lat-A washout and causes mature myofibrils to disassemble per (C). Inset shows that for these late embryo cardiomyocytes, the optimal elasticity for rapid recovery of striated pre-myofibrils is close to that of adult heart (Et  $\sim 10$ -15 kPa). Error bars are SEM ( $n \geq 3$  cells). (\*)  $p < 0.05$ .

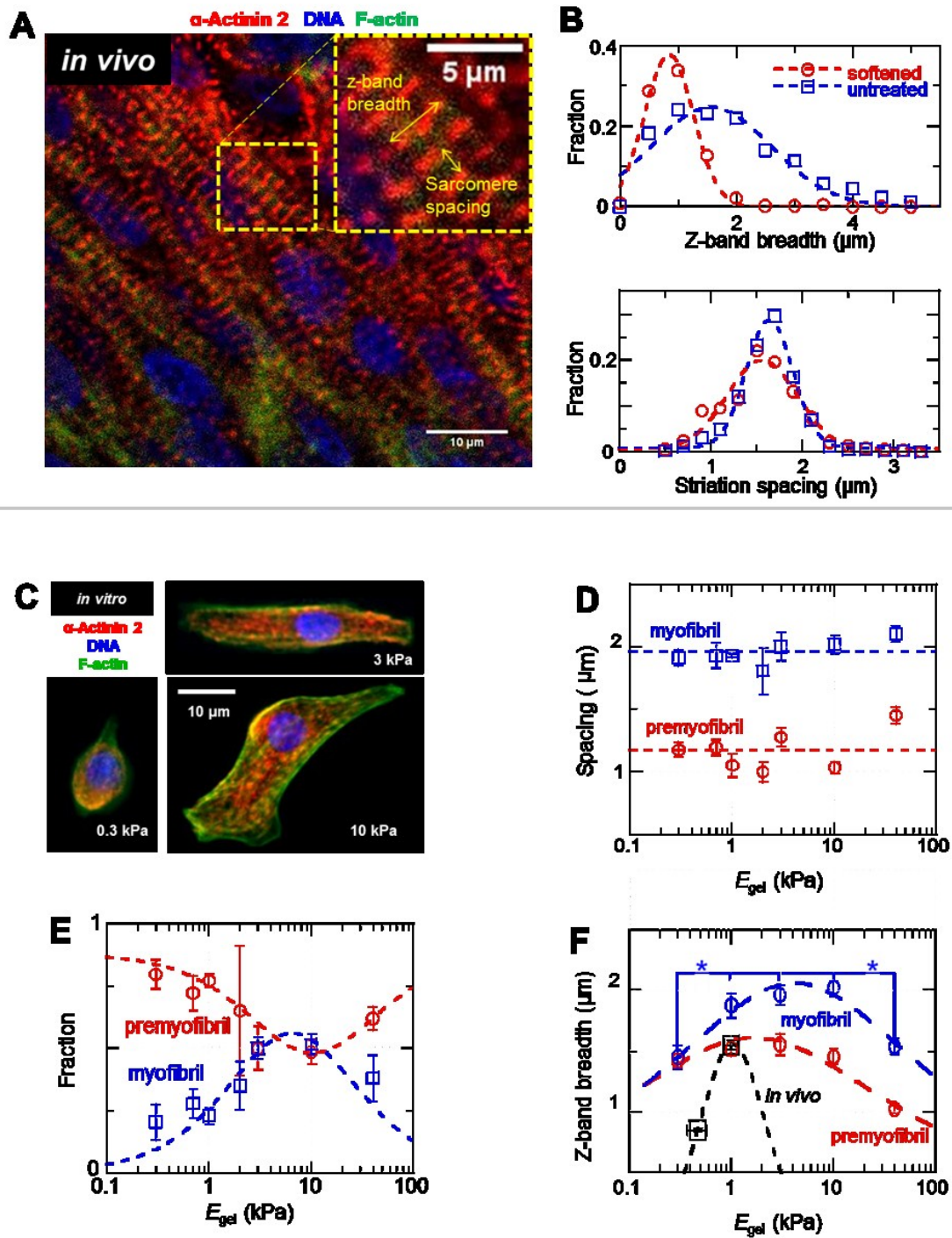
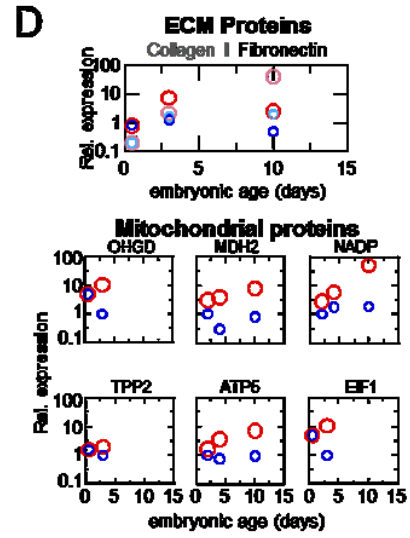
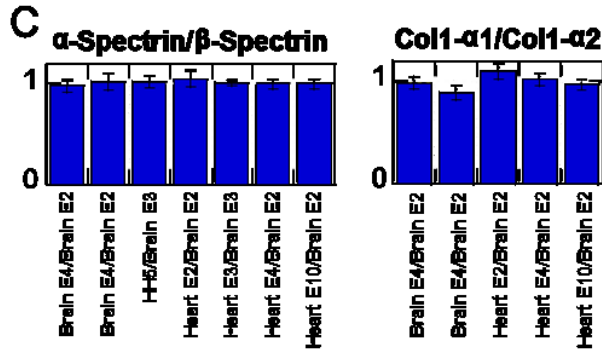
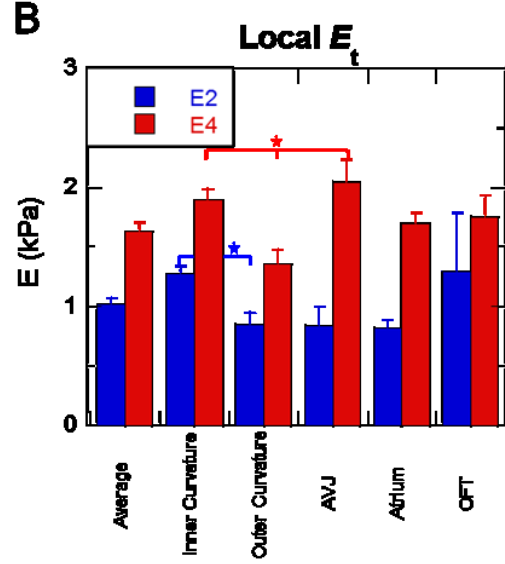
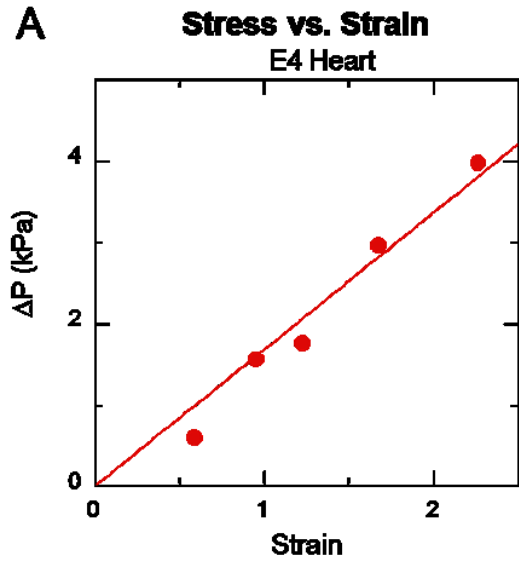


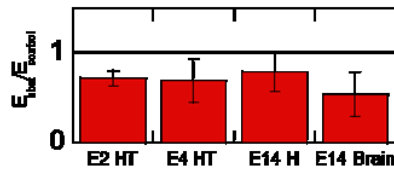
**Figure 2-4: Sarcomere breadth changes in softened heart and in isolated cardiomyocytes on compliant substrates.** (A) Untreated and softened whole E4 hearts were immunostained for sarcomeric  $\alpha$ -actinin-2, F-actin, and DNA and imaged by confocal microscopy. Sarcomere spacing and Z-disc breadth (inset) were measured to assess any structural changes. (B) Z-disc breadth is significantly decreased in the 47%-softened heart relative to untreated controls. The

decreased registry of myofibrils suggests a decreased coupling between adjacent myofibrils during contraction. Sarcomere spacing is consistent with mature myofibril sarcomere spacing and is not significantly different in the softened and untreated hearts. (C) E4 cardiomyocytes cultured on gels were stained in the same way as the whole hearts of figure A. Figure shows typical E4 cardiomyocytes on gels with stiffnesses of 0.3, 3.0 and 10 kPa. (D) Striation spacing was bimodal in distribution, indicating mature myofibrils (sarcomere spacing  $> 1.8 \mu\text{m}$ ) as well as pre-myofibrils (sarcomere spacing  $< 1.4 \mu\text{m}$ ). (E) Fraction of each type of striation per cell with myofibrils maximal on gels where pre-myofibrils are minimal. We fit the fraction of myofibrils with  $f_m = f$  (Eq. 1), (blue dashed line) and pre-myofibrils with  $f_p = 1 - f_m$ , finding  $E_m = 9 \pm 2 \text{ kPa}$ . (F) Z-disc breadth for myofibrils and pre-myofibrils were maximized on substrates of intermediate stiffness. The fits to Eq. 1 yield  $E_m = 1.7 \pm 0.3 \text{ kPa}$  for pre-myofibrils and  $E_m = 4.2 \pm 0.6 \text{ kPa}$  for myofibrils. Error bars are SEM ( $n \geq 3$  hearts or cells)





**E Myosin contractility contributes to stiffness in embryonic heart (~25%) and brain (~50%)**



**F Collagenase softens only heart (~40%)**

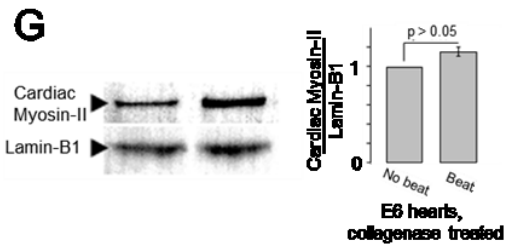
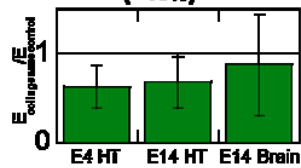


**Figure 2-S1: Anatomically distinct mechanics of embryonic tissue can be softened differentially by disrupting cytoskeleton or collagenous matrix.** (A) Example Stress/Strain curve of an E4 Heart Tube ventricle. From Eq. 1,  $E_t = 1.7 \pm 0.1$  kPa. (B) Anatomical differences in  $E_t$  are measured along the E2-E4 heart tubes that reflect functional developmental changes (AVJ = atrioventricular junction, OFT = outflow tract). (C) As a check for the protein quantification, we compared the relative amounts of  $\alpha$  and  $\beta$  Spectrins and Col Ia1 and Ia2. Since these spectrins and collagens should normally be found at ratios of 1:1 and 2:1, respectively, their normalized abundances should be equal across all samples, which is what we find. (D) Of the two ECM proteins identified, Collagen-I and Fibronectin, only Collagen follows the trends of the tissue mechanics. Several mitochondrial proteins were also identified to follow the trends of the tissue mechanics, but generally not as strongly and at a lower abundance than the excitation-contraction coupling proteins discussed in the text. (E) Treatment of E2, E4 and E14 heart and E14 brain (5 measurements each of  $n = 4, 4, 2, 2$ , respectively) with blebbistatin softens the tissues significantly, allowing us to estimate of the contribution of actomyosin contractile forces to tissue mechanics (~25% for heart and ~50% for brain). (F) Treatment of E4 and E14 heart and E14 brain (5 measurements each of  $n = 4, 2, 3$ , respectively) with collagenase shows that a significant softening of the heart tissue (~40%), but no softening of the brain tissue. Due to the thick epicardial layer of E4 heart, the softening of myocardium due to collagenase is likely underestimated. (G) Immunoblot of E6 hearts treated for 50 min with collagenase that had stopped beating ( $n = 3$ ) and continued beating ( $n = 2$ ) shows no significant difference in myosin expression. Error bars are  $\pm$  SEM ( $n \geq 3$  unless indicated).

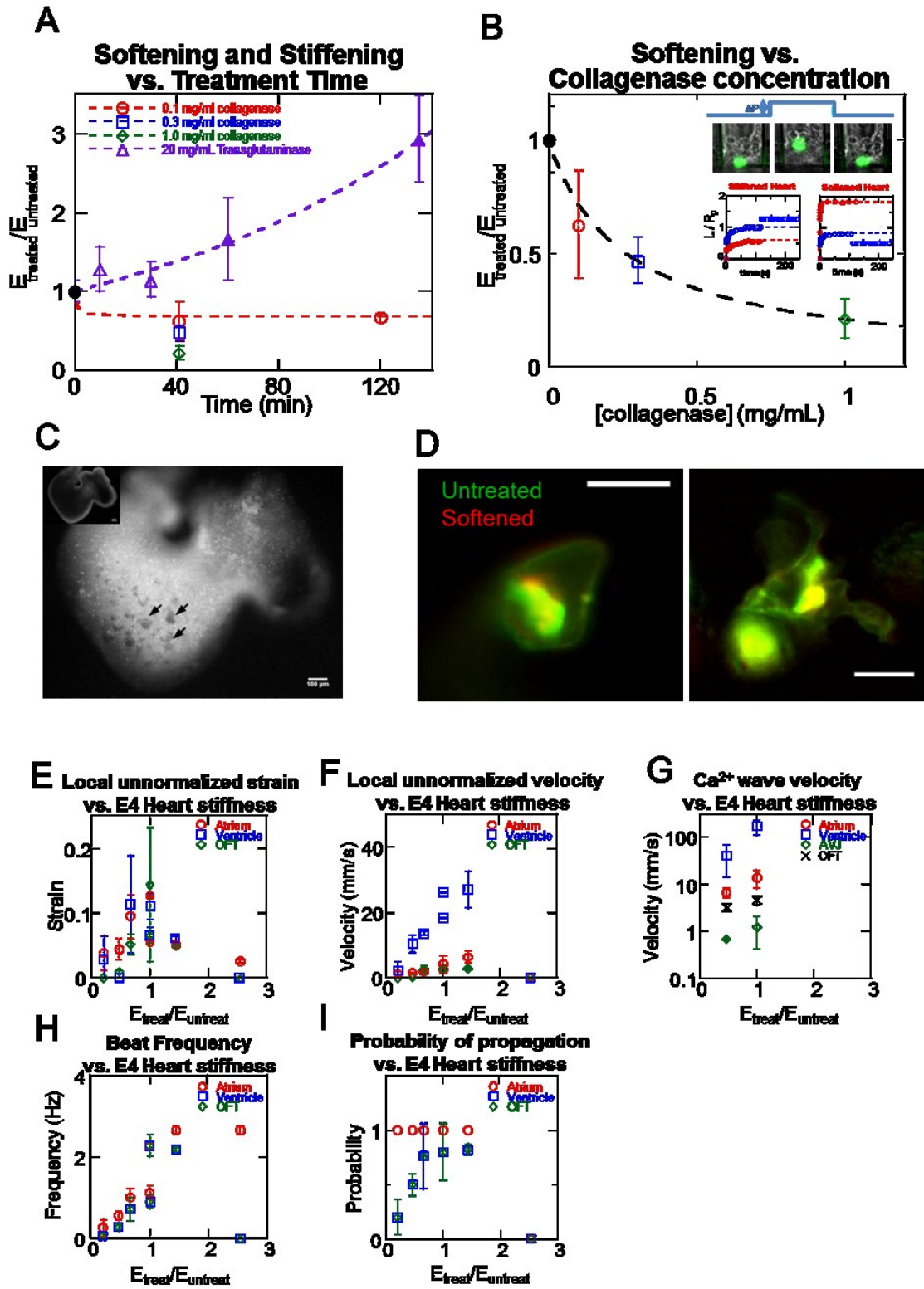


**Figure 2-S2: Effects of dose-dependent stiffening and softening of E4 embryonic cardiac tissue by transglutaminase and collagenase on intact tissue structure and function** (A) Change in tissue stiffness as a function of treatment time with 20 mg/mL transglutaminase (purple triangles, filled triangles represent the intermediate and extreme stiffening treatments used in the strain and velocity measurements) and different concentrations of collagenase (red circles 0.1 mg/mL, blue squares 0.3 mg/mL, green diamonds 1.0 mg/mL). Treatment with transglutaminase leads to stiffening whereas collagenase treatment softens the tissue. (B) Softening of tissue as a function of collagenase concentration for 30 min treatments. We assume the collagenase acts with Michaelis-Menten kinetics, so fit the data with  $\frac{E_{\text{treated}}}{E_{\text{untreated}}} = \frac{a}{b + [\text{collagenase}]}$ , finding  $a = 0.26 \pm 0.08$  mg/ml and  $b = 0.27 \pm 0.1$  mg/ml. Inset shows aspiration and relaxation of a 0.1 ml/mg collagenase softened E4 HT tissue including a GFP-expressing cell, demonstrating that individual cells return to their original shape and position upon relaxation from applied strain. Also in inset are sample aspiration curves for tissues before (blue) and after (red) softening and stiffening. (C) After 30 min, fluorescently labeled collagenase perfusion of an E4 HT shows that the tissue is fully perfused with the enzyme. Black arrows indicate possible trabeculae. (D) Overlays of SIRPA-GFP expression by transfected cells in beating E4 HTs before (green) and after (red) collagenase treatment show that treatment does not significantly alter cell membrane contour and thus likely does not significantly interfere with cell adhesions. (E) Un-normalized strain and (F) velocity measured from analysis of fluorescent imaging of GFP-transfected heart tubes that have been softened or stiffened. (G) Ca<sup>2+</sup> wave velocity in untreated and softened heart tubes. The Ca<sup>2+</sup> imaging allowed for more precise localization of the Ca<sup>2+</sup> wave than the strain wave, so the atrioventricular junction (AVJ) could be differentiated from the atrium and ventricle. The strain wave velocity measurements across the atrium and ventricle were made from the initiation of contraction to the AVJ and then from the AVJ to points in the presumptive right ventricle, respectively. Therefore the strain wave atrium and ventricle include time from the AVJ and so are measured to be slower than the Ca<sup>2+</sup> wave. The Ca<sup>2+</sup> wave is coincident with the initiation of contraction in the heart, and therefore shows the same trends in velocity as the strain wave with softening. (H) Beat frequency in each chamber decreases with softening and does not significantly change with stiffening, except in the stiffest condition in which the contraction wave does not propagate past the atrium. (I) Similarly, probability of contraction propagating decreases with softening but does not significantly change with slight stiffening and drops to zero in the extreme stiffening condition

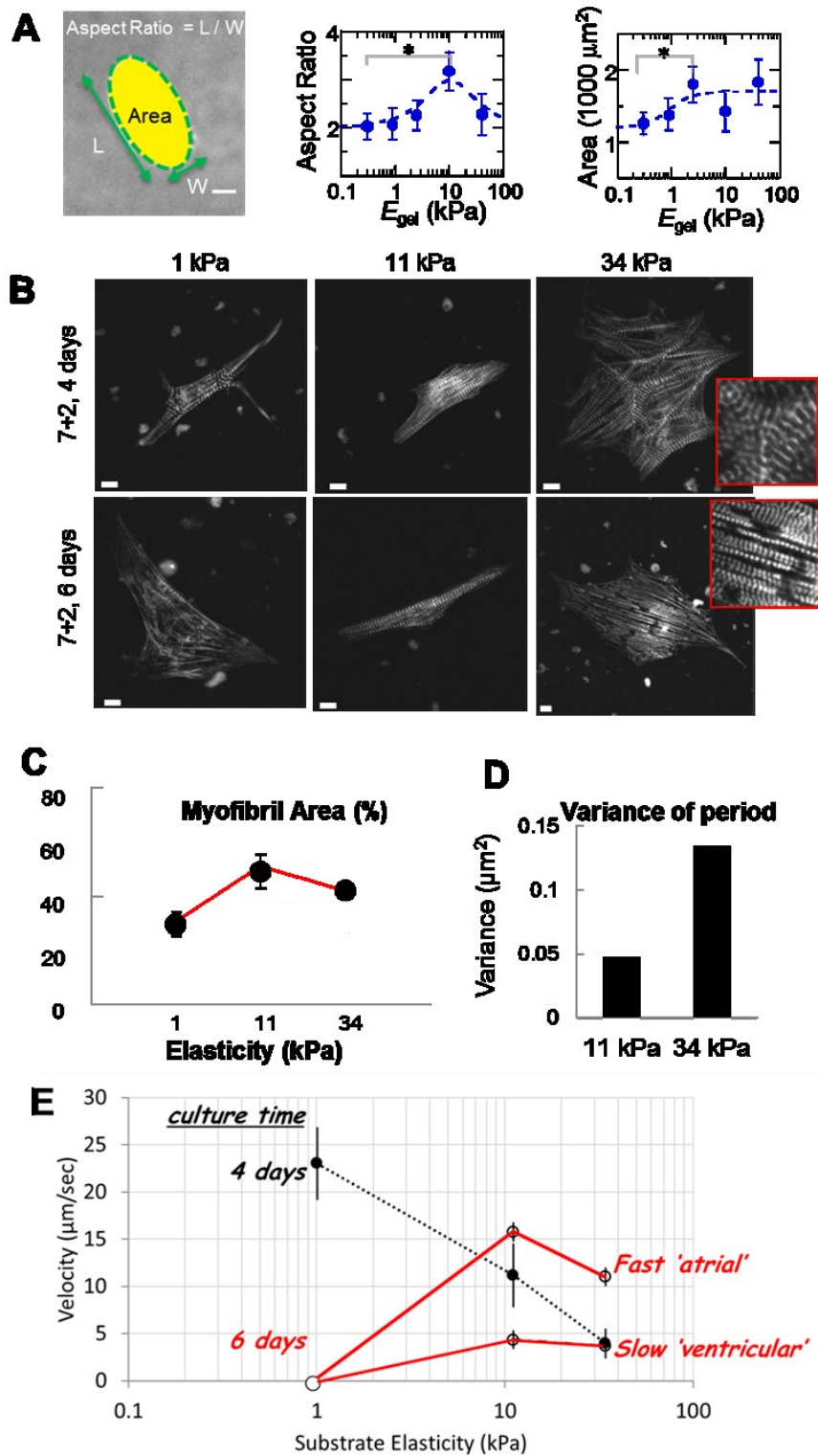


Figure 2-S3: Changes in E4 cardiomyocyte aspect ratio and area during contraction are optimized by intermediate substrate stiffness (A) Cell aspect ratio and area, schematized at

left, are significantly modulated by substrate elasticity. The peak in cell aspect ratio fits a Lorentzian (see Box 1) peaked at  $E_m = 10 \pm 4$  kPa, whereas cell area fits a generalized Hill equation with a mid-point of  $2 \pm 1$  kPa. (B) Representative images of ESC-CM stained for  $\alpha$ -actinin to visualize z-discs after being cultured on soft, intermediate, and stiff substrates for 4 days. (D,E,F) Representative image of ESC-CM after 6 days cultured on elastic substrates. Defects reminiscent of disclinations and dislocations in liquid crystals (upper inset) and cracks (lower inset) arise in the myofibril organization of ESC-CM cultured on stiff substrates. (C) Mature myofibril content quantified by % of total cell area is maximized on intermediate stiffness substrates after 4 days in culture. Myofibril content decreases further in cells grown on soft substrates and is maintained in intermediate to stiff substrates (data not shown). (D) Mature myofibril spacing of cells cultured on stiff substrates shows increased variance relative to that of cells grown on intermediate substrates. (E) Edge velocities of spontaneously beating ESC-CM cultured for 4 and 6 days on soft, intermediate, and stiff substrates. After just 4 days, edge velocity decreases with increasing stiffness, reflecting the increased load that the beating cell feels on different substrates. After 6 days, ESC-CM stop beating on the softest substrates, and two populations can be seen on the intermediate and stiff substrates, indicating possible further differentiation into fast-contracting "atrial" type cells and slow-contracting "ventricular" type cells

Name (Gene)	Brain E10/ Brain E2	Brain E4/ Brain E2	Emb Disc/ Brain E3	Heart E2/ Brain E2	Heart E3/ Brain3	Heart E4/ Brain E2	Heart E10/ Brain E2
Vitellogen II (VTGII)	-1.22	-0.13	5.36	2.92	2.84	0.16	-0.93
Vitellogen I (VTGI)	-0.69	0.07	5.57	2.96	2.8	0.27	-0.54
Apolipoprotein B (APOB)	-0.7	0.19	4.5	3.14	2.66	0.56	-0.23
Ovalbumin (SERPINB14)	-1.22	0.68		3.13		1.32	-0.78
Titin isoform N2-A (TTN)	0.49	1.22	2.95	2.56	3.75		2.38
Ovotransferrin (TFEW)	0.42	0.96		3.32		1.43	0.95
Fibronectin (FN)	1.67	2.32	1.89	2.9	3.04	2.7	2.4
T-complex protein 1 subunit epsilon (CCT5)	1.93	2.26		2.54		2.47	2.2
Paranemin	1.78	2.37	1.07	2.74	2.66	2.63	2.58
Spectrin alpha chain, brain (SPTA), Nonerythroid alpha-spectrin fragment overlap	2.28	2.25	2.25	2.47	2.58	2.53	2.87
Spectrin alpha chain, brain (SPTA)	2.36	2.09	2.27	2.3	2.56	2.46	2.77
Spectrin beta chain, brain 1 (SPTBN1)	2.32	2.12	2.22	2.19	2.53	2.47	2.76
Lamin B2 (LMNB2)	2.25	2.29		2.12		2.19	2.78
Creatine kinase B-type (CKB)	2.25	2.54		1.94		2.26	2.57
Talin (TLN)	2.18	2.34	1.87	2.28	2.63	2.59	2.84
Vimentin (VIM)	2.07	2.62		2.36		2.51	2.82
Eukaryotic translation elongation factor 1	2.05	2.4		2.28		2.31	2.49
SMARCA4 (BRG1)			2.05		1.84		
Heterogeneous nuclear ribonucleoprotein R (HNRNPR)	1.93	2.63		2.31		2.46	2.43
Malate dehydrogenase, cytoplasmic (MDH1)		2.48				2.7	3.08
Aspartate aminotransferase, mitochondrial (GOT2)	1.81	2.3		2.17		2.68	3.05
Smooth muscle gamma actin; alpha skeletal muscle; aortic smooth muscle; alpha cardiac muscle 1 [overlap]	0.75	1.42		2.81		2.52	3.25
Ubiquitin carboxyl-terminal hydrolase 10 (USP10)			1.72				

Succinyl-CoA:3-ketoacid-coenzyme A transferase 1, mitochondrial (OXCT1)	2.57			2.74		2.51	3.92
Nuclear pore complex protein Nup205 (NUP205)			2.56				
Albumin (ALB)	2.59	2.25		3.84		2.53	2.93
Collagen alpha-2(I) chain (COL1A2)	2.49	2.59		2.24			3.68
CCR4-NOT transcription complex subunit 1 (CNOT1)			1.82		1.75		
Sterol O-acyltransferase 1 (ACAT1)	2.4	2.52		2.33		2.92	3.55
Isocitrate dehydrogenase [NADP]	2.26	2.3		2.46		2.78	3.72
Collagen alpha-1(I) chain (COL1A1)	2.22	2.56	1.44	2.46	2.74		3.58
SERCA2 (ATP2A2)	2.57	2.32	2.62	2.58	3.33	2.89	2.97
Alpha actinin-1/2/4 (ACTN-1/2/4)	1.5	1.83	2.53	2.47	3.66	2.23	2.61
Sodium/potassium-transporting ATPase subunit alpha-1 (ATP1A1)	1.66		3.2	2.16	3.06	2.39	2.69
Radixin (RDX)	1.68	2.23		2.27		2.47	2.54
Glyceraldehyde-3-phosphate dehydrogenase (GAPDH)	1.86			2.31		2.5	2.57
ATP synthase subunit alpha (ATP5A1)	1.87			2.2		2.55	2.85
Similar to Cytoskeleton-associated protein 5 (CKAP5)	1.84		1.89	2.37		2.61	2.76
Malate dehydrogenase (MDH2)	1.48	1.91		2.49		2.61	2.89
ATP synthase subunit beta, mitochondrial (ATP5B)	1.48			2.38		2.6	3.02
CFR-associated protein p70	1.29			1.86		2.67	2.81
Prohibitin-2 (PHB2)	1.44	1.54		2.1		2.36	
Voltage-dependent anion-selective channel protein 2 (VDAC2)	1.72	1.63		2.12		2.52	2.28
T-complex protein 1 subunit alpha (CCT1)	1.73	2.3		1.84			2.18



similar to chaperonin-containing TCP-1 complex gamma (CCT3)	1.55	2.29				2.11	2.17
Transcriptional coactivator p100			2.3		2.41		
Peptidyl-prolyl cis-trans isomerase (FKBP4)	1.45	2.33		2.09		1.74	2.24
Spliceosome RNA helicase (DDX39B)	1.52	2.14		1.56			2.16
Calreticulin (CALR)	1.48			2.33		2.26	2.42
26S proteasome non-ATPase regulatory subunit 12 (PSMD12)	1.49	2.22		1.94		2.38	2.34
SMARCA5 (SMARCA5)			2.43		1.87		
Nucleoporin 133 kPa (NUP133)			2.52		1.34		
Fructose-bisphosphate aldolase C (ALDOC)	1.74	2.07		2.03		2.28	2.31
T-complex protein 1 subunit beta (CCT2)	1.47	2.05				2.14	2.07
Ribosomal protein L4 (RPL4)	1.27	2.15		2.1		2.16	2.26
60 kDa heat shock protein, mitochondrial (HSPD1)	1.12	1.7				2.19	2.11
Protein disulfide-isomerase (P4HB)	0.99	1.85					2.39
Probable global transcription activator SNF2L2 (SMARCA2)			2.31		1.77		
Stress-70 protein, mitochondrial (HSPA9)	0.83	1.87		1.59		2.1	2.23
Vinculin (VCL)	0.96	1.78	2.26	2.11	2.92		2.16
Microtubule-actin cross-linking factor 1 (MACF1)	2.5	1.25	1.59	2.7	1.82	1.61	1.19
Nuclease-sensitive element-binding protein 1 (YBX1)	2.1	1.15		2.1		1.66	1.61
Neurocan core protein (NCAN)	2.43	1.43		2.25		1.51	1.22
Similar to Transcription elongation regulator 1 protein (TCERG1)			1.73		1.74		
High molecular mass nuclear antigen			1.76		1.33		
Lamin-B1 (LMNB1)	2.17	1.42				1.6	1.18

SMC2 cohesin complex subunit (SMC2)			1.73		1.54		
Microtubule-associated protein (MAP2)	2.5	1.26		2.16		1.04	1.37
Heat shock protein HSP 90-alpha (HSP90AA1)	1.82	1.11		2.34		1.61	1.08
Microtubule-associated protein (MAPT)	3.39	1.37				1.91	1.61
Claustrin, MAP1B [overlap]	3.02	1.73	0.95	2.37	1.28		1.44
Microtubule-associated protein 1B (MAP1B)	2.83	1.86	0.99	2.58	1.24	1.84	1.46
Collapsin response mediator protein-1A (CRMP1A)	2.76	2.42		2.96			2.22
Cytoplasmic dynein (DYN1)	3.05	2.25	1.61	2.8	1.9	2.33	2.18
Tubulin beta-4 chain	3.09	2.42		2.77		2.38	
Neural cell adhesion molecule 1 (NCAM1)	2.89		1.31	2.59	2.49	2.27	2.2
Nuclear autoantigenic sperm protein (NASP)	0.63	1.7	2.52	1.7	1.92	1.26	0.93
Splicing factor 3b, subunit 3, 130kDa (SF3B3)	0.75	1.7	2.34	1.76	2.16	1.26	0.9
Filamin	1.08	1.67	1.64	1.69	2.09	1.29	1.45
Eukaryotic translation initiation factor 4 gamma 1 (EIF4G1)	1.2	1.74	1.59	1.8	2.27	1.66	1.37
60S acidic ribosomal protein P0 (RPLP0)	1.29	1.54		1.92		1.65	1.56
Elongation factor 1-alpha 1 (EEF1A)	0.77	1.86		1.71		2.03	1.69
ATP-dependent RNA helicase (DDX3X)	0.8	1.65		1.59		2.05	1.6
Nuclear calmodulin-binding protein (URP)			2.21		2.05		
Pyruvate kinase muscle isozyme (PKM2)	0.78	1.65		1.78		1.94	1.71
Alpha-enolase (ENO1)	0.99	1.68		1.57		1.85	1.67
Splicing factor 3A subunit 1 (SF3A1)			1.85				
Insulin-like growth factor 2 mRNA-binding protein 3 (IGF2BP3)	1.05	2.18		1.37		1.63	1.77
Phosphoglycerate kinase (PGK)	1.3			1.51			

Leucine-rich PPR motif-containing protein (LRPPRC)	1.29	1.77	2.83	1.56	2.33	1.71	
Heterogeneous nuclear ribonucleoprotein H1-like protein	1.14	1.81		1.76		1.81	1.88
SERPINE1 mRNA binding protein 1 (SERBP1)	1.05	1.78		1.71			
40S ribosomal protein SA (RPSA)	1.23	1.77		1.92		1.92	1.92
Nucleophosmin (NPM1)	0.3	1.59		1.89		1.8	1.49
DNA topoisomerase 2-beta (TOP2B)	2.34	2.11	1.21	2.3	1.81	1.79	1.84
Dynactin subunit 1 (DCTN1)	2.35	1.78	1.1	1.74	1.77	1.71	1.83
Collapsin response mediator protein-4B (CRMP4B)	2.95	1.55		2.5			
UDP-glucose:glycoprotein glucosyltransferase 1 (UGGT1)			2.74		2.32		
Tenascin (TNC)	2.61	1.59		2.63		1.74	1.35
Catenin alpha-2 (CTNNA2)	2.25			2.78		1.93	
SMC1 protein cohesin subunit (SMC1)					1.7		
Doublecortin (DCX)	2.68	1.73		2.2		1.64	1.52
Eukaryotic translation initiation factor 5B (EIF5B)					1.91		
Sister chromatid cohesion protein PDS5 homolog B (PDS5B)			1.75		1.67		
Myristoylated alanine-rich C-kinase substrate (MARCKS)	3.03					1.84	1.75
Heterogeneous nuclear ribonucleoprotein A3 (HNRPA3)	2.65					1.97	1.91
cardiac and cytoplasmic actin [overlap]	2.61	1.68		2.14		2.26	2.41
Hexokinase 1 (HK)	2.24	1.71		2.24		2.47	2.62
Exportin-5 (XPO5)			1.9		1.81		

Mitochondrial ubiquinol-cytochrome-c reductase complex core protein 2 (QCR2)	2.25	1.77				2.57	3.02
Nucleolin (NCL)			2.61		1.33		
Guanine nucleotide-binding protein G(I)/G(S)/G(T) subunit beta-3 (GNB3)	2.31	1.8		2.19		2.37	2.37
Reticulon-4 isoform A2 (NOGO)	2.37	2.21	1.53	1.86	2.27	2.27	2.15
Heterogeneous nuclear ribonucleoproteins A2/B1 (HNRNPA2B1)	2.39	2.19				2.2	2.22
Rab GDP dissociation inhibitor (GDI)	2.38	2.18		2.15			
Desmoplakin (DSP)			3.25		3.7		
AP-2 complex subunit alpha-2 (AP2A2)	2.36	2.35		2.21		2.12	2.35
Septin-7 (SEPT7)	2.11	2.12		2.15		1.92	2.36
Neuron-glia cell adhesion molecule (Ng-CAM)	2.1	1.81		2.15		2.1	2.14
SMC3 cohesin complex subunit (SMC3)					1.76		
Tubulin beta-2 chain		2.1		2.17		2.05	2.26
Protein disulfide-isomerase A3 (PDIA3)	2.16	2.19				2.05	2.48
Serine/arginine-rich splicing factor 1 (SRSF1)	2.05	2.23		1.69		1.9	2.12
AP-2 complex subunit beta (AP2B1)	2.18	2.14		1.81		2.15	2.15
2-oxoglutarate dehydrogenase, mitochondrial (OGHD)			2.7		3.02		
T-complex protein 1 subunit theta (CCT8)		2.21		1.84		2.11	2.16
Tubulin beta (TUBB)							
Tubulin alpha-1 chain (TUB1)		1.85				1.95	1.86

Thyroid hormone receptor associated protein 3 (THRAP3)			1.17		1.69		
26S proteasome non-ATPase regulatory subunit 2 (PSMD2)		2.21		1.93		1.93	1.76
78 kDa glucose-regulated protein (HSPA5)							2.23
Kinectin (KTN1)	2.27	2.17	2.82	1.92			2.11
Dihydropyrimidinase-related protein 2 (DPYSL2)	2.46	2.1		1.93		1.93	2.12
T-complex protein 1 subunit zeta (CCT6)	2.15	1.74		1.73		2.18	2.22
Heterogeneous nuclear ribonucleoprotein K (HNRNPK)	2.17	2.25		1.7		2.13	1.95
Kinesin-1 heavy chain (KIF5B)	2.43	2.16		1.43	2.15	2.14	1.91
Similar to scaffold attachment factor B (SAFB)		2.21	2.25	1.57	1.77	1.71	1.64
Coatomer subunit beta (COPB1)				1.46		1.88	1.79
GTP-binding nuclear protein Ran (RAN)			2.46		1.66		
Golgi apparatus protein 1 (GLG1)	2.12	2.28	2.38	1.55	1.84	1.91	1.77
Similar to Splicing factor Prp8 (PRPF8)	1.91	1.95	2.25	1.78	1.93	1.59	1.6
U5 small nuclear ribonucleoprotein 200 kDa helicase (SNRNP200)	1.91	1.93	2.23	2.11	1.92	1.56	1.81
T-complex protein 1 subunit eta (CCT7)	2.05	1.89		2.03		1.62	
Nonmuscle myosin heavy chain	1.72	1.92	1.92	1.71	1.94	1.77	1.92
Nonmuscle myosin heavy chain, Myosin-9 [overlap]	1.73	1.84	2.14	1.97	1.95	1.77	1.87
T-complex protein 1 subunit delta (CCT4)	1.59	1.72		1.85		1.91	1.8
Similar to THO complex 2 (THOC2)					1.81		

60S ribosomal protein L6 (RPL6)	1.55	1.59		1.45			1.68
Heterogeneous nuclear ribonucleoprotein H3 (HNRNPH3)	1.71	1.49		1.79		1.88	1.37
Nonmuscle myosin heavy chain / MYH9/11 [overlap]	1.55		2.36	1.85	2.15	1.72	1.85
Cullin-associated NEDD8-dissociated protein 1 (CAND1)	1.85		2.2	1.76		1.83	1.7
Eukaryotic initiation factor 4A-II (EIF4A2)	1.89			1.71		1.93	1.84
Similar to isoleucyl-tRNA synthetase (IARS)			2.42		2.2		
Fascin 1 (FSCN1)	1.84	1.93		1.72		1.9	1.68
Similar to Tripeptidyl peptidase 2 (TPP2)			2.18		2.29		
Protein SET (SET)	1.62			1.69		1.82	1.93
Similar to nuclear poly(C)-binding protein	1.83	2.18		1.74		1.74	1.8
Filamin B (FLNB)			2.92		2.11		
DEAD-box RNA helicase	1.59	2.3		1.73		1.81	1.84
Coatomer subunit alpha (COP1)	1.89		2.35	1.8	2.03	1.87	
Non-muscle myosin heavy chain IIa (MYH9)	1.4	1.84	2.36	2.12	2.12	1.65	
Heterogeneous nuclear ribonucleoprotein A3 (HNRNPA3)	1.41	1.82		2.24		1.76	1.53
Nonmuscle myosin heavy chain / MYH11 [overlap]	1.5	1.88		1.94		1.69	1.7
Vigilin (HDLBP)			1.87		2.16		
C-1-tetrahydrofolate synthase, cytoplasmic (MTHFD1)	1.5	1.93		1.79		1.57	1.25
Heterogeneous nuclear ribonucleoprotein U (HNRNPU)	1.5	1.93	2.15	1.71		1.59	1.49
Bifunctional aminoacyl-tRNA synthetase (EPRS)	1.44	1.79	2.22	1.56	2.2	1.66	1.62

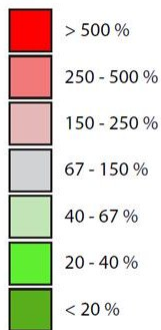
Alpha-centractin (ACTR1A)	1.83	1.73				2.18
Heat shock protein 70kDa (HSPA8)	1.58	1.91			1.84	
Alpha-actinin-4 (ACTN4)	1.68	1.91	2.51	2.19	2.95	1.84
26S proteasome non-ATPase regulatory subunit 1 (PSMD1)	1.74		2.24	1.93	2.54	1.84
Gizzard PTB-associated splicing factor	1.86			2.31		1.89
Exportin-1 (XPO1)			1.95	2.12	2.36	1.81
Leucyl-tRNA synthetase (LARS)	2.07	2.09	2.47		2.34	1.85
Heat shock 70 kDa protein 4 (HSPA4)	1.86		2.52	1.8	2.41	1.73
Putative Alanyl-tRNA synthetase, cytoplasmic (ARS)	1.95	2.22	1.71	1.76	2.19	1.92
Heat shock protein 4-like (HSPA4L)	1.95		1.26	1.76	2.41	1.78
Clathrin heavy-chain (CHC)	1.62	1.74	3.21		2.28	1.56
Actin, cytoplasmic (ACTG1)	2.14	1.54		1.52		1.61
Hypoxia up-regulated protein 1 (HYOU1)	2.1	1.79	2.49	1.93	2.05	1.68
Tubulin-specific chaperone D	2.13	1.89	2.66	2.17	2.17	1.41
Ran GTP binding protein 5	1.37	1.92	2.24	1.76	1.79	1.43
Similar to Nucleoprotein TPR (TPR)	1.42	1.87	2.12	1.49	1.66	1.42
Eukaryotic translation initiation factor 3 subunit A (EIF3A)	1.35	1.85		1.48	1.75	1.47
116 kDa U5 small nuclear ribonucleoprotein component (EFTUD2)	1.46	1.87	2.48	1.6	2.12	1.45
Exportin-2 (CSE1L)	1.48	1.82		1.55		1.47
Nucleoporin 155 kPa (NUP155)			2.75		1.91	
Transketolase (TKT)	1.72			1.63		1.39

Similar to RanBP7/importin 7 (IPO7)	1.48	1.85	2.3	1.42	1.47	1.27
Ubiquitin carboxyl-terminal hydrolase 7 (USP7)	1.75	1.75	2.39	1.39	1.55	1.51
Eukaryotic translation initiation factor 3 subunit B (EIF3B)	1.34		2.64	1.52	2.42	1.59
L-lactate dehydrogenase B chain (LDHB)	1.45	1.14		1.28		1.87
Heat shock protein 105 (HSPH1)	1.64			2.2	2.14	1.51
ATP-citrate lyase (ACLY)	1.88		1.75	1.69	1.93	1.46
Poly [ADP-ribose] polymerase 1 (PARP1)	1.63		1.77	1.38		1.4
Nuclear protein matrix 3 (MATR3)	1.74	1.93	1.57	1.74	1.79	1.54
Splicing factor 3B subunit 1 (SF3B1)	1.55	1.91	1.8	1.9	1.61	1.42
Heat shock cognate protein HSP 90-beta (HSP90AB1)	1.72	0.62		1.77		1.04
Serine/arginine repetitive matrix protein 1 (SRRM1)			0.77		1.87	
Fatty acid synthase Isoform 1 (FASN)	1.44	1.85	1.33	1.92	1.27	1.07
Myosin heavy chain, Chick atrial myosin heavy chain, Cardiac muscle myosin, Skeletal myosin heavy chain [overlap]	0.81	1.8	3.49	3.46	5	3.26
Similar to alpha-NAC, muscle-specific form	0.79	1.33	3.47	3.18	5.22	3.28
Myosin-3, Skeletal myosin heavy chain [overlap]	1.25	1.65	2.97	3.17	4.27	3.16
Alpha actinin-2 (ACTN-2)	1.39	1.74	2.82	2.94	4.4	2.84
Myosin heavy chain, Chick atrial myosin heavy chain [overlap]	1.22	1.71	2.91	2.73	4.29	3.07
Myosin-binding protein C, cardiac-type (MYBPC3)	1.74	1.81	2.46	3.08	3.99	3.21
Chick atrial myosin heavy chain	1.37	1.8	2.7	2.89	4.19	3.32



Annexin A6 (ANXA6)	1.57	1.81		2.6		3.38	3.91
Pan-muscle filamin isoform (CgABP260)	1.46	1.77	2.82	2.47	4.36	3.41	3.7
Myosin heavy chain, Chick atrial myosin heavy chain, Myosin-3, Cardiac muscle myosin, Skeletal myosin heavy chain [overlap]	0.86	1.6	2.84	3.08	4.14	3.43	3.69
Myosin heavy chain, Cardiac muscle myosin [overlap]	1.16	1.86	2.78	3.37	4.52	3.26	3.72
Myosin heavy chain	1.27		2.34	3.32	4.66	3.34	3.81
Smooth muscle gamma actin; alpha skeletal muscle; aortic smooth muscle; alpha cardiac muscle 1 [overlap]	1.73	1.79		4.01		4.32	4.47
Myosin heavy chain, Chick atrial myosin heavy chain, Myosin-3, Skeletal myosin heavy chain [overlap]	1.54	2.09	2.44	3.49	4.09	3.68	4.1
Xin actin-binding protein (XIRP1)	1.83	2.22	2.74	3.89	3.66	3.29	3.36

**Table 2-S1: Mass-Spec of early and late embryonic brain and heart tissue** Heat map of all identified proteins from two experiments: E2, E4, and E10 Heart and Brain tissue normalized to E2 Brain, and HH3-5 embryonic disc and E3 heart and brain normalized to E3 Brain. Proteins are clustered by the Manhattan Distance algorithm. Grey cells indicate undetected proteins for that experiment. The following is the heat-map key:



## Chapter 3: On the interplay between Cardiomyocytes and Collagen-secreting Cardiac Fibroblasts in the developing heart

*Requested Perspective: Majkut SF, Dingal D, Discher DE. (2014) Current Biology: Special issue on stress in development.*

*Initial model development by Dave Dingal.*

### 3-1: Introduction

Development of tissue with mechanical function could be based entirely on pre-programmed expression profiles, or perhaps there exist important feedback loops that involve sensing tissue mechanics. Heart is the first organ to form, and recent studies document a stiffness that changes daily but matches the contractile optimum of the cardiomyocytes at each stage [60]. The dynamically evolving balance between cardiomyocyte contractile ability and matrix stiffness paralleled daily increases in the levels of excitation-contraction proteins and collagen-I relative to protein mass. Cardiomyocytes express key excitation-contraction proteins but do not make matrix [61], while cardiac fibroblasts are distinctly specialized and secrete collagen-I and other matrix proteins but do not express muscle contractility proteins. Thus this contraction-matrix balance must be met by a balance of cardiomyocyte and fibroblast populations (**Fig. 3-1A**). Here we summarize current descriptions of fibroblast and cardiomyocyte population dynamics during development, and then a reasonably simple mathematical model is introduced to formally address how such a functional balance could be achieved between the two cell types during development. Structural proteins in the nucleus called lamins also change dramatically in normal

development, and recent studies that revealed lamins to be mechanoresponsive and to directly regulate cytoskeleton expression motivate an extension of our first matrix-myosin model to the nuclear lamins. The models presented may provide insight into some of the human genes most often linked to dilated cardiac myopathies, namely lamin-A and the myosin-II motors [62].

### **3-2: Cardiac fibroblast and collagen content during development:**

Cardiac fibroblasts (CF) are mesenchymal cells that arise primarily from the proepicardial region of the developing heart tube [63]. They are the primary extracellular matrix (ECM)-producing cells in the heart [61], but they also play significant roles in electrochemical and mechanical signaling in normal and injured developing and aging hearts [64]. In injuries such as infarcts in which cardiomyocytes die, CF's rapidly proliferate and contribute to a collagen-rich scar at the site of injury, while adult cardiomyocytes do not proliferate but do grow in size (hypertrophy) seemingly in an effort to contract the scarred tissue [65, 66].

Until recently, quantifying the CF population has been difficult due to a lack of reliable markers [67]. Discoidin Domain Receptor 2 (DDR2), periostontin, cadherin-11 in combination with common fibroblast-associated proteins such as vimentin and fibronectin have recently been used as CF markers and have allowed for more precise studies of when and where CF arise in the heart and how this cell population develops [68, 69, 70, 71]. However, quantitative studies of cellular population by numbers or volume fraction in tissue have thus far focused on late-embryonic to adult and aging hearts in various organisms [68, 72]. Relative fibroblast populations in adult hearts across species are typically attributed to requirements of increased collagen needed to withstand greater pressures in larger organisms, for example [73, 68, 74, 63]. Similarly, increased collagen and fibroblast population are associated with periods of significant growth and postnatal developmental events that involve stiffening [75, 68, 76] Pathological

stiffening in response to disease or injury is also associated with increased collagen and local fibroblast population [77, 78, 79].

There is limited information on cardiac fibroblasts in the early embryonic heart; however, collagen content across species and through development has been measured for decades [74]. Recent proteomic measurements of heart and brain during embryonic chick development show that this increase in matrix is matched by contractile proteins and parallel increased tissue mechanics (**Fig. 3-1B**). By the time the heart tube first begins beating, the cellular make-up is thought to be fairly homogenous and primarily composed of early cardiomyocytes [80]. DDR2 is not expressed until well into embryonic development, so there is still no good marker for the earliest CFs. Therefore, how the cellular makeup from the early heart tube evolves to the make-up of adult tissue is not clear, but they must increase to relatively stable levels in adulthood. (**Fig. 3-1C**).

Several studies have demonstrated cultured cardiac fibroblast functional mechanosensitivity to a variety of stimuli. Static or cyclic, uniaxial or biaxial strain has been shown to modulate ECM production by fibroblasts in a strain-dependent manner, with moderate strain inducing ECM production and large strain decreasing ECM production [81]. In vivo, such responses are likely complicated by mechanically stimulated paracrine signaling molecules that are also known to influence ECM production and proliferation rates of cardiac fibroblasts [82].

### **3-3: Systems biology in cardiac physiology and development**

To address these the problem of how these complicated mechanical and chemical effects ultimately affect fibroblast proliferation and collagen deposition and the associated increase in contractile capacity of the myocardium requires an integrative analysis of the known contributory factors. Thus a systems biology approach in which the relevant gene message and protein dynamics are integrated into an appropriate model that captures the relevant ECM and contractile protein behavior could prove extremely useful.

Systems biology approaches in cardiac physiology and pathophysiology have the potential to help build an integrated understanding of the electrophysiological and physical processes involved in cardiac function [83, 84]. Eventually, models developed using systems biology could even allow for identification of therapeutic drug targets [85, 86].

Fully understanding the details of how the balance of mechanical stiffness and contractile ability of myocardium is struck and changes with age and pathology ultimately requires a systems model that explicitly includes the various components of the developing heart ECM and cytoskeleton as well as any other functionally relevant signaling proteins integrated with a realistic physical model of the associated mechanics. However, as myocardial stiffening is paralleled by primarily actomyosin contractility proteins and collagen I out of hundreds of the most abundant proteins [87](**Fig. 3-1B**), we can initially consider a simplified system focusing on the interaction between the mechanical contribution of collagenous ECM deposited by cardiac fibroblasts and contractile cardiomyocytes. Furthermore, a recent study simultaneously measuring the production and degradation of mRNAs and proteins in NIH3T3 mouse fibroblasts showed that the half-lives of are fairly constant within functional groups suggesting similar dynamics within groups [88]. Therefore we could further simplify this system to consider the Collagen-I as a representative of the matrix proteins and Myosin-II as a representative of the contractile-related proteins of the myocardium.

Several studies have demonstrated functional mechanosensitivity of cultured cardiac fibroblast to a variety of stimuli. Static or cyclic, uniaxial or biaxial strain has been shown to modulate ECM production by fibroblasts in a strain-dependent manner, with moderate strain inducing ECM production and large strain decreasing ECM production [81]. In vivo, such responses are likely complicated by mechanically stimulated paracrine signaling molecules that are also known to influence ECM production and proliferation rates of cardiac fibroblasts [82].

### 3-4: Model for Mechanical coupling between Collagen and Myosin production

Since both static and cyclic strain encourage collagen production by cardiac fibroblasts, and both passive and active contraction increases in heart tissue through embryonic development, what is the mechanism that ultimately creates the balance between cardiac fibroblasts and cardiomyocytes? As contractility, and therefore myosin expression must always effectively strain the heart tissue, we consider the case that fibroblast proliferation is ultimately limited by the stiffness or crowdedness of their environment.

To explore possible general mechanisms, we considered a coupled rate equation between the relative concentrations of myosin and collagen mRNAs and proteins within developing cardiac and brain tissue. We hypothesize that since collagen is produced primarily by cardiac fibroblasts, the rate of collagen mRNA production is proportional to the fibroblast population, which is limited by the stiffness, or crowdedness of their environment. Since cardiomyocytes contain such high levels of contractile proteins, we consider them as the primary contributors of myosin in developing cardiac tissue. We start with simple coupled rate equations for collagen and myosin mRNA and protein [89]:

$$\frac{dC_m}{dt} = \tilde{a} - bC_m$$

$$\frac{dC_p}{dt} = gC_m - \tilde{h}C_p$$

$$\frac{dM_m}{dt} = jM_p - qM_m$$

$$\frac{dM_p}{dt} = rM_m - \tilde{s}M_p$$

Where  $C_p$  is collagen concentration,  $C_m$  is collagen mRNA concentration,  $M_p$  is myosin concentration,  $M_m$  is myosin mRNA concentration,  $g$  and  $r$  are translation rate coefficients, and  $b$  and  $q$  are mRNA degradation rate constants. mRNA production is proportional to protein level relative to cardiac cell concentration, with production rate coefficient  $j$  for myosin and  $\tilde{a}$  for collagen that is proportional to relative fibroblast proliferation rate. As cardiac fibroblasts are embedded in the interstitial ECM between myocardial layers, we expect fibroblast proliferation to be limited by the density of this network in some way. Confinement and stiffness in 2D culture has been demonstrated to affect fibroblast proliferation, and evidence is accumulating that fibroblasts from various origins cultured in 3D matrices proliferate less in stiffer environments [90]. We therefore choose  $\tilde{a}$  proportional to a CF population constrained by collagen content to have the form

$$\tilde{a} = a \frac{C_p^z}{a_0^z + C_p^z}$$

where  $z$  is a Hill coefficient. Protein degradation rates for collagen and myosin,  $\tilde{h}$  and  $\tilde{s}$ , respectively are tension dependent coefficients of the form:

$$\tilde{h} = h \frac{C_p^{A1-1}}{K^{A1} + C_p^{A1}}, \quad \tilde{s} = s \frac{M_p^{A2-1}}{k^{A2} + M_p^{A2}}$$

Where  $K = M_p^{x/A1}$  and  $k = C_p^{y/A2}$  are affinity constants for collagen proteases and myosin heavy-chain kinases that are proportional to stiffness contributions due to myosin contraction and collagenous matrix, respectively. Thus the degradation terms of collagen and myosin are Hill-type equations where the typical association-dissociation constant is proportional to  $K$ , a power of tension applied by active myosin contraction in the case of collagen, or to  $k$ , in response to ECM mechanics in the case of myosin. Collagen matrices have been shown to be stabilized from degradation by applied tension [91, 92] and myosin-IIs under tension can be preferentially un-

phosphorylated leading to increased incorporation into stress-fibers [93]. The mechanism for tension-stabilization for these polymers is not known, but Swift et al. (2013) argue that tension may cause changes of the network or polymers itself that sterically or conformationally prevent direct protease binding, in the case of collagen, or kinase binding that leads to dissociation and digestion, in the case of polymeric myosins [89]. The universality of stress stabilization against degradation by all proteases is not yet clear, and some evidence to the contrary exists from single-molecule studies of collagen [94]. However such studies are not inconsistent with the idea that a stressed network could be stabilized against degradation as proposed because, whereas in single molecule studies, the fibers could unwind, networked polymers under stress typically could not and stress may therefore lead to further tightening of coils and knots. Table 1. gives all parameters used. All linear coefficients, namely  $a$ ,  $b$ ,  $g$ ,  $h$ ,  $j$ ,  $q$ ,  $r$ , and  $s$  are of order  $\sim 1$  for both the heart indicating that protein and mRNA production and degradation are occurring on similar scales. In the case of the brain, the myosin protein production rate  $j$  is decreased relative to that of the heart giving the decreasing myosin trends over time and lower final collagen levels.

By extending simple coupled regulatory gene network to include mechanically regulated protein degradation and constrained fibroblast proliferation, we can qualitatively reconstitute our measurements of relative myosin and collagen content in the developing heart (model results in **Fig. 3-2** compared to measurements in **Fig. 3-1B**). In particular, collagen and myosin increase over days to reach stable steady-state values in the heart. By decreasing the rate of myosin production in brain,  $r$ , the brain myosin decreases to a steady low value while the collagen level increases only slightly to a value lower than the heart. This model is underconstrained by data, but it opens the door to avenues of inquiry that are important to address. For instance, growing evidence of biopolymer networks stabilized by tension suggests that this may be a generalizable biological phenomenon. The functional form may be complicated by e.g. mechanosensitive modulation of proteolytic enzymes or the polymer itself, but the Hill-type equation we propose here seems a sensible place to start.



### **3-5: From ECM to the nucleus**

So far, we have considered the interplay between extracellular matrix mechanics and cellular contractile capacity. Implicit in this interplay is communication of extracellular and intracellular mechanics with the translational machinery of the nucleus. Mechanosensitivity at the cell-ECM or cell-cell interface has been shown to contribute to biochemical signaling pathways that lead to changes in activity in the nucleus [95]. But mechanical signals from the extracellular environment can also be transmitted physically by the contractile cytoskeleton to the nucleus via connections through the nuclear membrane to the nuclear lamina [96]. The nuclear lamina is composed of a meshwork of filamentous proteins that confer mechanical stability to the nucleus and interact with chromatin and various proteins that regulate transcription. These proteins, Lamins, constitute a group of class V intermediate filaments found in all metazoans. In vertebrates, typically two types of Lamins, A and B, are expressed in tissue-specific ratios, with at least one Lamin B-type protein expressed ubiquitously. Of particular interest here, Swift et al. recently found that Lamin A:Lamin B ratio in adult tissues scales with tissue stiffness, and also enhances mechanically directed differentiation [89]. Thus not only do cardiomyocyte contractility and extracellular matrix during development feedback into each other, nuclear lamina structure and composition is in turn involved with this mechanical coupling.

### **3-6: Lamins in development**

Lamin expression has been shown to be both developmentally regulated and to play a role in tissue-specific maturation and differentiation. Developmental studies in mice [97], xenopus [98] and chickens [99] show that Lamin A is typically expressed first in muscle and not until late embryogenesis or shortly after birth, and continues to increase into adulthood. Quantitative measurements by Lehner et al (1987) in developing chick embryos demonstrated differential expression of Lamin B2, B1 and A in various tissues (**Fig. 3-3**, data from [99]). As far as we know, these are the only such measurements throughout early embryonic development in chickens. Lamin B2 was constitutively expressed at stable levels, but Lamin B1 and Lamin A

were variably expressed in tissues through time. Fig. 3-3 presents Lamin levels in heart and brain during chick development [99]. In brain, the total Lamin A and B1 normalized by Lamin B2 remained relatively constant (**Fig. 3-3A**). This total amount is dominated by Lamin B1 throughout the development and aging. Although the ratio of Lamin A to Lamin B2 was negligible before E10, it then increases to a non-negligible level into adulthood. In heart, measurements were not made during early embryogenesis. However, by late embryogenesis and into adulthood, Lamin A is the major variable isoform and constitutes much more of the heart cell nuclear lamina than in the brain.

### **3-7: Lamin A in cardiac development and disease**

In a general review of genetic mechanisms underlying dilated cardiac myopathy (DCM), mutations in the LMNA, the gene responsible for Lamin A/C, were identified among a list of the most common mutations associated with DCM and conduction system disorders [62]. A genetic study of families with autosomal dominant DCM and conduction-system disease have been shown to be caused by Lamin A/C defects in the coiled rod-domain and c-terminal domain [100]. How these mutations and defective Lamin expression results in impaired cardiac contraction and conduction is intimately related to the roles different types of Lamins play in healthy tissue development and adult function. LMNA gene defects account for 33% of DCM with atrioventricular block, a common conduction disorder [101]. In a later broader study of unrelated patients with DCM, LMNA mutations occurred in 6% of patients [102]. In these studies, no or mild serum creatine-phosphatase were measured, which is typically associated with muscular dystrophies or general muscle tissue damage. Instead, they saw damaged myocyte nuclei, which they hypothesize could lead to myocyte death and that accumulates over time, leading to DCM and conduction-disease phenotypes [101]. This type of cell death and tissue malfunction could also be caused by mislocalization of associated muscle specific genes [103] due to altered nuclear mechanics. In addition, altered lamin-A/C assembly and interaction with another nuclear protein, emerin, could lead to defective regulation of nuclear actin. This in turn would affect

nuclear-cytoplasmic shuttling of MKL1, a critical transcription factor to cardiac development and function [104] . Thus proper Lamin-A expression in developing and mature cardiac tissue is critical to tissue maintenance from a structural to transcriptional level.

### 3-8: Model of Lamin levels in response to Myosin:

We propose a model of coupled myosin and Lamin-A expression in cardiomyocytes much like the coupled myosin-collagen model. Here we start with simple regulatory equations and include tension-stabilized degradation of both Lamin and Myosin proteins, as before.

$$\frac{dL_m}{dt} = aL_p - bL_m$$

$$\frac{dL_p}{dt} = gL_m - \tilde{h}L_p$$

$$\frac{dM_m}{dt} = jM_p - qM_m$$

$$\frac{dM_p}{dt} = rM_m - \tilde{s}M_p$$

Where  $a, b, g, j, q,$  and  $r$  are rate constants and  $\tilde{h}$  and  $\tilde{s}$  are tension-stabilizing degradation coefficients

$$\tilde{h} = h \frac{L_p^{A1-1}}{K^{A1} + C_p^{A1}}, \quad \tilde{s} = s \frac{M_p^{A2-1}}{k^{A2} + M_p^{A2}}$$

Once again  $K = M_p^{x/A1}$  and  $k$  are affinity constants for lamin kinases and myosin heavy-chain kinases that are proportional to stiffness contributions due to myosin contraction and collagenous

matrix, respectively. **Table 2.** gives all parameters used. Unlike the myosin-collagen model, the lamin and myosin are produced by the same cell, so relative cell concentrations do not need to be taken into account. Like myosins, Lamins are thought to dissociate from their meshwork and get degraded when phosphorylated, but whether stress influences phosphorylation and degradation is understudied. We consider the steady-state solutions as a function of explicitly input  $k$  (**Fig. 3-4**). Steady-state Lamin A and myosin protein levels,  $L_{ss}$  and  $M_{ss}$ , respectively, follows a linear relation with explicit  $k$  input. Here we use the relation between relative Lamin A levels and tissue stiffness reported by Swift et al. (2013) [89],  $L_{ss} \sim E^{0.7}$  to infer a relation  $L_{ss} \sim k^{3.15} \sim E^{3.15 \cdot y}$ ,  $k \sim E^{0.22}$ . This in turn gives the relation between myosin levels and matrix stiffness  $M_{ss} \sim E^{0.46}$ . Ultimately, with more measurements of Lamin levels in developing chick tissue, this type of coupled modeling could be extended to include coupling of ECM to cytoskeleton to nucleus.

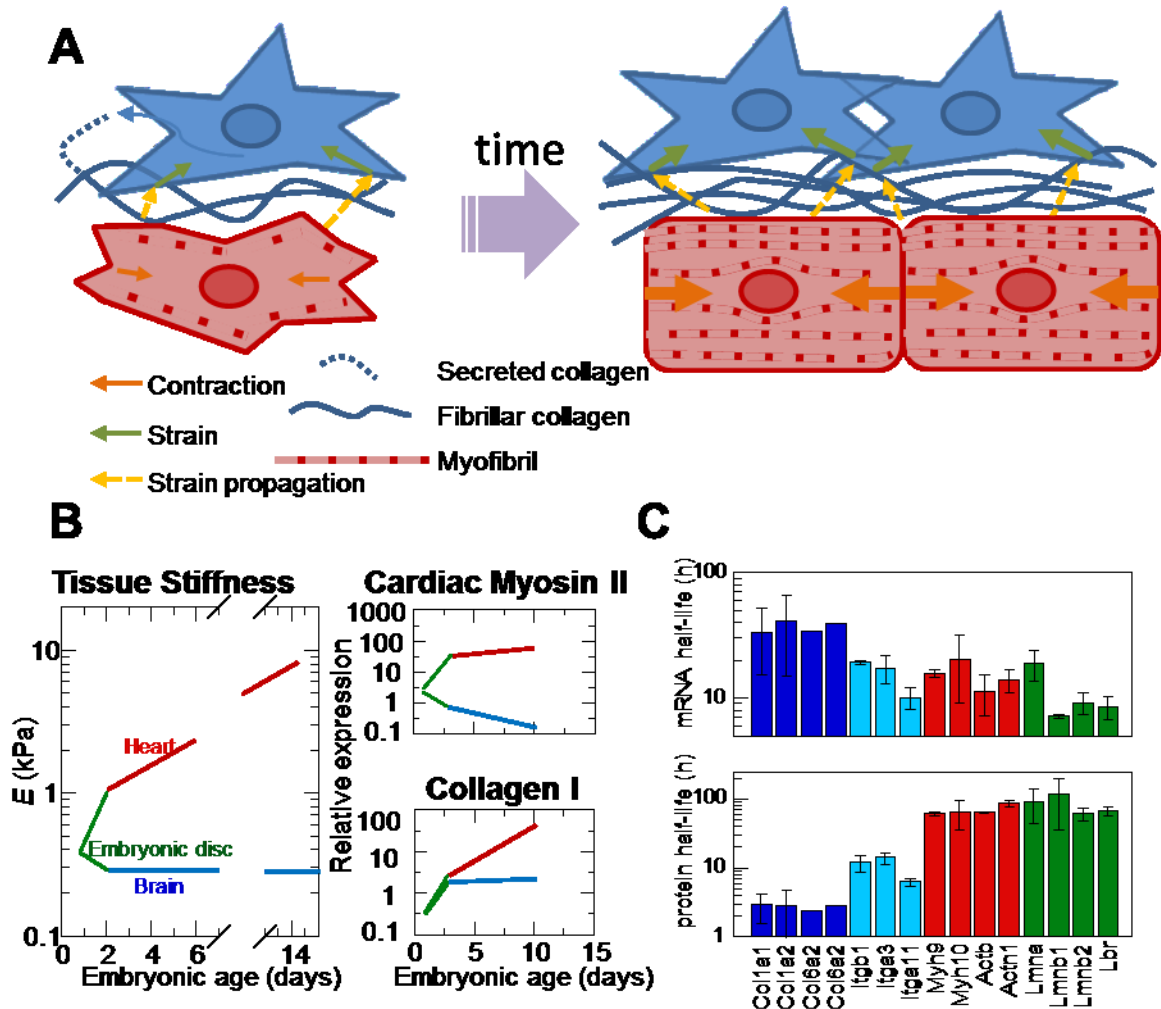
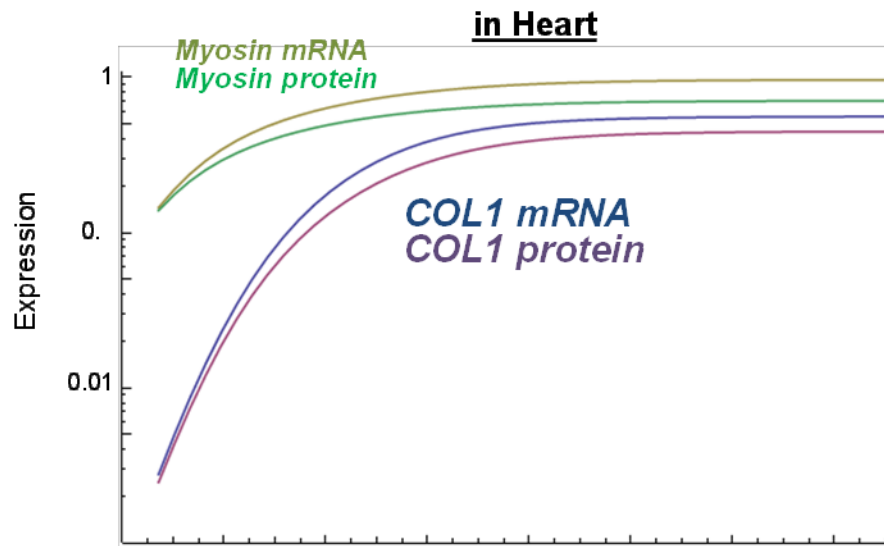


**Figure 3-1: Cardiomyocyte and Fibroblasts create a balance between contractile ability and ECM abundance during development (A)** Schema illustrating concept of how such a balance could be struck. Early in development, cardiomyocytes are relatively small with unorganized and relatively sparse myofibril content. Cardiac fibroblasts feel strain from passive and active contraction of surrounding cells (orange arrows) propagated through the ECM and cell-cell adhesions (yellow arrows) prompting them to divide and produce ECM in a strain and growth-factor responsive manner. The increased ECM due to increased CF population prompts increased production of myofibril proteins and encourages myofibril organization, which in turn increases contractile strain on the cardiac fibroblasts. We propose that fibroblast population growth is at least in part limited by stiffness and confinement, leading to an ultimate steady state of CM to FB volume fractions in normal adult tissue. **(B)** Tissue stiffness of embryonic chick heart and brain tissue was measured to increase throughout embryonic development in a way that is paralleled with both collagen-I and cardiac Myosin-II expression. **(C)** Half-lives of collagens (dark blue) and collagen-binding integrins (light blue), actomyosin contractility (red), and nuclear Lamin mRNAs and proteins measured coincidentally in NIH3T3 mouse fibroblasts. Half-lives of are fairly constant within functional groups suggesting similar dynamics within groups.

## Dynamic Myosin and Collagen I Protein and mRNA Expression

**A**



**B**

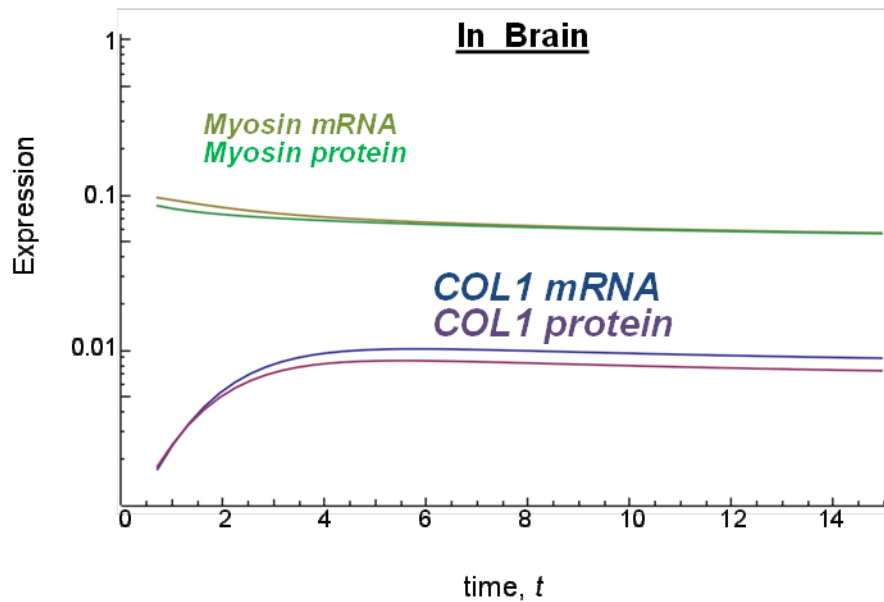


**Figure 3-2: Model Collagen-I and Myosin mRNA and Protein expression during development** Results from our coupled models of tissue-level concentrations of cardiac myosin II, primarily located within cardiomyocytes, and collagen-I, located extracellularly and produced primarily by cardiac fibroblasts, qualitatively recapitulate the trends we see in developing heart (A) and brain (B) tissue.

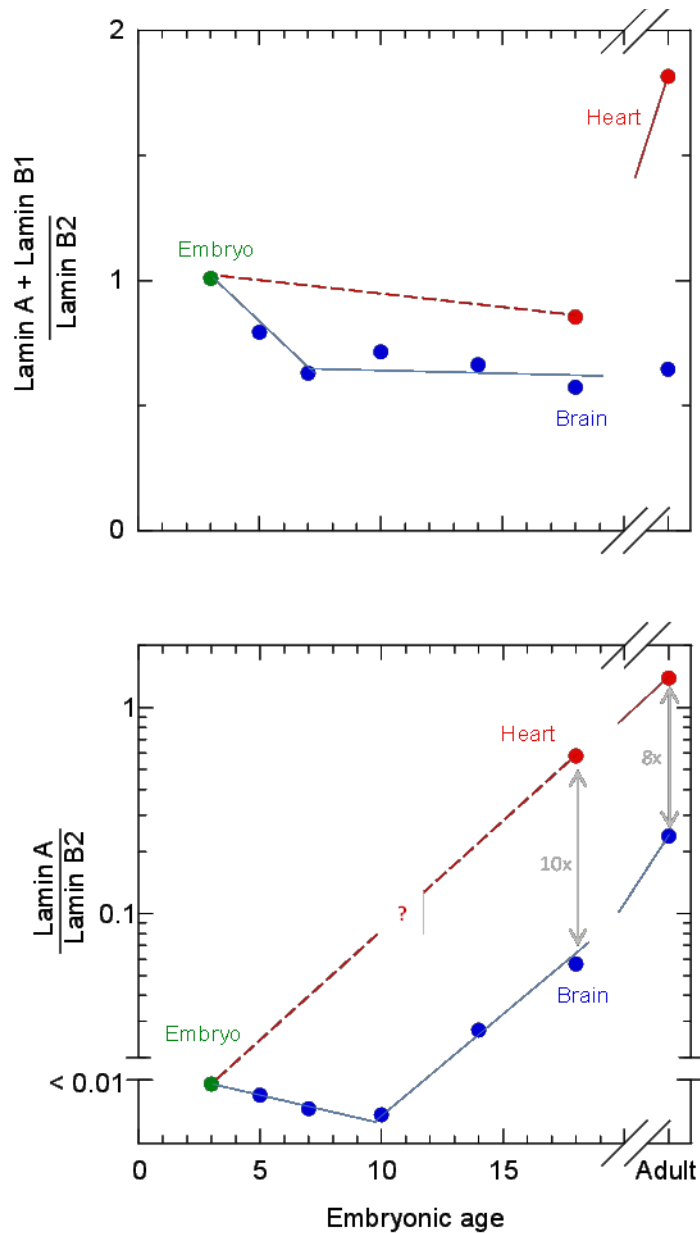


**Figure 3-3: Lamin levels in heart and brain during development** (adapted from Lehner et al. 1987). (A) Total variable Lamins A and B1 normalized by constant Lamin B2 in brain (blue) and heart (red). In brain, this total remained relatively constant; in heart, this total increases from late embryogenesis to adult levels. (B) This total amount is dominated by lamin B1 throughout the development and aging, although while the ratio of Lamin A was negligible before E10, it then increases to a non-negligible level adulthood, while it . In heart, measurements are more sparse and missing during early embryogenesis. However, by late embryogenesis and into adulthood, Lamin A is the major variable isoform and constitutes much more of the heart cell nuclear lamina than in the brain.

### Substrate Stiffness influence on Myosin and Lamin A Protein and mRNA Expression

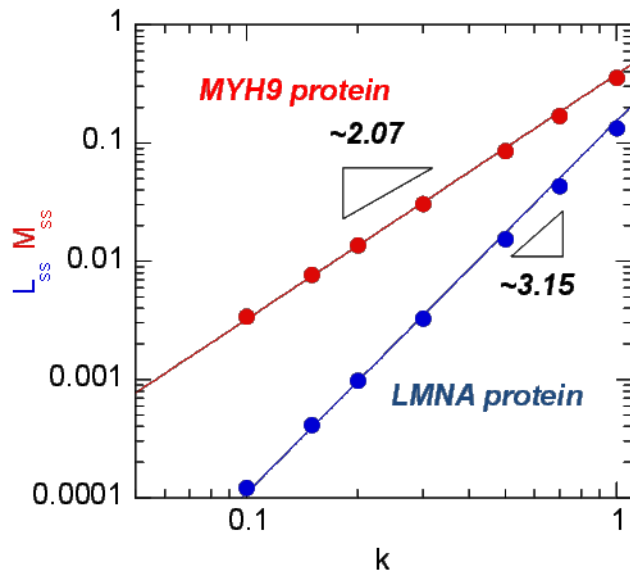


**Figure 3-4: Steady-state Lamin and Myosin levels given matrix elasticity** Steady-state Lamin A and myosin protein levels given explicit  $k$  input. Here we use the relation between relative Lamin A levels and tissue stiffness reported by Swift et al. (2013) [89],  $L_{ss} \sim E^{0.7}$  to infer a relation between  $k \sim E^{0.45}$ .



Constant	Heart	Brain
Rate constants		
a	6.2	6.2
b	5	5
g	3	3
h	6	6
j	4.1	4.1
q	3	3
r	1.3	0.005
s	4	4
Coupling constants		
z	0.99	0.99
$a_0$	0.9	0.9
A1	1.4	1.4
A2	3	3
Initial conditions		
$C_m(0)$	0.0006	0.0006
$C_p(0)$	0.0006	0.0006
$M_m(0)$	0.07	0.07
$M_p(0)$	0.07	0.07

**Table 3-1:Rate constants and coupling constants for Collagen-myosin coupled model**

Constant	
Rate constants	
a	1
b	2
g	3
h	4
j	3
q	2
r	1
s	4
Coupling constants	
z	3
A1	3
A2	3
Initial conditions	
Lm(0)	0.0006
Lp(0)	0.0006
Mm(0)	0.07
Mp(0)	0.07

**Table 3-2:Rate constants and coupling constants for Lamin-myosin coupled model**

## **CHAPTER 4: Method to visualize and study embryonic cardiomyocyte nuclei and Lamins in vitro and in vivo.**

### **4-1: Introduction**

The previous chapter argues that the nuclear lamina is influential in the mechanical regulation of cardiomyocyte function. Here we outline a method to image and manipulate the nuclear lamina of live beating embryonic cardiomyocytes in tissue and in culture.

### **4-2: Methods**

#### ***Chick culture and heart extraction***

Fertilized White Horn chicken premium eggs (Charles Rivers Labs) were incubated at 37°C in a humid incubator with low CO<sub>2</sub> with broad end up and rotated 180° once each day until the desired embryonic stage is reached. To extract E4 HTs, eggs are windowed on the broad end to expose the embryo, overlying membranes are removed, and the embryo is released from the extraembryonic tissue with fine forceps and gently lifted out of the egg and placed in room temperature PBS. The HT is

#### ***Whole tissue transfection***

Lipofectamine/plasmid complexes were prepared as prescribed by the manufacturers (Lipofectamine 2000, Invitrogen) and illustrated in **Fig. 4-2A**. For a single well of a 12-well dish, 15 micrograms of plasmid GFP-Lamin-A and 10 µL Lipofectamine were each diluted to total volumes of 50 µL in Opti-MEM (Gibco, 31985-070) and stayed at room temperature for 5 min before combining both solutions to make the final transfection solution which again sat at room temperature for an additional 25 min. 2-4 HTs per well were preincubated in 0.5 mL pre-warmed chick heart media during lipofectamine/plasmid complex formation. The lipofectamine/plasmid complex was added to the heart tubes in heart media and left to incubate at 37°C 5% CO<sub>2</sub> for 12-18 hours. Transfection media was replaced with prewarmed chick heart media and the heart

tubes continued incubating until use in stiffening or softening experiments and subsequent imaging.

### ***Cell isolation and culture on elastic substrates***

We isolated cells from heart tissue by dicing to sub-millimeter size and then digesting with Trypsin/EDTA (Gibco, 25200-072). We incubated tissue in approximately 1 mL Trypsin per E4 HT in a 15 mL conical tube for 13 min rotating on its side at 37°C, then for 2 min upright to let large tissue pieces settle before carefully removing supernatant which should contain blood cells, being careful not to disturb the settled tissue. We replacing with an equal volume of fresh Trypsin, and finally shaking for 15 more min. We stop digestion by adding an equal volume of chick heart media and release the cells from the tissue by pipetting up and down slowly (~2 mL/s) with a 5 mL glass pipette 5-8 times. Large pieces were then allowed to settle and the supernatant is plated on prepared PA gels. Cells were plated at concentrations of approximately  $2 \times 10^5$  cells/cm directly on collagen I coated PA gels of varying stiffness as described in Chapter 3.

### ***Imaging and analysis of cellular and nuclear strain***

Cardiomyocytes beating on PA gels were imaged after 24 hours in culture. Hoechst staining (1:1000, 33342 Sigma) on some non-transfected samples was performed for 10 minutes at room temperature, followed by 3x rinse with heart media to visualize nuclei, but they quickly stopped beating upon fluorescent imaging. Cells were imaged on an Olympus 1x81 microscope and recorded with a ccd camera with fluorescent and phase-contrast filters. Phase-contrast movies (23 fps) of beating cardiomyocytes with Hoescht-stained or GFP-Lamin A positive nuclei, as well as fluorescent movies of the nuclei (17 fps) were segmented using a Matlab program as described in Chapter 3 and the cell aspect ratio (AR) was tracked over time.  $(AR_{\text{relaxed}} - AR_{\text{contracted}})/AR_{\text{relaxed}}$  was calculated as a measure of cell and nuclear strain for at least 4 beats for each cell.

### 4-3: Results and Discussion

E4 cardiomyocyte contraction significantly deforms the nucleus (**Fig. 4-1A**). Live-cell imaging of Hoescht-stained nuclei in beating cardiomyocytes on 1 kPa PA gels shows significant deformation of both cell and nucleus (**Fig. 4-1B**).

Whole heart transfections with GFP-Lamin A (**Fig. 4-2A**) results in sparse cell transfections such that number of cells transfected increases in a dose-dependent manner with plasmid concentration (**Fig. 4-2B**). This allows for imaging of transfected nuclei in intact beating tissue, which could then be manipulated as described previously, e.g. collagenase or transglutaminase softening or stiffening of the collagenous ECM.

We isolated cells from transfected heart tubes and cultured them on collagen-coated PA gels of 1, 10, and 34 kPa for 24 hours. It should be noted that although although measurements of relative Lamin expression in the literature is missing at this early developmental stage, we can extrapolate from Fig 4-3 that it is low. Therefore transfected cells are necessarily perturbed both in that Lamin A transfection should stiffen the nucleus and possibly feed into increased myosin expression. 12-18 hours transfection and 24 hours in culture gives significant time for changes in gene expression in response to the transfection.

Preliminary results for nuclear deformation relative to cellular deformation for cells on gels agree with our naïve expectations for cells on rigid to very soft substrates (**Fig. 4-3**). Cells on rigid substrates (e.g. glass) should not be able to contract the substrate, and therefore should have not edge deformation. However, cardiomyocytes have been shown to beat on glass, so the nucleus should still respond to intracellular stresses. We find that for well-beating cells, cell strain and nuclear strain both increase with decreasing substrate stiffness. For cells that appear to beat very weakly, the nucleus also deforms very little. As the substrate softens and approaches the

optimum described in chapter 3, the cell should be able to deform its substrate more and more, and increasingly strain the nucleus. Finally as the substrate becomes too soft and the contractile cytoskeleton becomes less organized and loses contractile capacity, the cardiomyocyte strains its substrate less because its intracellular stress is less, which would be reflected in the nuclear deformation. Similarly, cells that beat uncharacteristically little on the 1 and 10 kPa gels here could be unhealthy or malfunctioning in some way and that is reflected in the lack of nuclear strain indicating that those cells just are not contracting well. This is in contrast to the cells on stiff substrates that to show similar cell edge strain, but significant nuclear strain, indicating that the contractile ability of the cells are incapable of deforming the substrate well, but still very functional. Therefore the nucleus serves as a useful indicator for cardiomyocyte contractile activity.

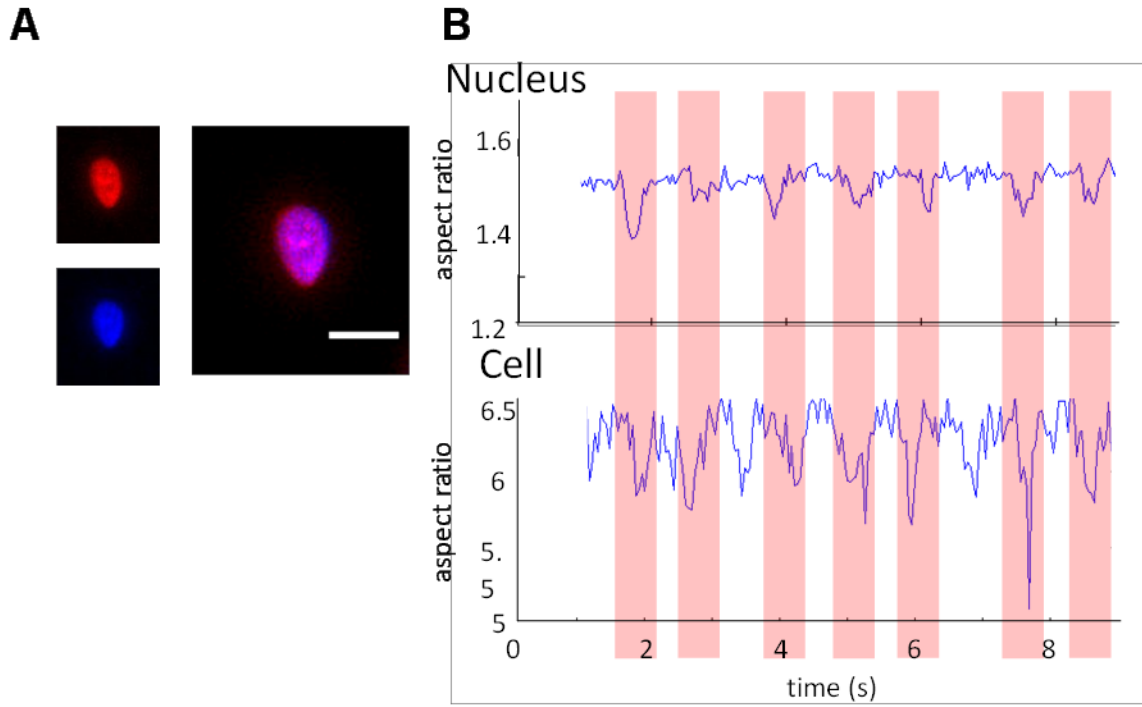


**Figure 4-1: . Contractile beating of embryonic cardiomyocytes on elastic substrates. (A)** Hoescht-stained nuclei of beating cardiomyocytes show nuclear strain during contraction. **(B)** Aspect ratio of nucleus and cell over time shows significant deformation of during contraction.

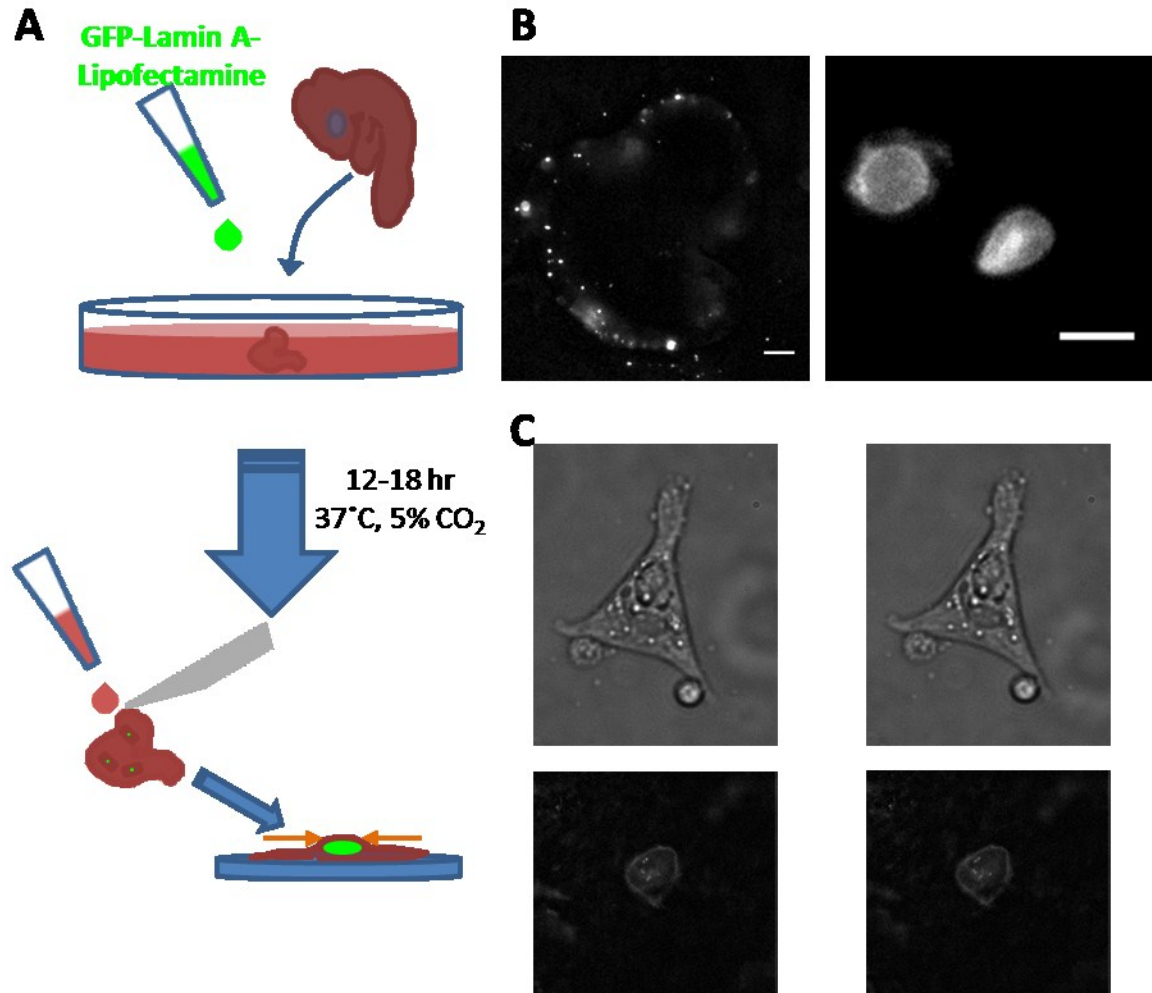


**Figure 4-2: Sparse transfection of embryonic heart tubes for perturbation and imaging of nuclear Lamins.** (A) Method for transfection of whole heart and isolation of cells for imaging. (B) Whole E4 HT transfected with GFP-Lamin-A at low and high resolution (inset). (C) Relaxed and contracted E4 cardiomyocyte and GFP-Lamin-A transfected nuclei on collagen-coated PA gels



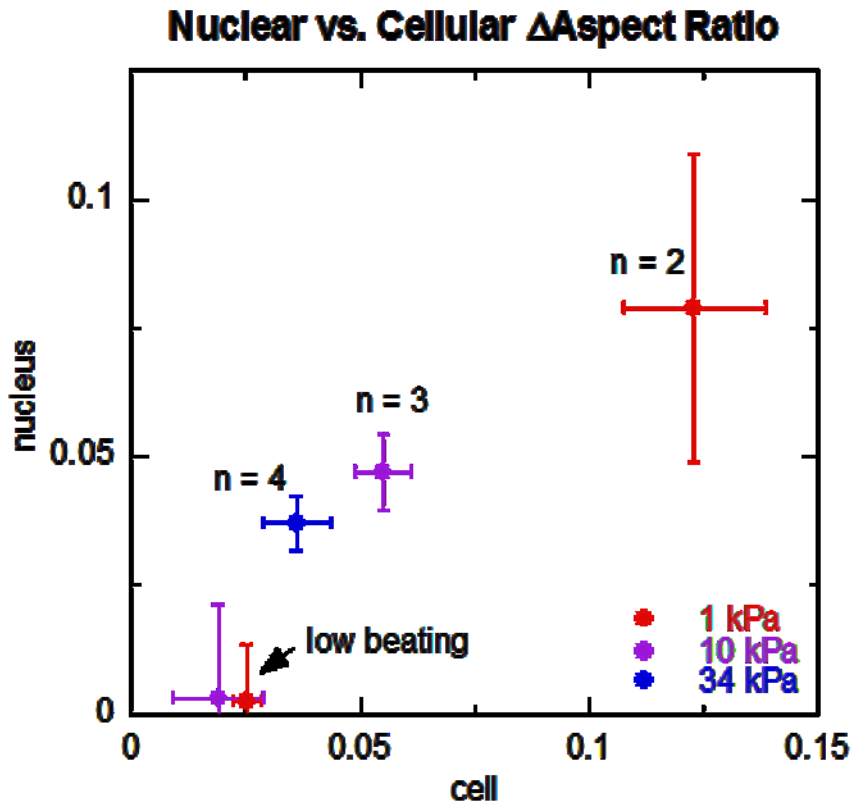


**Figure 4-3: Nuclear deformation vs. cellular deformation.** Nuclear fractional change in aspect ratio is plotted relative to cellular fractional change in aspect ratio. Expected behavior is illustrated in the inset. Cell strain and nuclear strain both increase with decreasing substrate stiffness. For cells that appear to beat very weakly, the nucleus also deforms very little, indicating much smaller intracellular strain.

## CHAPTER 5: Conclusions and future directions

### Conclusions:

In conclusion, this work attempts to characterize the dynamic mechanics of early heart development and the structural and molecular contributors and responses to those mechanics. We find that heart tissue stiffens during development, in contrast to brain which remains soft. These mechanical trends are paralleled by abundant cytoskeletal and ECM network proteins, in particular the contractile actomyosin cytoskeleton and Collagen-I, respectively. Disrupting these proteins decrease effective  $E_{\text{tissue}}$ . Both in intact tissue and isolated on elastic substrates, cardiomyocytes strain most on environments of physiological stiffness. Myofibril striation also optimized on intermediate stiffnesses. Unlike the optimized strain, contraction wave speed of intact myocardium goes proportionally with tissue stiffness, consistent with new theory presented here. The trends of myosin and collagen protein expression in developing tissues over time can be reconstituted with a coupled model including stress-stabilized degradation and extended to Lamin-Myosin interactions. Finally, as the nuclear Lamina is intimately linked with and can be strained by the contractile cytoskeleton of the cell, imaging the nucleus in intact tissue could prove a useful read-out to intercellular strain. We finish by presenting a useful and novel method of sparse fluorescent plasmid transfection in live intact embryonic cardiac tissue.

### Future Directions:

Chapter 2: The micropipette aspiration measurements of tissue stiffness were based on highly simplified models of tissue as an elastic half-space. More detailed or realistic models are currently being developed and could allow us to better understand the mechanics of the developing tissues in heart as well as viscous brain and embryo. Aside from giving a more

accurate measure of stiffness, a more detailed and realistic model that takes into account viscous properties of cells and ECM. One major advantage of micropipette aspiration is the dynamical strain information that it can provide, which our simplified model does not capture. Another very interesting and under-explored aspect of this research is the implications of the contraction wave model.

Chapter 3: The models of Chapter 3 point to a broad array of possible experimental and modeling avenues of inquiry. In particular, Lamin A, B1, and B2 levels could be more precisely and accurately measured throughout chick cardiogenesis using quantitative western immunoblotting. Absolute myosin, collagen, and Lamin A protein and mRNA expression could be quantified throughout development to get better estimates for some of the parameters of the models. The concept of strain-stabilized biopolymer networks is understudied, particularly in the case of Lamins. Finally, chapter 4 argues that matrix, cytoskeleton, and nuclear lamina are all intimately coupled, so the two models presented here should be further integrated to include all three structural proteins.

Chapter 4: As discussed in Chapter 4, with the technique of sparse transfection of intact tissue with various gfp-Lamin A constructs, we are well positioned to study the effects of over-expression or under- or defective expression of Lamin A on nuclear mechanics. The Discher lab has used various LaminA phospho-mimetic and disease related mutants that disrupt Lamin A assembly but still localize in the nucleus, thus acting as dominant-negative constructs in transfected cells. Of particular, a R453W mutant is a common mutant in Emory Dreyfuss Muscular Dystrophy, a form of the disease associated with the most common laminopathy-related cardiac defects, in particular DCM and conduction defects. Nucleii of cells transfected with GFP-WT Lamin A and GFP-mutant Lamin A could therefore be imaged and measured in intact

beating tissue, aspirated cells and tissue, and isolated cardiomyocytes on collagen-coated PA gels of various stiffnesses. Changes in nuclear mechanics could be measured in isolated cells and in tissue using micropipette aspiration. Nuclear morphology and strains could be correlated to tissue, cytoplasmic, and matrix strains during beating.

## BIBLIOGRAPHY

- [1] D. Gonzalez-Rodriguez, K. Guevorkian, S. Douezan and F. Brochard-Wyart, "Soft matter models of developing tissues and tumors," *Science*, vol. 338, no. 6109, pp. 910-917, 2012.
- [2] D. Discher, P. Janmey and Y. Wang, "Tissue cells feel and respond to the stiffness of their substrate," *Science*, vol. 310, no. 5751, pp. 1139-1143, 2005.
- [3] S. Khetan, M. Guvendiren, W. Legant, D. Cohen, C. Chen and J. Burdick, "Degradation-mediated cellular traction directs stem cell fate in covalently crosslinked three-dimensional hydrogels," *Nature Materials*, 2013.
- [4] K. Chien, I. Domian and K. Parker, "Cardiogenesis and the complex biology of regenerative cardiovascular medicine," *Science*, vol. 322, no. 5907, pp. 1494-1497, 2008.
- [5] A. Sachinidis, B. Fleischmann, E. Kolossov, M. Wartenberg, H. Sauer and J. Hescheler, "Cardiac specific differentiation of mouse embryonic stem cells," *Cardiovascular Research*, vol. 58, pp. 278-291, 2003.
- [6] L. Zwi, O. Caspi, G. Arbel, I. Huber, A. Gepstein, I. Park and L. Gepstein, "Cardiomyocyte differentiation of induced pluripotent stem cells," *Circulation*, vol. 120, pp. 1513-1523, 2009.
- [7] V. Segers and L. RT, "Stem cell therapy for cardiac disease," *Nature*, vol. 451, pp. 937-942, 2008.
- [8] A. Engler, C. Carag-Krieger, C. Johnson, M. Raab, H. Tang, D. Spelcher, J. Sanger, J. Sanger and D. Discher, "Embryonic cardiomyocytes beat best on a matrix with heart-like elasticity: scar-like rigidity inhibits beating," *Journal of Cell Science*, vol. 10, no. 24, pp.

3794-3802, 2008.

- [9] B. Friedrich and S. Safran, "How cells feel their substrate: spontaneous symmetry breaking of active surface stress," *Soft Matter*, vol. 8, pp. 3223-3230, 2012.
- [10] J. Jacot, A. McCulloch and J. Omens, "Substrate Stiffness affects the functional maturation of neonatal rat ventricular myocytes," *Biophysical Journal*, vol. 95, pp. 3479-3487, 2008.
- [11] D. Bers, *Excitation-Contraction Coupling and Cardiac Contraction Force*, 2nd ed., Boston, MA: Kluwer Academic Publishers, 2001.
- [12] V. Cadete, J. Sawicka, A. Doroszko, M. Wozniak and G. Sawicki, "Effects of the Rho-kinase inhibitor Y-27632 on the proteome of hearts with ischemia reperfusion injury," *Proteomics*, vol. 10, no. 24, pp. 4377-4385, 2010.
- [13] B. Bhana, R. Iyer, W. Chen, R. Zhao, K. Sider, M. Likhitpanichkul, C. Simmons and M. Radisic, "Influence of substrate stiffness on the phenotype of heart cells," *Biotechnology and Bioengineering*, vol. 105, no. 6, pp. 2151-2162, 2009.
- [14] J. S. N. Liu, M. Bruce, J. Wu and M. Butte, "Atomic force mechanobiology of pluripotent stem cell-derived cardiomyocytes," *PLoS-ONE*, vol. 7, no. 5, p. e37559, 2012.
- [15] P. Bajaj, X. Tang, T. Saif and R. Bashir, "Stiffness of the substrate influences the phenotype of embryonic chicken cardiomyocytes," *Journal of Biomedical Materials Research Part A*, vol. 95A, no. 4, pp. 1261-1269, 2010.
- [16] A. Rodriguez, S. Han, M. Regnier and N. Sniadecki, "Substrate stiffness increases twitch power of neonatal cardiomyocytes in correlation with changes in myofibril structure and intracellular calcium," *Biophysical Journal*, vol. 101, no. 10, pp. 2455-2464, 2011.

- [17] C. Johnson, H. Tang, C. Carag, D. Speicher and D. Discher, "Forced unfolding of proteins within cells," *Science*, vol. 317, no. 5838, pp. 663-666, 2007.
- [18] V. Cadete, J. Sawicka, D. Polewicz, A. Doroszko, M. Wozniak and G. Sawicki, "Effects of the Rho-kinase inhibitor Y-27632 on the proteome of hearts with ischemia reperfusion injury," *Proteomics*, vol. 10, no. 24, pp. 4377-4385, 2010.
- [19] M. McCain and K. Parker, "Mechanotransduction: the role of mechanical stress, myocyte shape, and cytoskeletal architecture on cardiac function," *European Journal of Physiology*, vol. 462, pp. 89-104, 2011.
- [20] J. Sanger, S. Kang, C. Siebrands, N. Freeman, A. Du, A. Stout and J. Sanger, "How to build a myofibril," *Journal of Muscle Research and Cell Motility*, vol. 26, pp. 343-354, 2005.
- [21] J. Sanger, J. Wang, Y. Fan, J. White and J. Sanger, "Assembly and dynamics of myofibrils," *Journal of Biomedicine and Biotechnology*, vol. 2010, 2010.
- [22] N. McKenna, C. Johnson and Y. Wang, "Formation and alignment of Z lines in living chick myotubes microinjected with rhodamine-labeled alpha-actinin," *Journal of Cell Biology*, vol. 103, no. 6, pp. 2163-2171, 1986.
- [23] C. Gregorio and P. Antin, "To the heart of myofibril assembly," *Trends in Cell Biology*, vol. 10, no. 9, pp. 355-362, 2000.
- [24] B. Friedrich, A. Buxboim, D. Discher and S. Safran, "Striated acto-myosin fibers can reorganize and register in response to elastic interactions with the matrix," *Biophysical Journal*, vol. 100, pp. 2706-2715, 2011.
- [25] S. Lahmers, Y. Wu, D. Call, S. Labeit and H. Granzier, "Developmental control of titin

- isoform expression and passive stiffness in fetal and neonatal myocardium," *Circulation Research*, vol. 94, pp. 505-513, 2004.
- [26] B. Fila, P. Bayly and L. Taber, "Mechanical stress as a regulator of cytoskeletal contractility and nuclear shape in embryo epithelia," *Annals of Biomedical Engineering*, vol. 39, no. 1, pp. 443-454, 2010.
- [27] J. Young and A. Engler, "Hydrogels with time-dependent material properties enhance cardiomyocyte differentiation in vitro," *Biomaterials*, vol. 32, no. 4, pp. 1002-1009, 2011.
- [28] E. A. Zamir, V. Srinivasan, R. Perucchio and L. A. Taber, "Mechanical Asymmetry in the Embryonic Chick Heart During Looping," *Annals of Biomedical Engineering*, vol. 31, pp. 1327-1336, 2003.
- [29] M. von Dassow and L. Davidson, "Natural variation in embryo mechanics: gastrulation in *Xenopus laevis* is highly robust to variation in tissue stiffness," *Developmental dynamics*, vol. 238, no. 1, pp. 2-18, 2009.
- [30] M. Krieg, Y. Arboleda-Estudillo, P. Puech, J. Kafer, F. Graner, D. Muller and C. Heisenberg, "Tensile forces govern germ layer organization in zebrafish," *Nature Cell Biology*, vol. 10, no. 4, pp. 429-436, 2008.
- [31] J. T. Butcher, T. C. McQuinn, D. Sedmera, D. Turner and R. R. Markwald, "Transitions in early embryonic atrioventricular valvular function correspond with changes in cushion biomechanics that are predictable by tissue composition," *Integrative Physiology*, vol. 100, pp. 1503-1511, 2007.
- [32] N. Hersch, B. Wolters, G. Dreissen, R. Springer, N. Kirchgebner, R. Merkel and B. Hoffmann, "The constant beat: cardiomyocytes adapt their forces by equal contraction upon



- environmental stiffening," *Biology Open*, vol. 2, no. 3, pp. 351-361, 2013.
- [33] M. McCain, H. Lee, Y. Aratyn-Schaus, A. Kleber and K. Parker, "Cooperative coupling of cell-matrix and cell-cell adhesions in cardiac muscle," *PNAS*, vol. 302, no. 2, pp. H445-H450, 2012.
- [34] A. Ulbricht, F. Eppei, V. Tapia, P. van der Ven, N. Hampe, N. Hersch, P. Vakeel, D. stadel, A. Haas, P. Saftig, C. Behrends, D. Furst, R. Volkmer, B. Hoffmann, W. Kolanus and J. Hohfeld, "Cellular mechanotransduction relies on tension-induced and chaperone-assisted autophagy," *Current Biology*, vol. 23, pp. 430-435, 2013.
- [35] A. Engler, S. Sen, H. Sweentey and D. Discher, "Matrix elasticity directs stem cell lineage specification," *Cell*, vol. 126, no. 4, pp. 677-689, 2006.
- [36] D. Theret, M. Levesque, M. Sato, R. Nerem and L. Wheeler, "The application of a homogeneous half-space model in the analysis of endothelial cell micropipette measurements," *Journal of Biomechanical Engineering*, vol. 110, pp. 190-199, 1988.
- [37] P. Georges, W. Miller, D. Meaney, E. Sawyer and P. Janmey, "Matrices with compliance comparable to that of brain tissue select neuronal over glial growth in mixed cortical cultures," *Biophysical Journal*, vol. 90, no. 8, pp. 3012-3018, 2006.
- [38] A. Chopra, V. Lin, A. McCollough, S. Atzet, G. Prestwich, A. Wechsler, M. Murray, S. Oake, J. Kresh and P. Janmey, "Reprogramming cardiomyocyte mechanosensing by crosstalk between integrins and hyaluronic acid receptor," *Journal of Biomechanics*, vol. 45, no. 5, pp. 824-831, 2012.
- [39] B. M. Friedrich, E. Fischer-Friedrich and S. A. Safran, "Sarcomeric pattern formation by

- actin cluster coalescence," *PLoS Computational Biology*, vol. 8, no. 6, p. e1002544, 2012.
- [40] M. Laflamme and C. Murry, "Regenerating the heart," *Nature Biotechnology*, vol. 23, no. 7, pp. 845-846, 2005.
- [41] L. Hazeltine, C. Simmons, M. Salick, X. Lian, M. Badur, W. Han, S. Delgado, T. Wakatsuki, W. Crone, B. Pruitt and S. Palecek, "Effects of substrate mechanics on contractility of cardiomyocytes generated from human pluripotent stem cells," *International Journal of Cell Biology*, vol. 2012, 2012.
- [42] J. W. Sanger, J. Wang, B. Holloway, A. Du and J. M. Sanger, "Myofibrillogenesis in Skeletal Muscle Cells in Zebrafish," *Cell Motility and Cytoskeleton*, vol. 66, no. 8, pp. 556-566, 2009.
- [43] A. Shwarek-Maruszewska, P. Hotulainen, P. Mattila and P. Lappalainen, "Contractility dependent actin dynamics in cardiomyocyte sarcomeres," *Journal of Cell Science*, vol. 112, pp. 2119-2126, 2009.
- [44] G. P. Farman, K. Tachampa, R. Mateja, O. Cazorla, A. Lacampagne and P. P. de Tombe, "Blebbistatin: use as inhibitor of muscle contraction," *Pflugers Archiv*, vol. 455, no. 6, pp. 995-1005, 2008.
- [45] B. M. Friedrich, E. Fischer-Friedrich, N. S. Gov and S. A. Safran, "Sarcomeric pattern formation by actin clustercoalescence," *PLoS Computational Biology*, vol. 8, no. 6, p. e1002544, 2012.
- [46] A. Du, J. Sanger and J. Sanger, "Cardiac myofibrillogenesis inside intact embryonic heart," *Developmental Biology*, vol. 318, no. 2, pp. 236-246, 2008.
- [47] M. Ieda, T. Tsuchihashi, K. Ivey, R. Ross, T. Hong, R. Shaw and D. Srivastava, "Cardiac

- Fibroblasts Regulate Myocardial Proliferation through B1 Integrin Signaling," *Developmental Cell*, vol. 16, pp. 233-244, 2009.
- [48] A. del Rio, R. Perez-Jimenez, R. Liu, P. Roca-Cusachs, J. Fernandez and M. Sheetz, "Stretching single talin rod molecules activate vinculin binding," *Science*, vol. 323, no. 5914, pp. 638-641, 2009.
- [49] T. Baudino, W. Carver, W. Giles and T. Borg, "Cardiac fibroblasts: friend of foe?," *American Journal of Physiology Heart and Circulatory Physiology*, vol. 291, pp. H1015-H1026, 2006.
- [50] J. Shin, J. Swift, K. Spinler and D. Discher, "Myosin-II inhibition and soft 2D-matrix maximize multinucleation and cellular projections typical of platelet-producing megakaryocytes," *Proceedings of the National Academy of Science*, vol. 108, pp. 11458-11463, 2011.
- [51] K. Dahl, S. Kahn, K. Wilson and D. Discher, "The nuclear envelope lamina network has elasticity and a compressibility limit suggestive of a molecular shock absorber," *Journal of Cell Science*, vol. 117, pp. 4779-4786, 2004.
- [52] P. Rodriguez, T. Harada, D. Christian, D. Pantano, R. Tsai and D. Discher, "Minimal "self" peptides that inhibit phagocytic clearance and enhance delivery of nanoparticles," *Science*, vol. 339, no. 6122, pp. 971-975, 2013.
- [53] Y. Ono, C. Schwach, P. Antin and C. Gregorio, "Disruption in the tropomodulin1 (Tmod1) gene compromises cardiomyocyte development in murine embryonic stem cells by arresting myofibril maturation," *Developmental Biology*, vol. 282, no. 2, p. 336-348, 2005.
- [54] P. Devreotes, "Dictyostelium discoideum: a model system for cell-cell interactions in

- development," *Science*, vol. 245, no. 4922, p. 1054, 1989.
- [55] P. Gillespie and R. Walker, "Molecular basis of mechanosensory transduction," *Nature*, vol. 413, no. 6852, pp. 194-202, 2001.
- [56] C. Kung, "A possible unifying principle for mechanosensation," *Nature*, vol. 436, pp. 647-654, 2005.
- [57] A. Levine and T. Lubensky, "Response function of a sphere in a viscoelastic two-fluid medium," *Physical Review E*, vol. 63, no. 4, p. 041510, 2001.
- [58] P. Alford and L. Taber, "Epicardial strains in embryonic chick ventricle at stages 16-24," *Circulation Research*, vol. 75, no. 5, pp. 896-903, 1994.
- [59] F. de Jong, T. Opthof, A. Wilde, M. Janse, R. Charles, W. Lamers and A. Moorman, "Persisting zones of slow impulse conduction in developing chicken hearts," *Circulation Research*, vol. 71, pp. 240-250, 1992.
- [60] S. F. Majkut, T. Idema, J. Swift, C. Krieger, A. Liu and D. Discher, "Heart stiffening in early embryos parallels matrix and myosin levels to optimize beating," *Current Biology*, 2013.
- [61] M. Eghbali, M. Czaja, M. Zeydel, F. Weiner, M. Zern, S. Seifert and O. Blumenfeld, "Collagen chain mRNAs in isolated heart cells from young and adult rats," *Journal of Molecular and Cellular Cardiology*, vol. 20, no. 3, pp. 267-276, 1988.
- [62] E. McNally, J. Golbus and M. Puckelwartz, "Genetic mutations and mechanisms in dilated cardiomyopathy," *Journal of Clinical Investigation*, vol. 123, no. 1, pp. 19-26, 2013.
- [63] C. Souders, S. Bowers and T. Baudino, "Cardiac fibroblast: the Renaissance cell,"

- Circulation Research*, vol. 105, pp. 1164-1176, 2009.
- [64] S. Bowers, I. Banerjee and T. Baudino, "The extracellular matrix: At the center of it all," *Journal of Molecular and Cellular Cardiology*, vol. 48, no. 3, pp. 474-482, 2010.
- [65] M. St. John Sutton and N. Sharpe, "Left ventricular remodeling after myocardial infarction: pathophysiology and therapy," *Circulation*, vol. 101, pp. 2981-2988, 2000.
- [66] W. Briest, "The role of extracellular matrix in the development of experimental cardiac hypertrophy," in *Communicating Current Research and Educational Topics and Trends in Applied Microbiology*, vol. 2, A. Mendez-Vilas, Ed., Badajoz, Formatex, 2007, pp. 830-838.
- [67] E. Goldsmith, A. Hoffman, M. Morales, J. Potts, R. Price, A. McFadden, M. Rice and T. Borg, "Organization of the fibroblasts in the heart," *Developmental Dynamics*, vol. 230, no. 4, pp. 787-794, 2004.
- [68] I. Banerjee, J. Fuseler, R. Price, T. Borg and T. Baudino, "Determination of cell types and numbers during cardiac development in the neonatal and adult rat and mouse," *American Journal of Physiology: Heart and Circulatory Physiology*, vol. 293, no. 3, pp. H1883-H1891, 2007.
- [69] P. Snider, K. Standley, J. Wang, M. Azhar, T. Doetschman and S. Conway, "Origin of cardiac fibroblasts and the role of Periostin," *Circulation Research*, vol. 105, pp. 934-047, 2009.
- [70] P. Camellit, C. Green, I. LeGriecce and P. Kohl, "Fibroblast network in rabbit sinoatrial node: structural and functional identification of homogeneous and heterogeneous cell coupling," *Circulation Research*, vol. 94, pp. 828-835, 2004.

- [71] P. Camelliti, T. Borg and P. Kohl, "Structural and functional characterisation of cardiac fibroblasts," *Cardiovascular Research*, vol. 65, pp. 40-51, 2005.
- [72] A. Ruiz-Villalba, A. Ziogas, M. Ehrbar and J. M. Perez-Pomares, "Characterization of epicardial-derived cardiac interstitial cells: differentiation and mobilization of heart fibroblast progenitors," *PLoS ONE*, vol. 8, no. 1, p. e52694, 2013.
- [73] R. Neuman, "Hydroxyproline content of the developing chick embryo," *Experimental Biology and Medicine*, vol. 1, no. 75, pp. 37-39, 1950.
- [74] J. Woessner Jr., R. Bashey and R. Boucek, "Collagen development in the heart and skin of the chick embryo," *Biochimica et Biophysica Acta - Protein Structure*, vol. 140, no. 2, pp. 329-338, 1967.
- [75] J. Jacot, J. Martin and D. Hunt, "Mechanobiology of cardiomyocyte development," *Journal of Biomechanics*, vol. 43, no. 1, pp. 93-98, 2010.
- [76] M. Eghbali, M. Eghbali, T. Robinson, S. Seifert and O. Blumenfeld, "Collagen accumulation in heart ventricles as a function of growth and aging," *Cardiovascular Research*, vol. 23, no. 8, pp. 723-729, 1989.
- [77] J. Jalil, C. Doering, J. Janicki, R. Pick, S. Shroff and K. Weber, "Fibrillar collagen and myocardial stiffness in the intact hypertrophied rat left ventricle," *Circulation Research*, vol. 64, pp. 1041-1050, 1989.
- [78] R. Dean, L. Balding, R. Candido, W. Burns, Z. Cao, S. Twigg and L. Burrell, "Connective tissue growth factor and cardiac fibrosis after myocardial infarction," *Journal of Histochemistry and Cytochemistry*, vol. 53, pp. 1245-1256, 2005.

- [79] M. Berry, A. Engler, Y. Woo, T. Pirollo, L. Bish, V. Jayasankar, K. Morine, T. Gardner, D. Discher and H. Sweeney, "Mesenchymal stem cell injection after myocardial infarction improves myocardial compliance," *American Journal of Physiology: Heart Circulation Physiology*, vol. 290, pp. H2196-H2203, 2006.
- [80] A. Gittenberger-de Groot, M. Vrancken Peeters, M. Mentink, R. Gourdie and R. Poelmann, "Epicardium-derived cells contribute a novel population to the myocardial wall and the atrioventricular cushions," *Circulation Research*, vol. 82, no. 10, pp. 1043-1052, 1998.
- [81] D. MacKenna, S. Summerour and F. Villarreal, "Role of mechanical factors in modulating cardiac fibroblast function and extracellular matrix synthesis," *Cardiovascular Research*, vol. 46, no. 2, pp. 257-263, 2000.
- [82] R. Kakkar and R. Lee, "Intramyocardial fibroblast myocyte communication," *Circulation Research*, vol. 106, pp. 47-57, 2010.
- [83] A. McCulloch and G. Paternostro, "Cardiac Systems Biology," *Annals of the New York Academy of Sciences*, vol. 1047, pp. 283-295, 2005.
- [84] D. Noble, "Modeling the heart-from genes to cells to whole organ," *Science*, vol. 295, pp. 1678-1682, 2002.
- [85] S. Sperling, "Systems biology approached to heart development and congenital heart disease," *Cardiovascular Research*, vol. 91, pp. 269-278, 2011.
- [86] K. Ryall, D. Holland, K. Delaney, M. Kraeutler, A. Parker and J. Saucerman, "Network reconstruction and systems analysis of cardiac myocyte hypertrophy signalling," *Journal of Biological Chemistry*, vol. 287, no. 50, pp. 42259-42268, 2012.

- [87] S. Majkut, T. Idema, J. Swift, C. Krieger, A. Liu and D. Discher, "Heart-specific stiffening in early embryos parallels matrix and myosin expression to optimize beating," *Current Biology*, 2013.
- [88] B. Schwanhausser, D. Busse, N. Li, G. Dittmar, J. Schuchhardt, J. Wolf, W. Chen and M. Selbach, "Global quantification of mammalian gene expression control," *Nature*, vol. 473, pp. 337-342, 2011.
- [89] J. Swift, I. Ivanovska, A. Buxboim, T. Harada, P. Dingal, J. Pinter, J. Pajeroski, K. Spinler, J. Shin, M. Tewari, F. Rehfeldt, D. Speicher and D. Discher, "Nuclear Lamin-A scales with tissue stiffness and enhances matrix-directed differentiation," *Science*, vol. 341, pp. 1240104-1-15, 2013.
- [90] K. Bott, Z. Upton, K. Schrobback, M. Ehrbar, J. A. Hubbell, M. P. Lutolf and S. C. Rizzi, "The effect of matrix characteristics on fibroblast proliferation in 3D gels," *Biomaterials*, vol. 31, no. 32, pp. 8454-8464, 2010.
- [91] B. Flynn, A. Bhole, N. Saeidi, M. Liles, C. DiMarzio and J. Ruberti, "Mechanical strain stabilizes reconstituted collagen fibrils against enzymatic degradation by mammalian collagenase matrix metalloproteinase 8 (MMP-8)," *PLoS ONE*, vol. 5, no. 8, p. e12337, 2010.
- [92] R. Camp, M. Liles, J. Beal, N. Saeidi, B. Flynn, E. Moore, S. Murthy and J. Ruberti, "Molecular mechanochemistry: Low forces switch slows enzymatic cleavage of human type I collagen monomer," *Journal of American Chemical Society*, vol. 133, no. 11, pp. 4073-4078, 2011.
- [93] M. Raab, J. Swift, P. Dingal, P. Shah, J. Shin and D. Discher, "Crawling from soft to stiff



- matrix polarizes the cytoskeleton and phosphoregulates myosin-II heavy chain," *Journal of Cell Biology*, vol. 199, no. 4, pp. 669-683, 2012.
- [94] A. Adhikari, J. Chai and A. Dunn, "Mechanical load induces a 100-fold increase in the rate of collagen proteolysis by MMP-1," *Journal of the American Chemical Society*, vol. 133, no. 6, pp. 1686-1689, 2011.
- [95] D. Discher, P. Janmey and Y. Wang, "Tissue cells feel and respond to the stiffness of their substrate," *Science*, vol. 310, no. 5751, pp. 1139-1143, 2005.
- [96] F. L. D. Haque, D. Smallwood, Dent, CL, C. Shanahan, Fry, AM, R. Trembath and S. Shackleton, "SUN1 interacts with nuclear lamin A and cytoplasmic nesprins to provide a physical connection between the nuclear lamina and the cytoskeleton," *Molecular and Cellular Biology*, vol. 26, no. 10, pp. 3738-3751, 2006.
- [97] R. Rober, K. Weber and M. Osborn, "Differential timing of nuclear lamin A/C expression in the various organs of mouse embryo and young animal: a developmental study," *Development*, vol. 105, pp. 365-378, 1989.
- [98] R. Benavente, G. Krohne and W. W. Franke, "Cell type-specific expression of nuclear lamina proteins during development of *Xenopus laevis*," *Cell*, vol. 41, no. 1, pp. 177-190, 1985.
- [99] C. Lehner, R. Stick, H. Eppenberger and E. Nigg, "Differential expression of nuclear lamin proteins during chicken development," *Journal of Cell Biology*, vol. 105, no. 1, pp. 577-587, 1987.
- [100] D. Fatkin, C. MacRae, T. Sasaki, M. p. M. Wolff, M. Frenneaux, J. Atherton, H. Vidaillet, S. G. U. Spudich, J. Seidman and C. seidman, "Missense mutations in the rod domain of the

Lamin A/C gene as causes of dilated cardiomyopathy and conduction-system disease," *New England Journal of Medicine*, vol. 341, no. 23, pp. 1716-1724, 1999.

- [101] E. Arbustini, A. Pilotto, A. Repetto, M. Grasso, A. Negri, M. Diegoli, C. Campana, L. Scelsi, E. Baldini, A. Gavazzi and L. Tavazzi, "Autosomal dominant dilated cardiomyopathy with atrioventricular block: a Lamin A/C defect-related disease," *Journal of the American College of Cardiology*, vol. 39, no. 6, pp. 981-990, 2002.
- [102] S. Parks, J. Kushner, D. Nauman, D. L. S. Burgess, A. Peterson, D. Li, P. Jakobs, M. Litt, C. Porter, P. Rahko and R. Hershberger, "Lamin A/C mutation analysis in a cohort of 324 unrelated patients with idiopathic or familial dilated cardiomyopathy," *American Heart Journal*, vol. 156, no. 1, pp. 161-169, 2008.
- [103] N. Zuela, D. A. Bar and Y. Gruenbaum, "Lamins in development, tissue maintenance and stress," *EMBO reports*, vol. 13, pp. 1070-1078, 2012.
- [104] C. Y. Ho, D. E. Jaalouk, M. K. Vartiainen and J. Lammerding, "Lamin A/C and emerin regulate MKL1-SRF activity by modulating actin dynamics," *Nature*, vol. 497, pp. 507-511, 2013.